

UNCLASSIFIED

AD . 4 2 6 4 4 8

DEFENSE DOCUMENTATION CENTER

FOR

SCIENTIFIC AND TECHNICAL INFORMATION

CAMERON STATION, ALEXANDRIA, VIRGINIA



UNCLASSIFIED

NOTICE: When government or other drawings, specifications or other data are used for any purpose other than in connection with a definitely related government procurement operation, the U. S. Government thereby incurs no responsibility, nor any obligation whatsoever; and the fact that the Government may have formulated, furnished, or in any way supplied the said drawings, specifications, or other data is not to be regarded by implication or otherwise as in any manner licensing the holder or any other person or corporation, or conveying any rights or permission to manufacture, use or sell any patented invention that may in any way be related thereto.

426448

CATALOGED BY DDC

AS FOR AD NO. NEWPORT BEACH, CALIFORNIA



MHD research, inc.

RESEARCH ON THE PHYSICS
OF
PULSED MHD GENERATORS

FINAL REPORT

Advanced Research Projects Agency
Nonr-3859(00)
Project Code 9800
Order No. 209 62 (Amend =4)
December 1963

By: Malcolm S Jones Jr.
V. H. Blackman
F. C. Brumfield
E. W. Evans
C. N. McKinnon

FINAL REPORT

**RESEARCH ON THE PHYSICS
OF
PULSED MHD GENERATORS**

Advanced Research Projects Agency

Nonr-3859(00)

Project Code 9800

Order No. 209 62 (Amend. =4)

December 1963

By: Malcolm S. Jones, Jr.

V. H. Blackman

R. C. Brumfield

E. W. Evans

C. N. McKinnon

This work has been sponsored by the
Advanced Research Projects Agency
through the Power Branch of the Office
of Naval Research. Reproduction in
whole or in part is permitted for any
purpose of the U. S. Government

ABSTRACT

Two systems are discussed for producing short pulses of electrical power by MHD principles. The first system is driven by condensed explosives and produces pulses lasting from $1\ \mu$ sec to $100\ \mu$ sec. The peak power generated to date is 23 MW, with an energy output of 750 joules. The conversion efficiency, chemical to electrical, is 1%. Higher conversion efficiencies can be readily achieved.

The second system uses the combustion of aluminum with cesium nitrate as the energy source for a supersonic MHD channel. The measured conductivity of the combustion products was 1000 mho/m. The highest measured peak power output was 29 watts. The experimental data indicate a large electrode drop which must be overcome before currents can flow in the generator. A favorable scaling potential is indicated.

TABLE OF CONTENTS

	ABSTRACT	i
	TABLE OF CONTENTS	ii
	LIST OF ILLUSTRATIONS	iv
	LIST OF TABLES	vii
1.	INTRODUCTION AND SUMMARY	1
	1.1 General introduction and statement of problem	1
	1.2 Summary of Explosive-driven MHD Generator Experiments	2
	1.3 Summary of Long duration pulsed power experiments	4
2.	PULSED POWER FROM CONDENSED EXPLOSIVES	7
	2.1 Introduction	7
	2.2 Theory	8
	2.3 Description of the Apparatus	11
	2.4 Power Generation Experiments	23
	2.5 Technical studies	32
	2.5.1 Variation in velocity with initial pressure	32
	2.5.2 Seeding studies	43
	2.5.3 Conductivity Measurements	53
	2.5.4 Variation in output with load resistance	62
	2.5.5 Variation in output with magnetic field	70
	2.5.6 Scaling and aspect ratio studies	72
	2.5.7 Variation in blast pressure with initial channel pressure	75

TABLE OF CONTENTS (cont'd)

2. 5. 8	Explosive Parameters	80
2. 5. 9	Load Placement Studies	89
2. 5. 10	Probe Studies	94
3.	LONG DURATION PULSED POWER	101
3. 1	Introduction	101
3. 2	Experimental Apparatus	101
3. 2. 1	Design Objectives	101
3. 2. 2	Combustion Chamber	102
3. 2. 3	Test Section	107
3. 2. 4	Electrodes	108
3. 2. 5	Magnet	108
3. 2. 6	Exhaust System	110
3. 2. 7	Conductivity and Power Measure- ment Instrumentation	110
3. 2. 8	Pressure Measurement Instrumentation	111
3. 2. 9	Recording System	112
3. 3	Power Generation Experiments	112
3. 4	Conductivity Measurements	121
4.	CONCLUSIONS	127
	APPENDIX A	
	APPENDIX B	
	REFERENCES	
	DISTRIBUTION LIST	

LIST OF ILLUSTRATIONS

Figure 2. 1	Schematic view of explosive-driven MHD generator	12
Figure 2. 2	View of complete facility	13
Figure 2. 3	Dissembled view of 1" x 1" explosive driven MHD channel	14
Figure 2. 4	Dissembled view of 1" x 4" explosive driven MHD channel	17
Figure 2. 5	Schematic diagram of the current pickup loop and integrator circuit.	21
Figure 2. 6	Oscilloscope trace showing voltage and current output of 1" x 4" explosive driven MHD generator.	24
Figure 2. 7	Electrical energy delivered to load	26
Figure 2. 8	Power output of 1 inch by 4 inch explosive-driven MHD generator.	30
Figure 2. 9	Power output as a function of load resistance for 1" x 1" explosive driven MHD generator.	31
Figure 2. 10	Front arrival at several electrode stations for various initial pressures	34
Figure 2. 11	Front arrival at several electrode stations for low initial pressures	35
Figure 2. 12	Initial velocity of front of conductive detonation products	36
Figure 2. 13	Variation of pressure in air shock driven by detonation product rarefaction wave.	41
Figure 2. 14	Comparison of seeded and nonseeded charges in 1 inch by 1 inch explosive-driven MHD generator.	44
Figure 2. 15	Comparison of generator characteristics for bulk and surface seeding with PEX and RDX charges.	46
Figure 2.16	Reduction in velocity of detonation product front as cesium picrate seed is added to front surface of duPont 20B charge.	48

LIST OF ILLUSTRATIONS (cont'd)

Figure 2. 17	The voltage-current relationships across the generator electrodes, $B = 0$.	54
Figure 2. 18	Typical oscilloscope trace from explosive driven MHD generator.	56
Figure 2. 19	Voltage-current characteristic of explosive driven MHD generator for conductivity determination.	58
Figure 2. 20	Voltage current characteristic of explosive driven MHD generator with 0. 5 inch diameter electrodes.	59
Figure 2. 21	Output characteristics of 1 inch by 1 inch explosive-driven MHD channel for various load resistances.	64
Figure 2. 22	Output voltage of 1" x 1" explosive-driven MHD generator. Initial pressure 10 mm Hg of air.	65
Figure 2. 23	Output voltage of 1" x 1" explosive-driven MHD generator. Initial pressure 10 mm Hg of argon.	67
Figure 2. 24	Open circuit voltage versus applied field.	71
Figure 2. 25	Normalized voltage-current plots for explosive driven MHD generators.	74
Figure 2. 26	High Reynolds number scaling of explosive-driven MHD channels with initial pressure 10 mm Hg of argon.	76
Figure 2. 27	Pressure rise as a function of initial air pressure in explosive-driven channel.	77
Figure 2. 28	Typical oscilloscope trace during probe experiments.	95
Figure 2. 29	Typical oscilloscope traces from four probes.	97
Figure 2. 30	Change in velocity of conductive detonation products as a function of extracted energy in explosive-driven MHD generator.	99

LIST OF ILLUSTRATIONS (cont'd)

Figure 3.1	Long duration pulse power facility	103
Figure 3.2	Dissembled view of supersonic MHD channel	104
Figure 3.3	Power generation apparatus for series 3 charges showing heated electrodes	105
Figure 3.4	Cross section of combustion chamber and nozzle plate.	106
Figure 3.5	Schematic for the 60 cycle conductivity measurement	109
Figure 3.6	Load current vs. time	115
Figure 3.7	Voltage output and burning pressure	117
Figure 3.8	Voltage and conductance data for Series 4 charge run.	120
Figure 3.9	Current record from Conductivity Measurements	125

LIST OF TABLES

TABLE 2.1	Effect of Seed Level on Power Outputs in the 1 inch by 4 inch Generation	49
TABLE 2.2	Effect of Argon Pressure on 1 inch by 4 inch Channel Output	49
TABLE 2.3	Operating Characteristics of the 1 inch by 4 inch Generator for Helium, Argon, and Air in the Channel	52
TABLE 2.4	Correlation of Pressure Rise Data with Mach Number in Explosive-Driven MHD Channel	79
TABLE 2.5	Comparison of Explosive Charge Holder Density and Charge Geometry	83
TABLE 2.6	Comparison of DuPont 20B and Falcon Research W Charges in 1 inch by 1 inch Explosive-Driven MHD Generator	86
TABLE 2.7	Charge Comparisons	88
TABLE 2.8	Data taken during Probe Experiments in 1 inch by 1 inch Channel	100
TABLE 3.1	Charges Used in Long Pulse Power Generation	115

1.0 INTRODUCTION AND SUMMARY

1.1 General Introduction and Statement of Problem

One of the most interesting aspects of MHD power conversion is the potential for obtaining high power densities in the energy conversion section. For example, in experiments with a small size explosive-driven MHD generator, which are reported herein, power densities as high as 2×10^{10} watts per cubic meter were obtained. Even in the open cycle fossil fueled generators which are being extensively investigated, power densities of 10^8 watts per cubic meter can be obtained. This potential offers many possibilities for the use of an MHD generator, which would be relatively small in size and light in weight per unit output, as a source of pulsed electrical power or more descriptively pulsed electrical energy. Many possible applications for pulsed electrical energy can be mentioned. Examples include high power radar sets, sonar systems, laser light pumps, X-ray tubes, and emergency communication systems. In addition, there are other uses in research programs involving the powering of advanced test facilities such as spark driven shock tubes, controlled thermonuclear fusion experiments, etc., which require very large amounts of electrical energy, i. e., greater than a megajoule, in short pulses.

The objective of the present program has been to investigate the feasibility of using MHD generators to meet these pulsed energy source requirements. Because of the wide distribution of desired pulse lengths it has been necessary to consider two separate thermal sources for driving pulsed generators. These are condensed explosives, such as are used in shaped charges or for demolition work, and deflagrating explosives which include solid

rocket propellants. These two thermal sources would, in principle, allow energy "storage" systems to be developed with output pulse lengths in the range from microseconds up to several seconds. Systems with pulse lengths in the range from microseconds up to several milliseconds could be constructed for the replacement of capacitor banks in certain applications.

The work reported herein includes the experimental and analytical work performed over the three month period from 1 July 1963 to 30 September 1963. This work is reviewed briefly below, and more extensively in Sections 2.0 and 3.0 of this report. The work performed at the beginning of the program on negative ion formation in combustion product flows was fully reported in the First Semiannual Technical Report⁽¹⁾ and will not be repeated here. Section 2.0 of this report described the work with condensed explosives to produce short pulses of energy. Section 3.0 describes the work with solid propellant materials to produce pulses of longer duration which was reported in detail in the technical reports^(1,2).

1.2 Summary of Explosive-Driven MHD Generator Experiments

The most extensive experimental effort under this program was conducted using condensed explosives. The time scale of the power pulse in these experiments varied from about 5 to 50 μ sec depending upon the length of electrodes in the generator. (Times of between 1 and 200 μ sec would be characteristic of the power pulse for practical systems based on an explosive-driven MHD converter.) Power pulses of up to 23 MW have been generated by this technique in a channel 1 inch by 4 inches by 18 inches long. The total electrical energy delivered to the load in this case was 750 joules. The energy was derived from the detonation of 15 gms of RDX explosive in a shaped charge

geometry, seeded on the front surface with 0.4 gms of cesium picrate. The conversion efficiency, chemical to electrical, is 1%. Higher efficiencies can be obtained by using stronger magnetic fields and a longer generator.

Extensive experimental and theoretical work has been performed on the explosive-driven MHD generator concept to determine the basic physical processes occurring in the generator and to obtain data to scale the results to larger sized units with usable outputs. From these studies it has been determined that very highly conductive detonation products are produced by seeding condensed explosives with low ionization potential material. In these experiments the seed was cesium picrate. The measured conductivity of the seeded detonation products is 1100 mho/meter. The detonation products flow at a very high velocity (10 km/sec) through an MHD channel which has a transverse magnetic field of the order of 2.2 w/m^2 (22 kilogauss). The electrical power is generated by relative motion of the ionized gas through the magnetic field. Electrical current is extracted by means of copper electrodes in contact with the detonation products, and conducted to an external load. The detonation products are slowed as kinetic energy is converted to electrical energy and removed from the system.

To support this analysis, studies have been performed to determine the effects of changes in the various parameters on the generation process in order that the optimum systems for energy conversion can be predicted. These studies have included the following:

- 1) Measurement of the effective velocity and conductivity of the conducting detonation products as a function of the density and composition of gas initially in the channel, and the type and shape of explosive.

- 2) Determination of electrical characteristics such as the optimum load resistance, ideal position for placement of the load, effects of electrode size, effects of magnetic field strengths, and the effect of generator size and aspect ratio upon scaling parameters.

On the basis of these studies it is believed possible to predict the characteristics of explosive-driven MHD generators with a fair degree of accuracy to meet a specified pulse requirement with the applicable time range.

The above topics are discussed in complete detail in Section 2.0 of this report. Analytical studies relating to scaling factors and possible geometries are presented as Appendix A to this report. An engineering analysis of the possible configuration of a potential pulse power system to produce one-quarter of a megajoule is contained in Appendix B. Due to the type of magnet coil cooling used, the system presented in Appendix B is mainly of interest for a satellite application.

1.3 Summary of Long Duration Pulsed Power Experiments

The goals of the long duration pulsed power experiments are to produce pulses of electrical power lasting from 1 millisecond to several seconds. A series of experiments have been conducted wherein special propellant charges consisting of cesium nitrate and aluminum have been used as the thermal energy source in a supersonic MHD channel. In order to simulate the use of permanent magnets in some pulsed power applications, low magnetic fields have been used. The peak electrical power measured in this system was 29 watts dissipated in a 1 ohm load. Electrical measurements indicated that supersonic velocities were obtained in the flow channel.

In an auxiliary set of measurements it was determined that the conductivity of the ionized combustion products was of the order of 1000 mho/meter. These measurements also indicated that a very large electrode drop (~ 50 volts) had to be overcome before appreciable currents could flow. These data suggest that any future work on this system be conducted on a scale such that the output voltage is many times the observed electrode drop. This would indicate the use of larger charges, to obtain the same supersonic velocity in a larger channel, and higher magnetic fields.

The fact that it was possible to achieve a highly conductive, high velocity, flow stream indicates an attractive potential for future development.

2.0 PULSED POWER FROM CONDENSED EXPLOSIVES

2.1 Introduction

The purpose of this portion of the program has been to investigate methods for the production of pulses of electrical power from condensed explosives by MHD principles. Pulse power sources of the explosion tube type have potential advantages of simplicity, compactness, portability, convenience, reliability, and storability. The use of various types and geometric forms of chemical explosive sources should make possible operation at various power levels (one KW to thousands of MW) and for variable periods of time, (1 microsecond up to 1 millisecond).

In the present experiments, the characteristics of the electrical output from a seeded shaped charge detonated in the explosion tube have been studied. The hot, partially ionized combustion gases from the detonation pass at high velocity through the power generation section. In the MHD section, the electric power is generated by the relative motion of the ionized gas through a transverse magnetic field. The electric current is extracted by means of copper electrodes connected to an external load.

There are a large number of factors which have been investigated in order to establish criteria for the design of explosive-driven MHD generators, and which are required for an intelligent scaling from the present small size experiment. These investigations have covered: (1) the choice of explosive and explosive geometry, (2) the choice of pressure and composition of gases initially in the channel, (3) the selection of the optimum load across the electrodes, and (4) the effect of electrode geometry, magnetic field intensity, and the channel aspect ratio upon power output. The velocity, pressure, and con-

ductivity of the detonation products was also determined. During these experiments power outputs as high as 23 MW were demonstrated, with an integrated output of 750 joules. This was equivalent to a chemical to electrical conversion efficiency of 1%. Higher conversion efficiencies appear readily attainable using these principles.

2.2 Theory

The generation of pulsed power by MHD means from condensed explosives is a direct outgrowth of steady state experimentation and theoretical development. It is instructive to recall that the electrical power produced in a continuous electrode, MHD generator for matched load conditions is given by:

$$P = \frac{\sigma}{1 + \epsilon^2} u^2 B^2 K (1 - K) V, \quad (2.2.1)$$

where

- P = power in watts,
- V = interaction volume in meters³,
- σ = scalar electrical conductivity in mhos/meter,
- u = velocity in meters per second,
- B = magnetic field in webers per meter²,
- ϵ = ratio of electron mean free path to the Larmor radius,

and K is given by:

$$K = \left(\frac{\sqrt{1 + \epsilon^2} - 1}{\epsilon^2} \right)^2. \quad (2.2.2)$$

For the high particle densities which occur in detonation product flows, the electron mean free path is small compared to the Larmor radius, therefore, $\beta \ll 1$ and $K = 1/2$. Equation (2.2.1) then becomes:

$$P = \frac{\sigma u^2 B^2 V}{4} . \quad (2.2.3)$$

Equation (2.2.3) only applies when the magnetic Reynolds number, Re_M , is very small. The magnetic Reynolds number is defined as follows:

$$Re_M = \mu \sigma u L , \quad (2.2.4)$$

where

μ = magnetic permeability,

L = a length characteristic of the duct,
usually the diameter .

Detonation velocities of 10^4 m/sec can be obtained with shaped charges and conductivity of 10^3 mhos/meter has been measured. Therefore in a laboratory scale experiment with $L = 0.04$ m,

$$Re_M = 4\pi \times 10^{-7} \times 10^3 \times 10^4 \times 4 \times 10^{-2} = 0.5 .$$

We must therefore conclude that, in laboratory devices which are driven by condensed explosives, Equation (2.2.3) must be modified to some extent since Re_M is not much smaller than one, and the currents which can flow in the conducting fluid may cause a substantial modification of the magnetic field intensity. If large devices are considered, i. e., $L \sim 1$ m then

$$Re_M > 10 .$$

Equation (2.2.1) is definitely no longer valid, and the large Reynolds number expression must be used for the power density. In Reference 3, this condition is shown to be given in the limiting case by the relation

$$P = \frac{2B^2}{\mu} Au, \quad (2.2.)$$

where A is the cross sectional area of the channel. For $Re_M \sim 1$ the power density will be between that given in Equations (2.2.3) and (2.2.5). Equation (2.2.5) arises from the fact that when $Re_M \gg 1$, the currents induced in the plasma conductor give rise to a magnetic field. This field is equal in magnitude to the initial field ahead of the moving conductor and in a direction such that the field value is doubled ahead of the conductor while the field behind the current sheet drops to zero. Thus the breaking pressure given by

$$P_z = \int (j \times B)_z dz$$

(where z is along the direction of motion) becomes

$$\frac{2B^2}{\mu}.$$

Therefore, the rate at which work is done is given by the product of this breaking pressure and the rate at which volume is swept up, e.g., Equation (2.2.5).

Equation (2.2.5) will apply in the case where the generator is feeding a very low impedance load so that large currents can flow. For high impedance loads, the device will perform more in the manner of a conventional MHD generator. This characteristic is shown in the experimental data which is presented in the following sections, particularly Section 2.5.6, which examines the variation in output with load impedance.

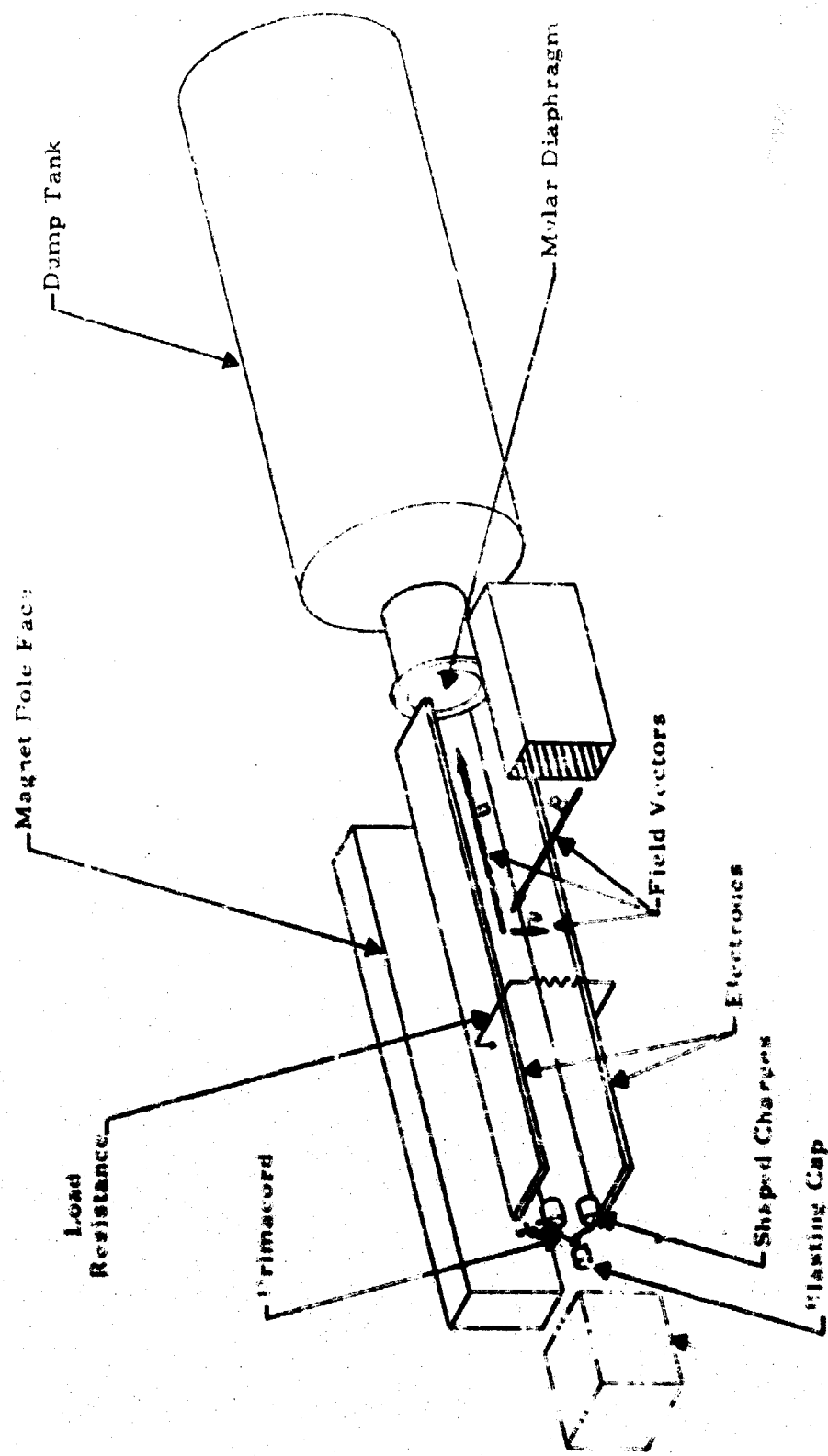
It is interesting to notice that the power production for the case of $Re_M \gg 1$ is independent of σ and only depends on u to the first power. Thus, in large scale pulse power devices it does not improve power output to increase σ much beyond the point where $Re_M \sim 3-4$. It then becomes more important to maximize the velocity with which the conducting slug moves against the field, and to maximize the magnet field. It should be remarked that the removal of electrical energy from the system will result in the slowing down of the detonation products, which is experimentally observed.

2.3 Description of the Apparatus

The experimental apparatus used for the experiments consists of five basic parts as shown in the schematic in Figure 2.1. These are: (1) explosion tube or driver section; (2) the MHD channel or test section; (3) di instrumentation; (4) electromagnet, and (5) evacuated dump tube. Figure 2.2 is a photograph of the complete facility; Figure 2.3 is a photograph of the interior of a 1 inch by 1 inch generator.

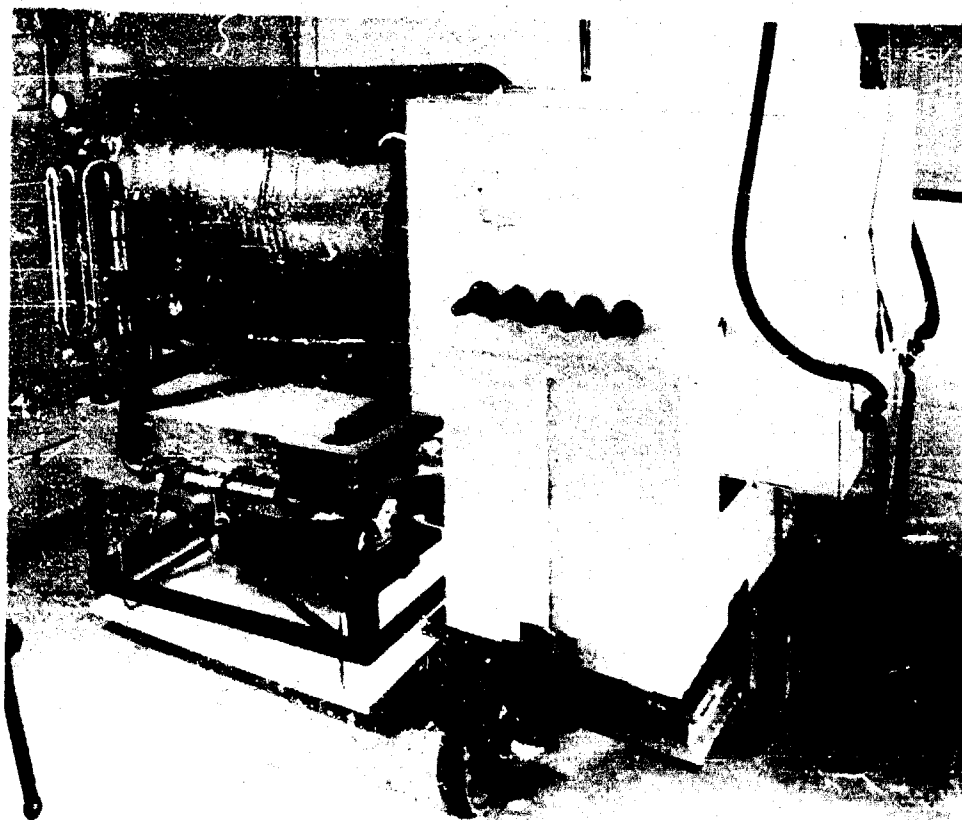
Several types of explosion tubes have been used depending on the geometry of the channel being used. The tube shown in Figure 2.3 has contained approximately 50 explosive shots. The noticeable bulge of the tube was caused by the high peak pressure load on each detonation which causes an increase in diameter of about 0.006 inches for each shot. Only a small fraction of the energy, of the order of 2%, goes into the high-speed jet which is produced by the shaped charge. The explosive driver, the black object in Figure 2.3 just below the explosion tube, is a 7.5 gram commercial shaped charge (duPont 20B jet).

Subsequent redesign of the explosion tube reduced this gradual deformation.



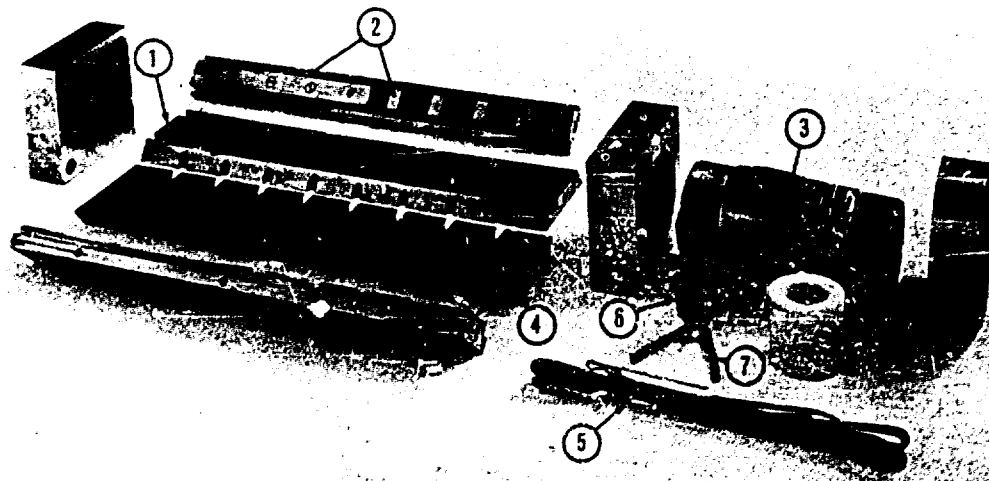
Schematic view of explosive-driven MHD generator.

Figure 2.1



View of complete facility

Figure 2.2



1. Bakelite sidewalls
2. Electrodes
3. Explosive tube
4. Iron sidewall
5. Blasting cap and leads
6. Shaped charge
7. Primacord
8. Standoff spacer

Figure 2.3

Disassembled view of 1" x 1" explosive driven MHD channel

perforator). The explosive in the jet perforator is generally a waxed RDX (cyclo-trimethylene-trinitramine) composition. The copper liner of the perforator is removed prior to firing the charge. Firing is initiated by an electric blasting cap which sets off the explosive primacord, shown attached to the bottom of the shaped charge. The primacord serves as an explosive train to carry the detonation to the booster at the base of the RDX charge. The explosive is seeded with a low ionization potential compound (cesium picrate) in a fashion which is described in a subsequent section. The charge is held in the center of the explosion tube by a polystyrene spacer which provides standoff of the condensed explosive from the metal walls.

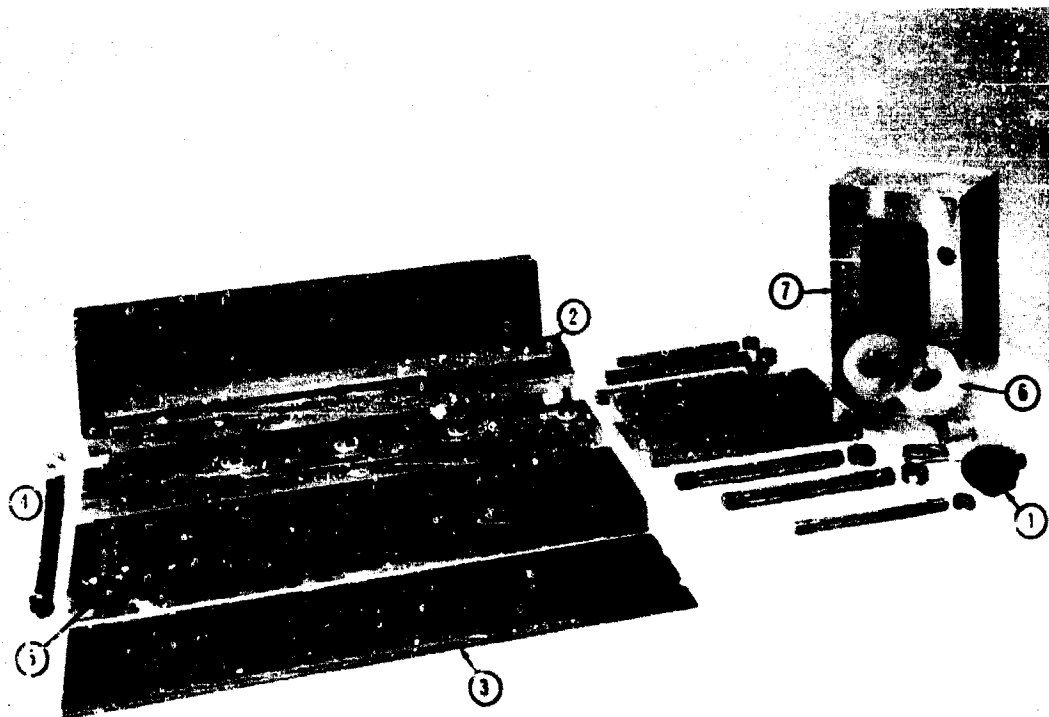
The driven section, or MHD generator proper, shown in Figure 2.3 is a steel channel. The walls of this test section are 0.75 inch thick. The top and bottom spacer bars which hold the electrodes are of stainless steel; the channel sidewalls are made of soft magnetic steel. The purpose of soft steel is to reduce the width of the gap in the magnet. With a lower reluctance, a given power source can produce a higher magnetic field in the test section. The inside walls of the channel are insulated with fiber reinforced phenolic strips (micarta). The test section is fitted with copper electrodes which are flush with the inside walls. In some experiments the electrodes are spaced on two inch centers down the channel as shown in Figure 2.3. In other experiments continuous electrodes the length of the generator were used. The electrodes are unheated copper, 1.0 inch wide, but of varying lengths in the flow direction. Electrodes have been studied with the following lengths in the flow direction: 0.25 inch, 0.50 inch, 2.00 inches, and 16 inches. The short electrodes shown in Figure 2.3 are 0.5 inch long. The space between the

electrodes is filled with phenolic strips to maintain a smooth contour. In addition to experiments in the 1 inch by 1 inch channel, an MHD channel of 1 inch by 4 inch (in the direction of $u \times B$) was constructed. It was the purpose of the experiments in this channel to study the effect of aspect ratio and scaling parameters. In the large generator, 18 inch long electrodes were used. The channel was normally driven by two duPont 20B charges placed approximately 2 inches apart, one above the other. A photograph of this test section is shown as Figure 2.4.

Readout of data has been accomplished with Tektronix 551 dual-beam oscilloscopes equipped with Polaroid cameras. A small triggering electrode situated at the explosion end of the test section senses the $u \times B$ voltage developed by the jet to trigger the oscilloscope sweeps. Resistive loads are fastened across the electrode pairs on the outside of the channel as is indicated schematically in Figure 2.1. The resistive loads pass through the slots milled into the outside of the side plates (shown in Figure 2.3) so as to provide a minimum inductance path.

The cylindrical dump tank and muffler at the left side of Figure 2.2 is evacuated by a vacuum pump. The exit from the test section into the tank is sealed with a mylar diaphragm which is ruptured by the explosive jet. The dump tank is employed strictly in order to muffle the noise produced by the explosive charge. As will be explained later, the channel can be evacuated by a separate vacuum system, and then filled to a low pressure with a gas to be studied such as air, argon, helium, etc.

The magnet shown was formerly used in combustion powered MHD generation experiments. Magnetic fields of 22 kilogauss can be produced in the one-inch channel with the present power supply, which is a 70 KW motor generator set.



1. Shaped charge
2. 18" x 1" electrode
3. Bakelite sidewall liner
4. Generator load
5. Slot for interior surface of sidewall for resistive load
6. Standoff spacer
7. Explosion chamber

Figure 2.1

Disassembled view of 1.54" explosive driven MHD channel

To determine the variation of selected parameters with the initial density of the gas in the channel, experiments were conducted in an auxiliary test facility which could be instrumented with some degree of flexibility because the large electromagnet, which is shown in Figure 2.2, was eliminated. The interior details of the explosive chamber and the channel were similar to the experimental apparatus shown in Figure 2.3. The flow channel was 1 inch by 1 inch by 18 inches long with provision for 8 electrodes on 2-inch centers. Since the channel was to be evacuated by a mechanical vacuum pump, provision was made for "O" ring seals on all surfaces to provide vacuum tight joints. Both ends of the channel were sealed with a mylar diaphragm, so that the channel pressure could be controlled independently of the pressure in the explosive driver tube or the pressure in the dump tank. The pressure was measured with either a Wallace and Tiernan gauge or a manometer.

This instrumented facility was used to measure the following three quantities as a function of the initial pressure in the channel:

1. the time of arrival of the conducting gases at various stations along the channel, i. e., velocity,
2. the peak pressure in the channel, and
3. the conductivity of the seeded detonation products.

The results of these experiments are reported in Section 2.5.

In the power generation experiments, the primary emphasis was placed upon the measurement of the voltage and current in the external load. Because of inductive effects, the voltage drop V across the external load is the sum of the ohmic drop and an inductive drop, i. e.,

$$V = IR + L \frac{dI}{dt} ,$$

where I is the current, R is the load resistance, L the load inductance, and di/dt is the time rate of change of the current. Therefore, during the early part of the pulse when the current is rising, the voltage drop is greater than IR , and correspondingly when the current is falling the voltage drop will be less. Therefore, it is not possible to determine the current from the measured voltage drop across the load resistor unless di/dt and L are also known. Since time rates of change of current as high as 10^9 amperes/sec were observed, a load inductance of 5×10^{-8} henries resulted in a 50 volt inductive signal. This signal in many cases was larger than the voltage drop which in a typical case might be due to a current of 10^4 amperes through an 0.5 milli-ohm load resistor, or 5 volts.

The voltage across the load was measured by means of coaxial cables which were connected to the differential inputs of a Tektronix type CA pre-amplifier. The recorded signal was the algebraic sum of the signals from the two ends of the load resistor. The cables were terminated in their characteristic impedance to avoid reflections. The outer shields were not grounded at the input end. The measurement was done in this fashion so that the load could be floated with respect to ground potential. The trigger electrode was placed upstream at the inlet end of the channel and was used to trigger the oscilloscope sweep. The recording oscilloscope was grounded to the test section at only one point, through the coaxial cable to the trigger electrode, so that ground loops were avoided.

The current through the load was measured by an inductive pick-up technique. The basic principle is to sense the magnetic field caused by the current through the load circuit. In practice the time rate of change of the

magnetic field, dB/dt is sensed as a voltage by a pick-up coil placed near the conductor and then integrated with respect to time. For a pick-up coil of N turns, each with a mean area of, A , cm^2 , at an average distance of r cm from the conductor, the induced voltage signal is:

$$E_i = 10^{-8} NA dB/dt = 2NA dI/dt \times \frac{10^{-9}}{r} . \quad (2.2.7)$$

The voltage signal E_i is then integrated electronically in an RC network to produce a signal proportional to the current. This system can be calibrated by determining the response to a known current, or by determining the electrical characteristics of the system including: (1) the mutual inductance between the pick-up coil and the circuit in which the current to be measured is flowing, (2) the number of turns on the coil, and (3) the resistance and capacitance of the integrating network.

If a toroidal pick-up coil is used, the response is independent of the location of the current carrying conductor, provided that the toroid is uniformly wound and encircles the current carrying conductor. When using a toroidal coil the coefficient of coupling between the conductor in which the current is being measured and the pick-up coil can be expressed as the ratio L/N where L is the inductance of the toroidal coil and N is the number of turns on the pick-up coil. The details of a typical coil and integrator are shown in Figure 4.5. For the coil used in the present experiments, the inductance L was approximately $22\mu h$, and the coil had 220 turns. To eliminate signals due to externally generated time varying magnetic fields, (when viewed from the above toroid appears as a one-turn coil) the toroid is wound so that the return lead provides a back turn. This turn, to a first approximation, cancels out any

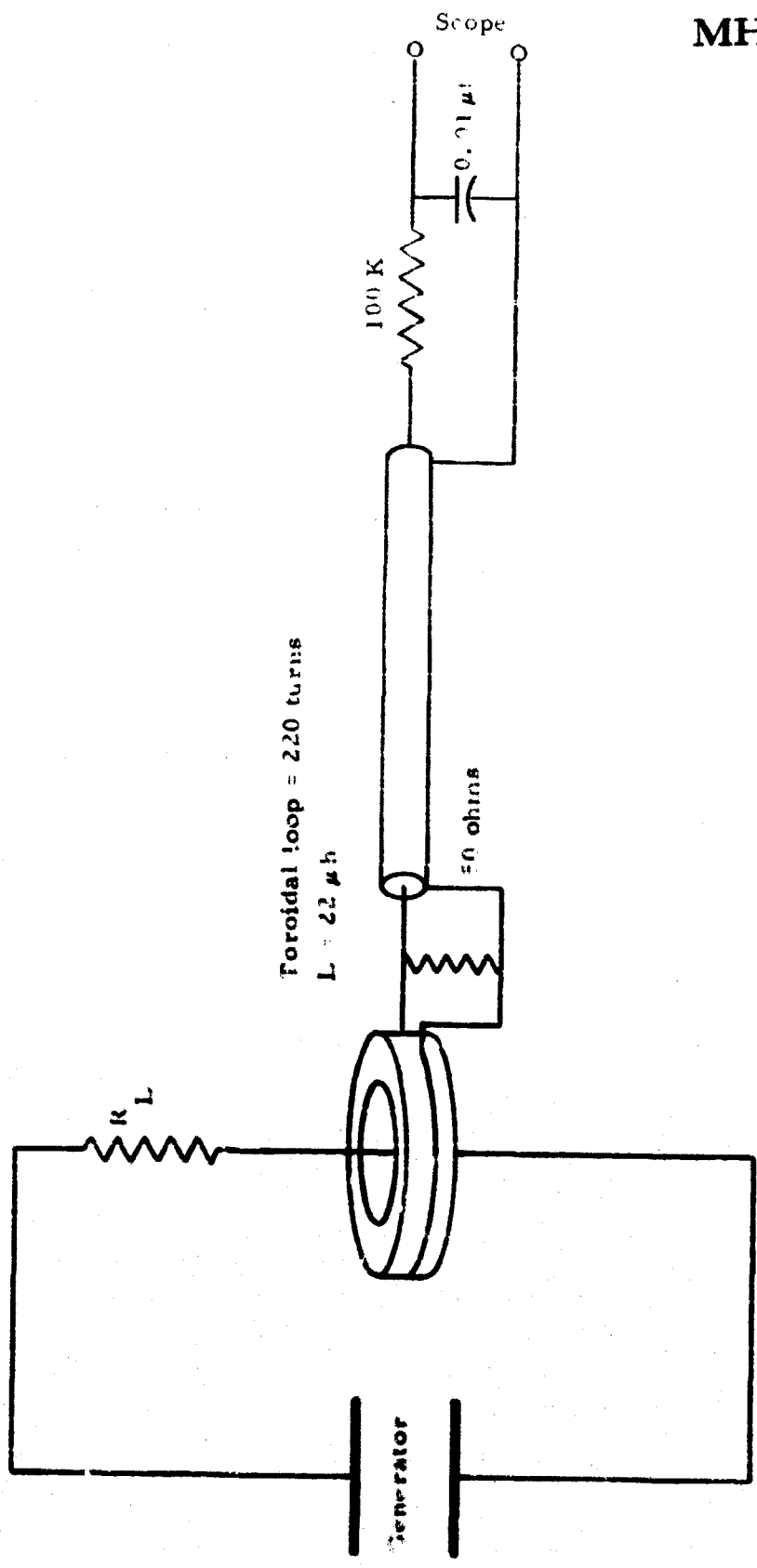


Figure 2.5
Schematic diagram of the current pickup loop and integrator circuit.
This circuit allows for an independent measurement of the current.

voltage signal induced in the toroid by magnetic fields whose source is external to the toroid. This requirement is especially important in devices where the magnetic Reynolds number approaches unity and there is considerable displacement of the magnetic flux lines by the moving conducting fluid.

For a typical case, where the integrating network has the following values, $R = 10^5$ ohms, and $C = 0.01 \mu f$, so that $RC = 10^{-3}$ sec, the voltage output of the integrator is given as

$$V(t) = \frac{L}{N} \times \frac{1}{RC} I(t) = 10^{-4} I(t) \frac{\text{volt}}{\text{ampere}} \quad (2.2.8)$$

In the actual measurements the calibration factor was 1.07×10^4 amperes/volt. When using the simple RC integrating network, one of the major requirements is that the RC time constant be long compared to the duration of the event to be measured. However, the larger the RC product, the smaller the output signal, as indicated by Equation (2.2.8), so that the measurement of small currents, say 100 amperes, for times of the order of a fraction of a second may present accuracy problems because of the decay of the signal on the capacitor. One solution to this problem is to use the Miller effect to increase the effective time constant of the integrator by a factor equal to the gain of the feedback amplifier. However, in the present experiments, it was not necessary to use a Miller integrator system.

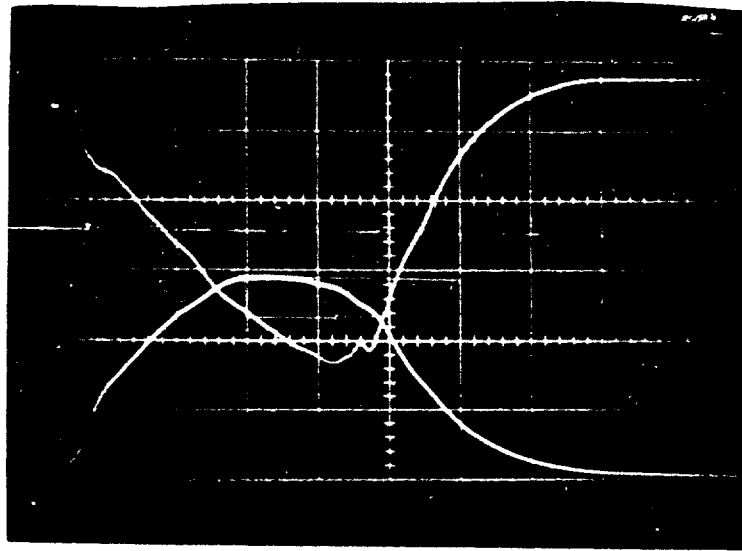
The current measuring system in these experiments was calibrated by two methods. As a first step, the obvious measurements were made of the elements appearing in Equation (2.2.8), i. e., measurements of the inductance and number of turns on the coil, and the capacitance and resistance of the integrator.

The first calibration was made by passing 60 cycle current through a wire which threaded the toroid. The 60 cycle current was measured with an ammeter. Since the 60-cycle period was long compared to the RC time constant available, the only measurement possible was to determine the response to dI/dt and assume that the integrator would work properly. Since a sinusoidal test signal was used, the measured response divided by the angular frequency of $2\pi f$, was equivalent to integration with $RC = 1$. In the second calibration method a capacitor bank was used to pass a current through an inductive load. The current could be calculated from the measured frequency of the ringing circuit, the capacitance of the bank, and the initial value of the charging voltage. The results of both methods agreed to within 10%, which is the approximate precision to which the voltage on the capacitor bank could be set and read. This independent measurement of the current through the load gave complete confidence in the electrical measurements, since it agreed with the current value calculated from the voltage measured and the known value of the load resistance within acceptable accuracy. As noted later for high energy outputs the load resistor heated up, thus changing resistance. Then an independent measure of current became imperative.

2.4 Power Generation Experiments

The primary objective of this program is the generation of electrical power. Therefore considerable attention has been given to the attainment of high energy conversion efficiencies and high power outputs. The details of a typical power production experiment are described below.

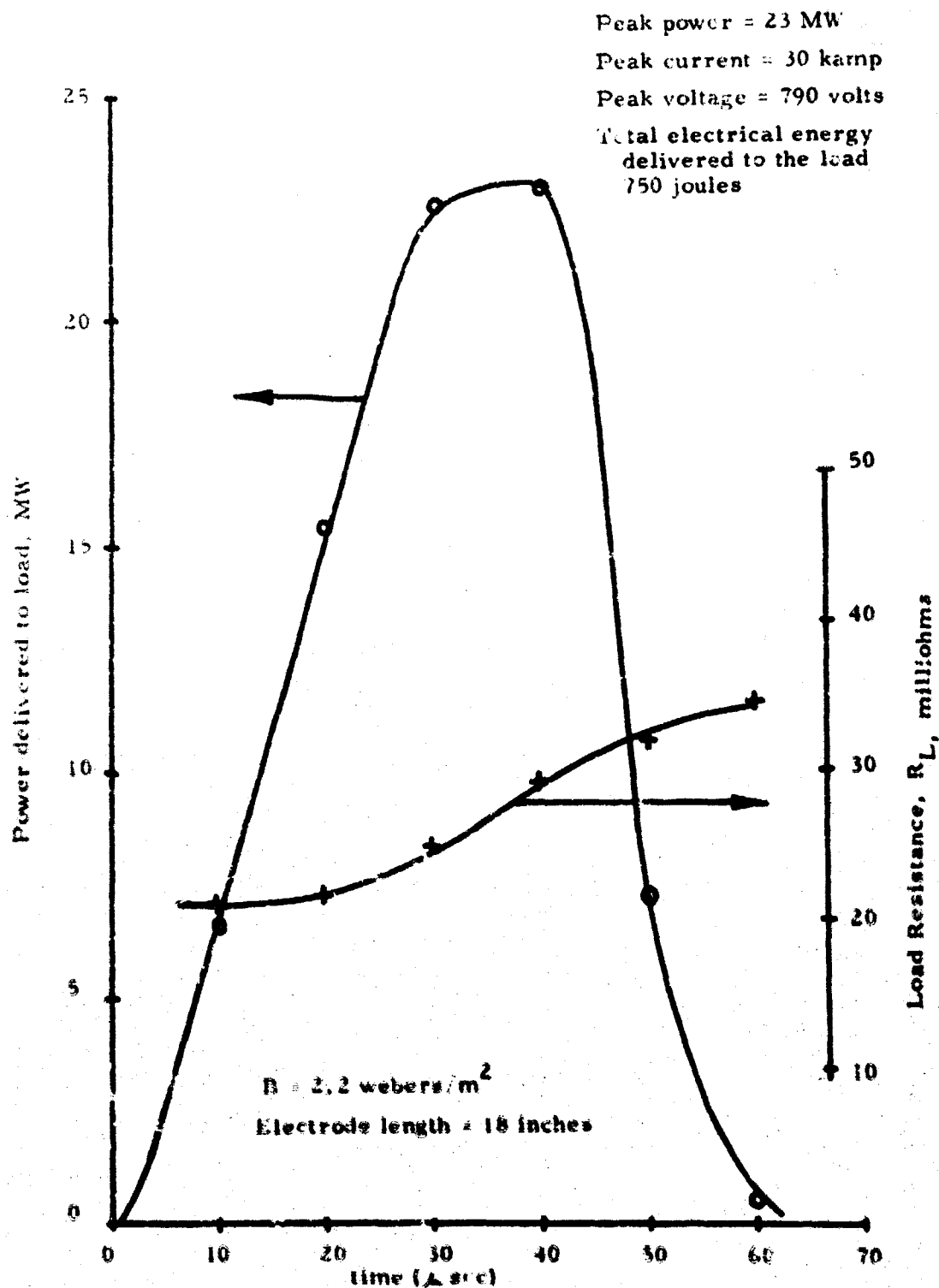
Figure 2.6 is a typical oscilloscope trace of the current and output voltage of the 1 inch by 4 inch explosive driven MHD generator with 18 inch



Oscilloscope trace showing voltage and current output of 1" x 4" explosive driven MHD generator. Sweep speed 10 microseconds/cm. Upper trace is output voltage at 200 volts/cm, lower trace is current at 10,700 amperes/cm. For this experiment the magnetic field was 2.2 w/m^2 and the channel was filled with 10 mm Hg of helium. The initial value of the load resistance was 0.0201 ohms.

Figure 2.6

long continuous electrodes which were described in Section 2.3 and shown as Figure 2.4. For this experiment the magnetic field was 2.2 w/m^2 . The channel had previously been evacuated and was filled to an initial pressure of 10 mm Hg. The load resistor, shown in Figure 2.4 had an initial resistance of 20.1 milliohms. For this experiment the channel was powered with two duPont 20B shaped charges, as shown in Figure 2.4, which were each seeded with 200 mg of cesium picrate. The sweep speed of Figure 2.6 is 10 microseconds per centimeter. The upper trace, which shows the voltage, has a gain of 200 volts/cm, while the current, shown in the lower trace, is 10.7 kA/cm. The peak current, which occurs about 30 microseconds after the start of the trace is 30.0 kA. The peak voltage which occurs at a later time, i. e. , about 45 microseconds, is 750 volts. The power output of the generator which is the product of the current and the voltage, is shown as a function of time in Figure 2.7. The peak power in this pulse is about 23.0 MW which continues for approximately 15 microseconds after the time of peak current. The total pulse length is 60 microseconds. The value of the load resistance, as determined from the voltage divided by the current, is also shown as a function of time. It can be seen that the resistance increases as the load heats up. The energy delivered to the load which can be calculated by summing the area under the power versus time curve in Figure 2.7 is 750 joules. For this experiment where two 20B charges were used to drive the channel, the chemical energy in the 15 grams of RDX contained in the charges is approximately 75,000 joules. Therefore, the overall conversion efficiency of the system, chemical energy to electrical energy, is presently 1%. There is evidence to believe that additional energy could be removed by: (a) increasing the channel length, (b) increasing the magnetic field, and (c) increasing



The electrical power excursion delivered to the load as a function of time from initial pickup for the 1 x 4 inch channel. The gas in the channel was helium at an initial pressure of 10 mm Hg. Also shown is the change in the load resistance as a function of time due to the heating of the load.

the utilization of the explosive through appropriate changes in geometry.

In support of the above, we can note that the gases are still conductive when they leave the generator, so that additional energy could be converted by lengthening the generator. It should also be noted that in the present experiment, where the magnetic Reynolds number is approximately unity for the 10 cm channel depth, the best that can be done is to convert all of the energy in the magnetic field in the generator volume into electrical energy in the load, see Appendix A. On this basis the 1 inch by 4 inch generator is already almost 30% efficient since $B^2/2\mu \times \text{volume} = 2500$ joules.

Measurements described in Section 2.5.3 show that only about 20% of the mass of the charge is directed down the flow channel. Therefore, assuming that by appropriate changes in geometry it is possible to work on the entire mass of the explosive for a longer period of time, conversion efficiencies of between 10 and 30% appear achievable. Clearly, it is desirable to go to the highest field strengths possible and drive the maximum volume with minimum amount of explosive to obtain the maximum efficiency.

As an independent check of the energy delivered to the load, a calorimetric calculation was performed for the load resistor used with the 1 inch by 4 inch channel. The initial load resistance at 20 °C for the pulse shown in Figure 2.6 was 0.020 ohms. As energy is dissipated in the load during the pulse, the load is heated and the resistance increases as noted, to a value of 0.035 ohms. This increase in resistance is calculated from the independently measured voltage and current across the load. From the increase in resistance, the increase in temperature

can be calculated from the relation

$$R = R_0 \{1 + \alpha (T - T_0)\},$$

where R_0 is the initial resistance, and T_0 the initial temperature.

The temperature coefficient of resistivity, α , for the tempered steel used as the load was 0.0032 in $^{\circ}\text{C}$.

The increase in temperature for the test shown in the figure was

$$\Delta T = 234^{\circ}\text{C}.$$

The specific heat of the steel was approximately

$$c_p = 0.125 \text{ cal/gm.}$$

and the mass of the resistance was

$$m = 5.8 \text{ gms.}$$

Therefore, the energy required to heat the load 234°C was

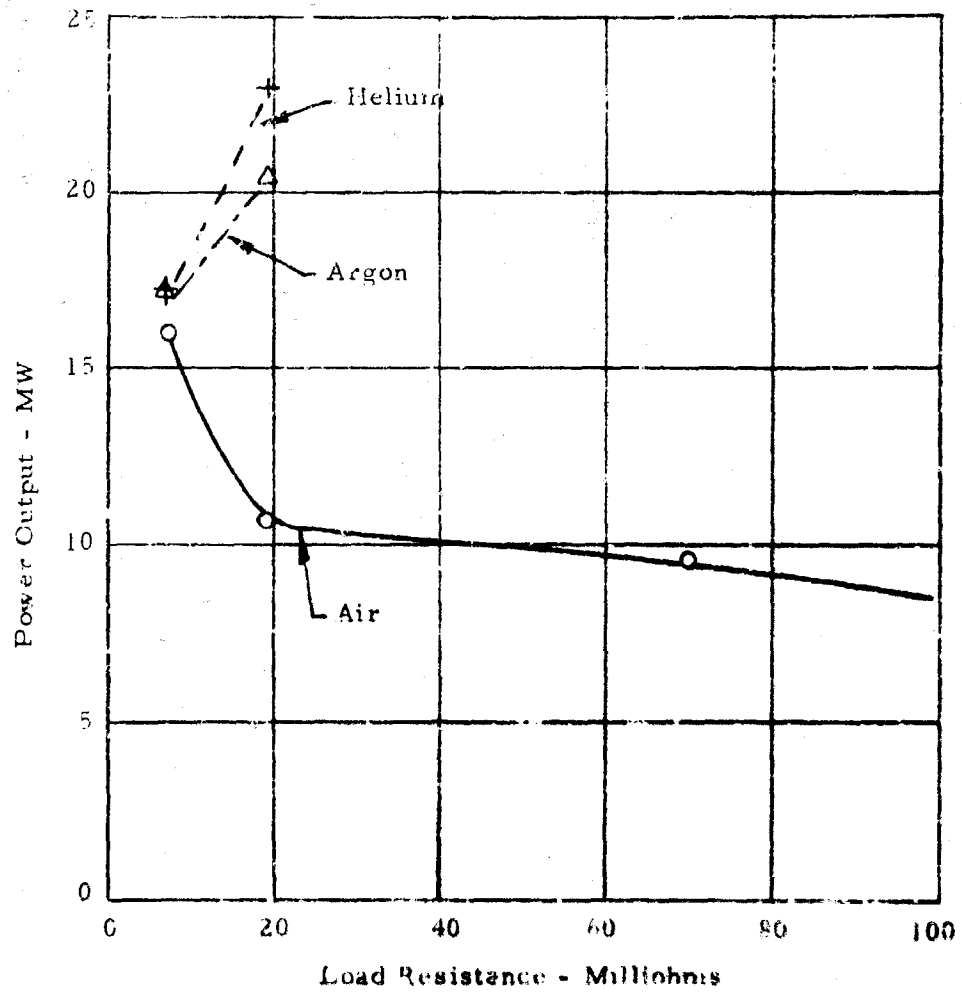
$$\begin{aligned} Q &= m c_p \Delta T = 170 \text{ calories} \\ &= 710 \text{ joules.} \end{aligned}$$

This value agrees to within 0.5% of the value calculated from the electrical measurements, which is excellent agreement considering that other points, such as connections, etc., must absorb energy. This calculation and the agreement gives complete confidence in the basic measurement technique for current and voltage.

To investigate the effect of load resistance upon power output, the data from the shot shown in Figure 2.6 is plotted together with other data taken in the 1 inch by 4 inch generator as Figure 2.8. This figure gives power outputs as a function of load for three separate gases initially in the channel: air, argon, and helium. It is seen that the highest power output was obtained using helium with a load resistance of 20 milliohms. The limited data which is available, and shown in Figure 2.8, does not indicate whether the optimum load resistance has been chosen.

To examine this question in detail, the power output for the 1 inch by 1 inch generator is plotted as a function of load resistance in Figure 2.9. The data on which this figure is based is similar to the data which was shown in Figure 2.6 except that the voltage levels are somewhat lower because of the smaller electrode separation. Figure 2.9 shows that the maximum power output in the 1 inch channel was achieved with a load resistance of 5 milliohms which would indicate that the optimum load for the larger channel should be about four times as high, or 20 milliohms (neglecting electrode effects). The power output in the smaller channel was approximately a factor of two larger when argon was used as the filling gas. The superiority of argon and helium over air as a filling gas is also shown in Figure 2.8. Both sets of data indicate that the explosive-driven generator must feed a very low impedance load in order to efficiently transfer energy.

Having seen that appreciable power outputs can be achieved and that performance does not fit the conventional, low Reynolds number, MHD generator theory, a number of experiments have been conducted to investigate the effect of various parameters in MHD generator operation. The following section discusses this experimental program in some detail.



Power output of 1 inch by 4 inch explosive-driven MHD generator. Initial pressure, 10 mm Hg. Magnetic field, 2.2 w/m^2 .

Figure 2.8

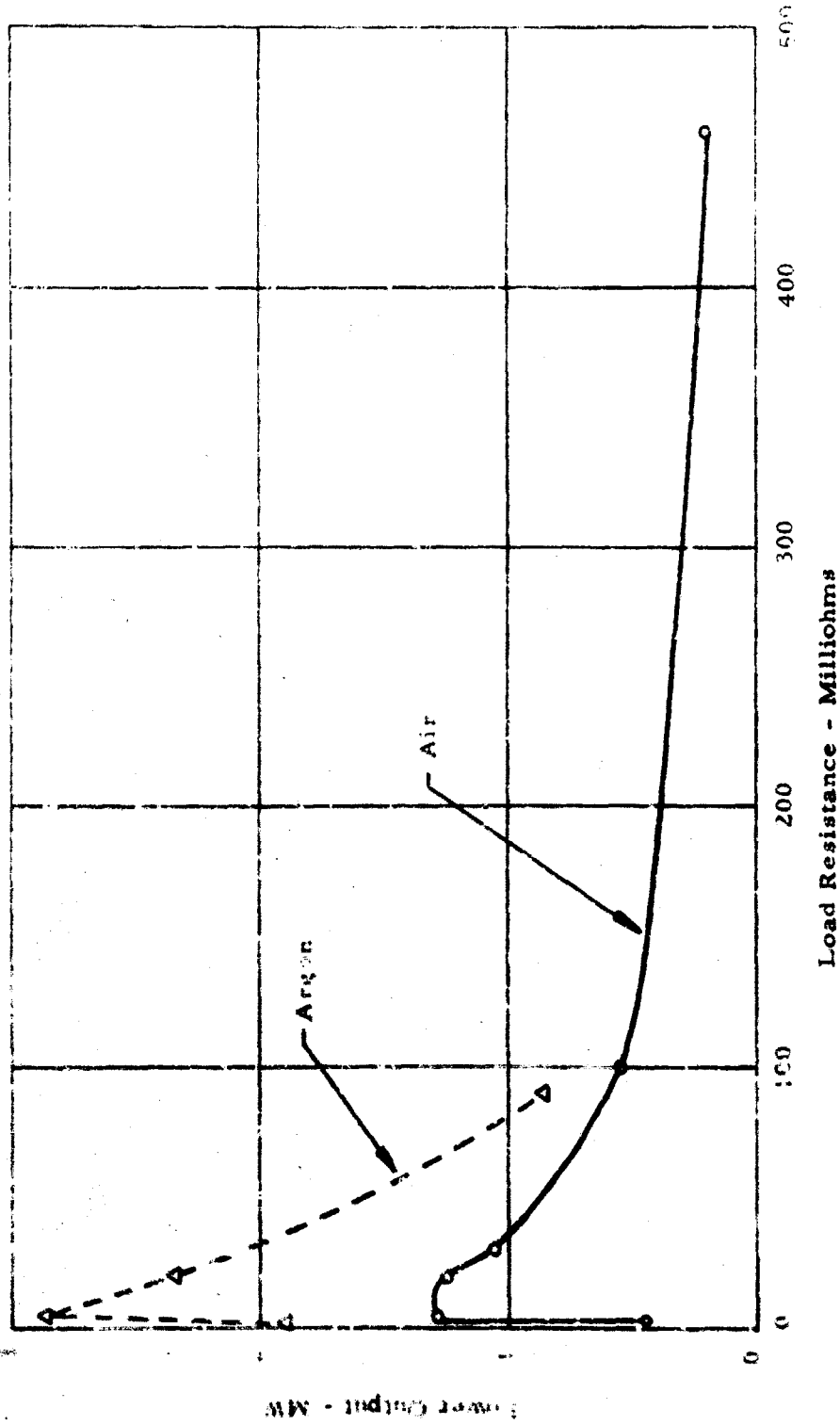


Figure 2.9

Power output as a function of load resistance for
 1" x 1" explosive driven MHD generator with
 initial pressure 10 mm Hg of either air or argon.
 Magnetic field 1.7 W/M².

2.5 Technical Studies

Inasmuch as the present studies simultaneously cover several areas of technology, i. e., explosives, MHD power generation, shock waves, ionization in explosives, etc., it was necessary to conduct a rather extensive program to investigate the effects of the many parameters upon the output characteristics of the explosive-driven MHD generator. Since the power output of the generator depends primarily upon the velocity of the working fluid, the strength of the magnetic field, the conductivity of the working fluid, and the characteristics of the electrical load, the major emphasis was placed upon measuring these quantities and determining the effect upon the electrical output of the generator as these quantities were changed. A number of subsidiary studies were conducted in support of these objectives. These included measurements of the pressure in the channel, geometrical variation studies, and studies of the optimum explosive composition and geometry. These studies are presented in the following sections. With the considerable amount of information which has been gathered during the course of the studies, a fairly clear understanding of the operation of a linear, pulsed MHD generator has been obtained.

2.5.1 Variation in Velocity with Initial Pressure

One of the important parameters in determining the output of the explosive-driven MHD generator is the velocity of the conductive zone, since the output power varies directly with velocity, in the high magnetic Reynolds number case, and as the square of the velocity for low magnetic Reynolds numbers. In the initial experiments where the channel was at atmospheric pressure, it was

determined that the velocity of the detonation products was approximately 6 km/sec. However, it was found that, if the pressure or density of the air initially in the flow channel was reduced, a higher velocity was observed. Therefore a systematic investigation of the variation in velocity with initial pressure was conducted.

In these experiments, the velocity of propagation of the conducting detonation products was measured by determining the time of arrival of the front of the conducting region at various stations along the channel. The timing pulses were generated by discharging capacitors across several of the electrode pairs in an auxiliary channel which was instrumented for these measurements. Arrival of the detonation products or a shock wave at the electrode pairs allowed the capacitor to discharge through the conducting gases and produced a voltage pulse across a 100 ohm resistor placed in series with the capacitor. Figure 2.10 is an X-t diagram showing the time of arrival of the front at various stations for several values of initial channel pressure. Figure 2.11 gives additional data for lower initial pressures.

The consistency of the velocity data obtained on different shots is excellent, with a variation of only a few percent in an extended series. The velocity, as determined from the slope of the X-5 curve near the origin, varies from an initial value of about 5 km/sec for an initial pressure of 0.1 mm Hg of air. Some attenuation can be noted with distance down the channel, particularly at the higher pressures. Figure 2.12 is a plot of this data showing the initial velocity as a function of initial pressure in the channel. The data suggest that, in the region

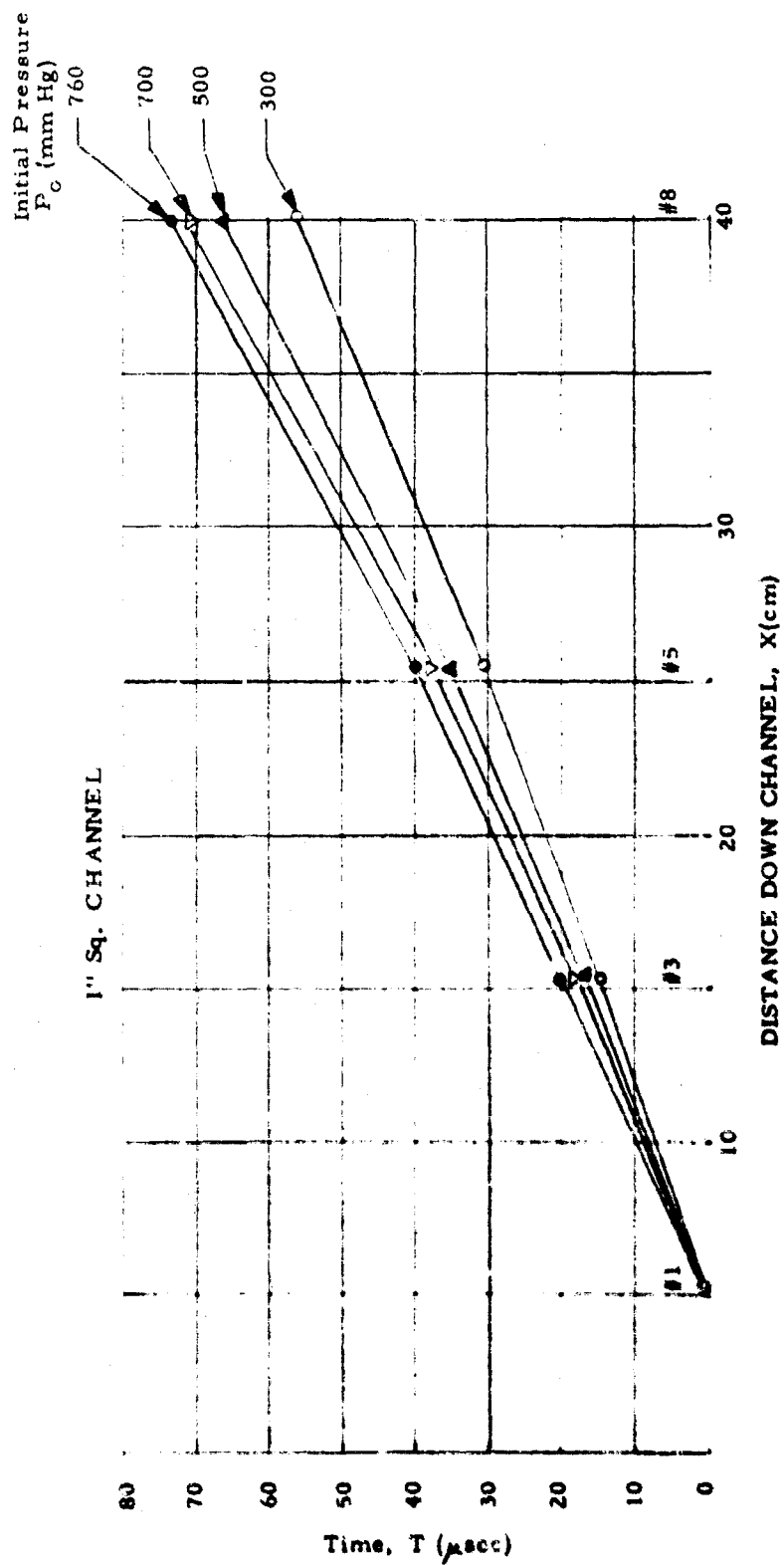


FIGURE 2.10

Front Arrival At Several Electrode Stations For Various Initial Pressures

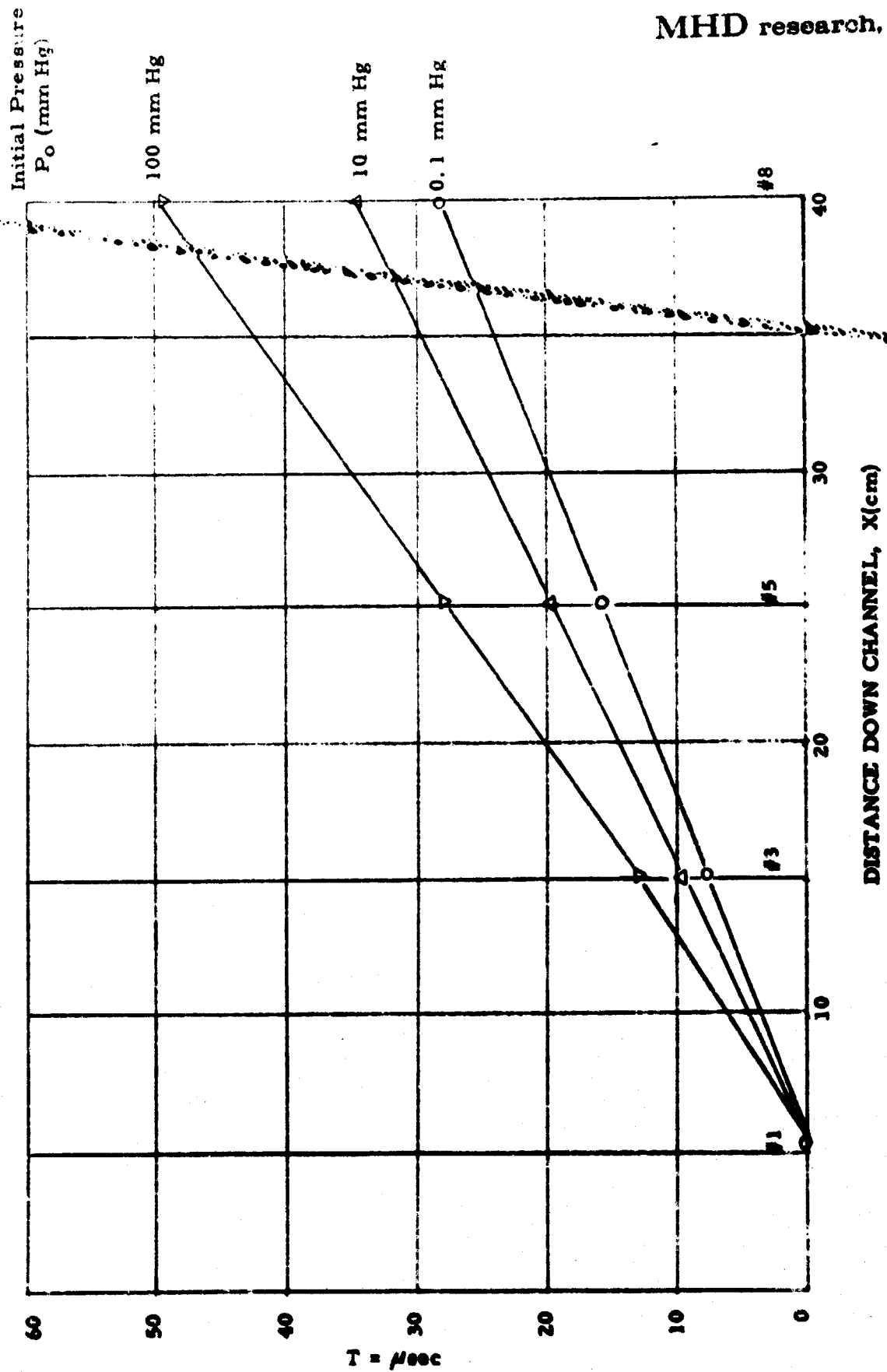
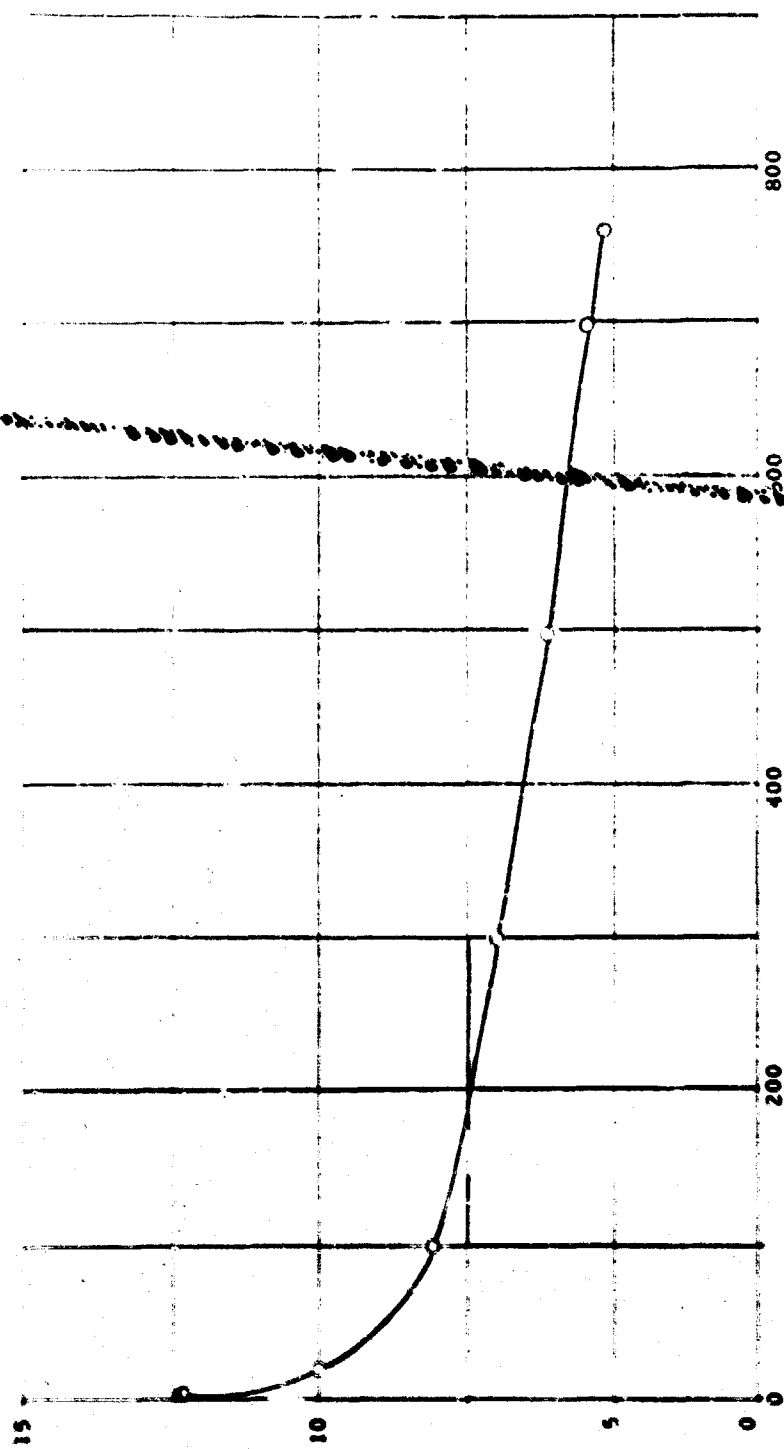


FIGURE 2.11
Front Arrival at Several Electrode Stations for Low Initial Pressure



Initial Pressure - mm Hg of Air

FIGURE 2. 12

Initial Velocity of Front of Conductive Detonation Products

between 100 mm Hg and atmospheric pressure, the velocity of the front increases slowly as the pressure is reduced. For initial pressures below 100 mm Hg, the velocity increases much more rapidly. For 10 mm Hg, the pressure used in the majority of the experiments, the velocity is 10 km/sec, with little attenuation along the channel. While higher velocities could have been achieved by evacuating the channel to lower initial pressures, it was difficult to reliably attain lower pressures after a number of shots in the apparatus because of deformation of the sealing surfaces.

It should be noted for the record that, for most of the shots in the 1 inch by 1 inch channel, mylar diaphragms were placed at both ends of the channel, and only the channel proper was at the low pressure. The explosive was at atmospheric pressure. During the runs in the 1 inch by 4 inch channel, the initial experiments were carried out with the charge at atmospheric pressure. However, in the later experiments it was possible to eliminate the upstream diaphragm. This meant that the entire volume of the generator which included the charge, the explosion tube and the channel could be evacuated and then filled with a test gas such as argon or helium. Because of the out-gassing of the polyurethane which was initially used in the stand-off spacer for this explosive, it was difficult to pump out the test section to a low pressure. However, when a cardboard spacer was used in place of the polyurethane, this difficulty was eliminated.

One of the major problem areas has been the explanation of the variation in velocity with initial pressure which is shown by the data of Figures 2.10 and 2.11.

Four theoretical models were explored in some detail to determine a possible reason for the change in velocity with initial channel pressure.

These models were:

1. blast wave model,
2. the fast jet model,
3. the solid propellant driven shock tube model, and
4. shock wave model.

The details of these studies are contained in Reference 2. It was found that none of these models could adequately explain the observed variation.

The blast wave model⁽⁴⁾ predicted that the position of the front should vary with time as

$$t = \frac{2}{3} \left(\frac{E}{\rho_0 B} \right)^{1/2} R^{3/2} \quad (2.5.1)$$

where E is the energy release, ρ_0 the initial gas density and B a constant which depends upon the specific ratio of the shocked gas and the geometry of the shock wave. The atmospheric pressure data fitted this relation quite well. However, at lower pressures, i. e., as ρ_0 approached zero, the above relation does not fit the data.

The fast jet model⁽⁵⁾ was patterned after the fast jets observed from the collapse of cylindrical liners of light metals by condensed explosives. This model was discarded when it was discovered that the same high velocities were obtained at low pressure when using flat faced charges instead of the cone shaped charge.

In the solid propellant driven shock theory⁽⁶⁾, as presented, no variation with initial pressure was predicted. The data are obviously at variance with this theory, and it was accordingly rejected.

Considerable effort was expended in examining the applicability of the shock wave model. This theory predicted that if the conductivity were due to shock heating of the air and the cesium seed material, the conductivity would vary markedly as the initial pressure was changed inasmuch as the shock speeded up, attaining a higher Mach number. The shock wave theory predicted that for a constant driver gas pressure in the explosive, the Mach number should vary approximately as the inverse square root of the initial pressure, as in the blast wave model. The shock wave model also predicted a variation in shock peak pressure with initial pressure, as will be described in a subsequent section wherein the pressure measurements are discussed. It was found that the shock wave model failed three experimental tests in that (a) the variation in conductivity with initial pressure, or velocity, was much smaller than predicted, (b) the velocity did not vary as the inverse square root of the initial pressure, and (c) by the use of propane, which has a specific heat ratio of $\gamma = 1.11$, instead of $\gamma = 1.4$ as for air, it was found that the velocities and conductivities were independent of the specific heat ratio of the gas initially in the channel in contradiction with the models which use conductivity to shock heating of the air initially in the channel.

Perhaps the best explanation of the observed variation of velocity with initial pressure can be derived from a discussion of the emergence of a detonation wave from the surface of a condensed explosive. It can be shown⁽⁷⁾ that for the expansion of the detonation products into empty space the velocity of the gases, u , is given by a relation of the form

$$u = D - c_x + \frac{2}{\gamma - 1} c_x = D + 5.67 c_x \quad (2.5.2)$$

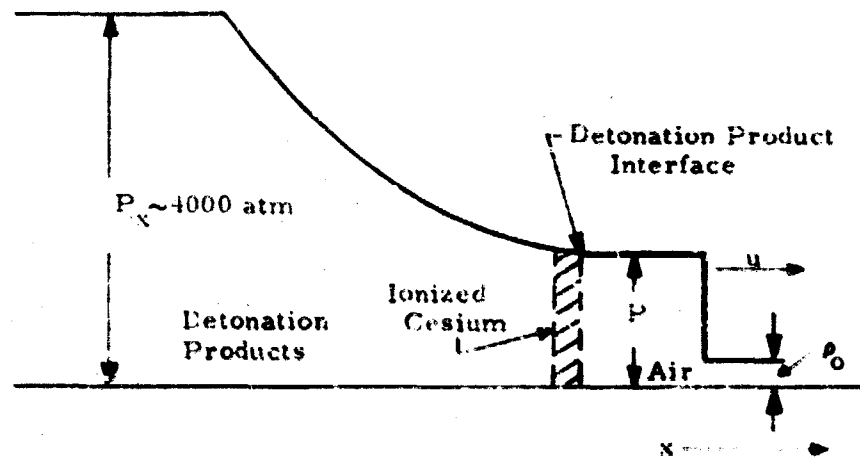
where D is the detonation velocity, and c_x is the velocity of sound in the explosion products after they have expanded to the point where the isentropic relation is applicable. In most cases c_x is approximately 1 km/sec, and $\gamma = 1.3$, so that for RDX at a density of 1.7 gm/cm^3 , where D is approximately 8 km/sec, the maximum velocity should be about 13.5 km/sec for one dimensional expansion into empty space, which is in reasonable agreement with the value of 12.7 km/sec which was observed.

For completeness we will consider the case where the explosive is expanding into air and a shock wave is formed ahead of the detonation products. We will let the pressure in the air shock be equal to P . The pressure in the detonation products will be reduced to this value as shown in Figure 2.13. We will assume that for the strong shock in air that $\gamma = 1$ so the velocity of the shock u is given as

$$u = \sqrt{\frac{P}{\rho_0}} \quad (2.5.3)$$

where ρ_0 is the initial air density. The velocity u should be equal to the velocity of the explosion product in the rarefaction wave, as given above, but modified by the fact that the velocity of sound in the detonation products is also reduced. Equating the velocity at the interface between the explosion products and the thin layer of shocked air we obtain

$$u = \sqrt{\frac{P}{\rho_0}} = D - c_x + \frac{2}{\gamma-1} c_x \left[1 - \frac{P}{P_x} \right]^{\frac{\gamma-1}{2}} \quad (2.5.4)$$



Variation of pressure in air shock driven by detonation product rarefaction wave.

Figure 2.13

For a typical explosive, P_x is approximately 4000 atmospheres. In air at atmospheric density, $\rho_0 = 1.3 \times 10^3 \text{ gm/cm}^3$. Substituting these values we can solve Equation (2.5.4) by numerical methods to find that the pressure in the air wave, P , is approximately 1/10 of P_x , or 400 atmospheres, and the particle velocity is approximately the detonation velocity.

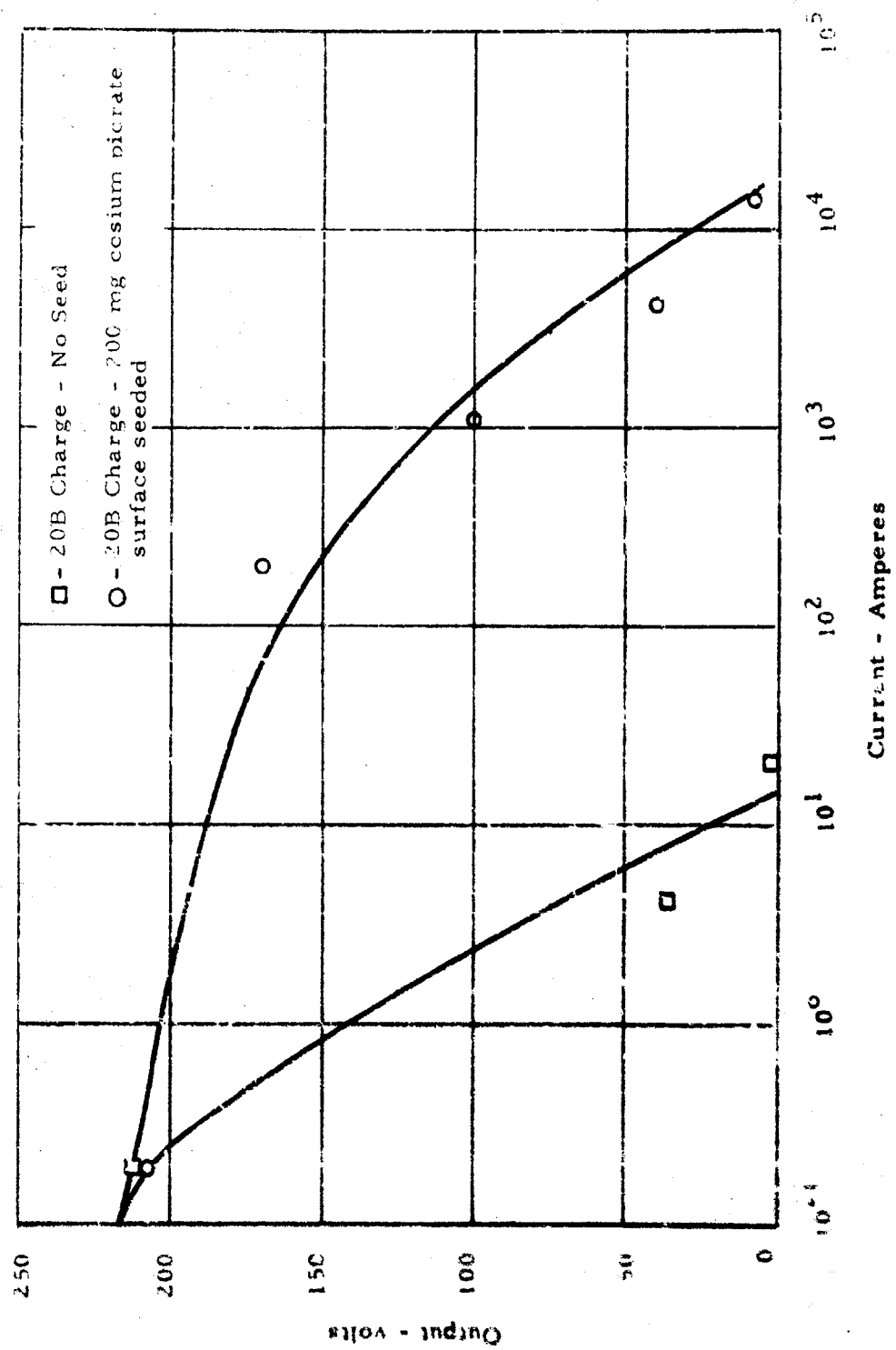
The above model is in excellent agreement with the observed data when it is considered that the measured velocity is determined by the transient time between two stations and is therefore an average velocity, whereas the initial velocity is much higher, near the detonation velocity as predicted. (For example see Figure 2.16.)

The important feature of this theory is that there is a maximum limiting velocity as the initial gas density is reduced in agreement with the experimental data. The highest velocities are obtained when using an explosive with a high detonation velocity, D , and when expanding into a vacuum. If other gases are present, i. e., air or argon as in some of the experiments reported herein, then the velocity will be reduced by a factor which is dependent upon both the isentropic properties of the explosive and the shock properties of the ambient gases. However, because of the ionization which might occur in the ambient gases due to the strong shock, there is the possibility that the maximum power production conditions will occur at some optimum pressure where the product uP is maximized, and not at the highest particle velocities u , which would occur if the charge were exploded in vacuo. The optimum pressure for energy conversion may be different from the optimum pressure for power output because as the pressure is increased and the velocity is reduced, the pulse is lengthened. If the power level remains constant, the longer pulse will yield more energy. Further work in this area is indicated.

2.7.2 Seeding Studies

In the early experiments it was quickly noted that seeding of the explosive with a low ionization potential material was required in order to produce appreciable amounts of power, i. e., obtain high electrical conductivity. In a typical set of experiments in the 1 inch by 1 inch channel where the magnetic field strength was 15 kilogauss and the channel was initially at atmospheric pressure, an unseeded 7.5 gm charge gave an open circuit voltage of 150 volts. The generator had an approximate internal impedance of 150 ohms as determined from the voltage-current plot. The maximum power delivered to the load was about 28 watts. When identical 7.5 gm charges were seeded on the surface with 0.2 gms of cesium carbonate, the open circuit voltage rose to 230 volts, the internal impedance dropped to 0.5 ohms, and the power to the load increased to 74 KW. These data indicate that the internal impedance decreased by a factor of 300, i. e., the conductivity increased by a similar factor. Experiments were then conducted with an active seed material, i. e., one that liberates energy. Cesium picrate was selected as the most satisfactory seed from many considerations. With 0.2 gms of cesium picrate seed on the surface of the 7.5 gms charges and identical channel conditions another factor of five was obtained in power output over the value obtained with cesium carbonate. Figure 2.14 shows the results of a set of experiments undertaken to show clearly the effect of using cesium picrate seed material. Figure 2.14 is a voltage-current plot of data taken under identical conditions using seeded and unseeded charges. The seed was 200 mg of cesium picrate placed in the inside surface of the cone of the charge. The data is of significance in that each point corresponding to a common load resistance was taken without

use of a load resistor. It is possible that the seed was not the same in all cases.



Comparison of seeded and non-seeded shaped charges in 1 inch by 1 inch explosive-driven MHD generator.

internal impedance between these two series of experiments was approximately a factor of 70. Note that the data of Figure 2.14 is plotted in semilog fashion because of the wide range of currents covered. These results clearly establish the desirability of seeding the explosive with low ionization potential materials.

Two types of seeding were studied: bulk and surface seeding. Unfortunately two different types of explosives were used so that this effect was incorporated into the experiment along with the change in seeding system. The bulk seeding experiment was carried out with PBX explosive which had been seeded with 24% by weight of cesium picrate and then pressed into the contour of the duPont 20B charge. The bulk seeded PBX was compared with the duPont 20B charge, which contains waxed RDX, surface seeded with 200 mg of cesium picrate. In addition, some of the bulk seeded charges had surface seeding added. The results of this experiment are shown in Figure 2.15. It is seen that the bulk seeded PBX was somewhat better than the surface seeded RDX, by 15 to 20%, for the conditions of this experiment. The combination bulk and surface seeding of the PBX charge gave an output which was slightly lower than the surface seeded RDX.

One reason for the above result is believed to be due to the fact that the yield of the PBX explosive is greater than the RDX, so that a higher detonation velocity would be expected for the PBX and hence a higher channel velocity. Time of flight measurements indicate that this is the case. It is suggested that further tests should be conducted to compare bulk seeded RDX to surface seeded RDX and similar tests with PBX and other explosives.

One effect which has been observed with the surface seeding studies is that the application of seed material slows down the detonation products. This

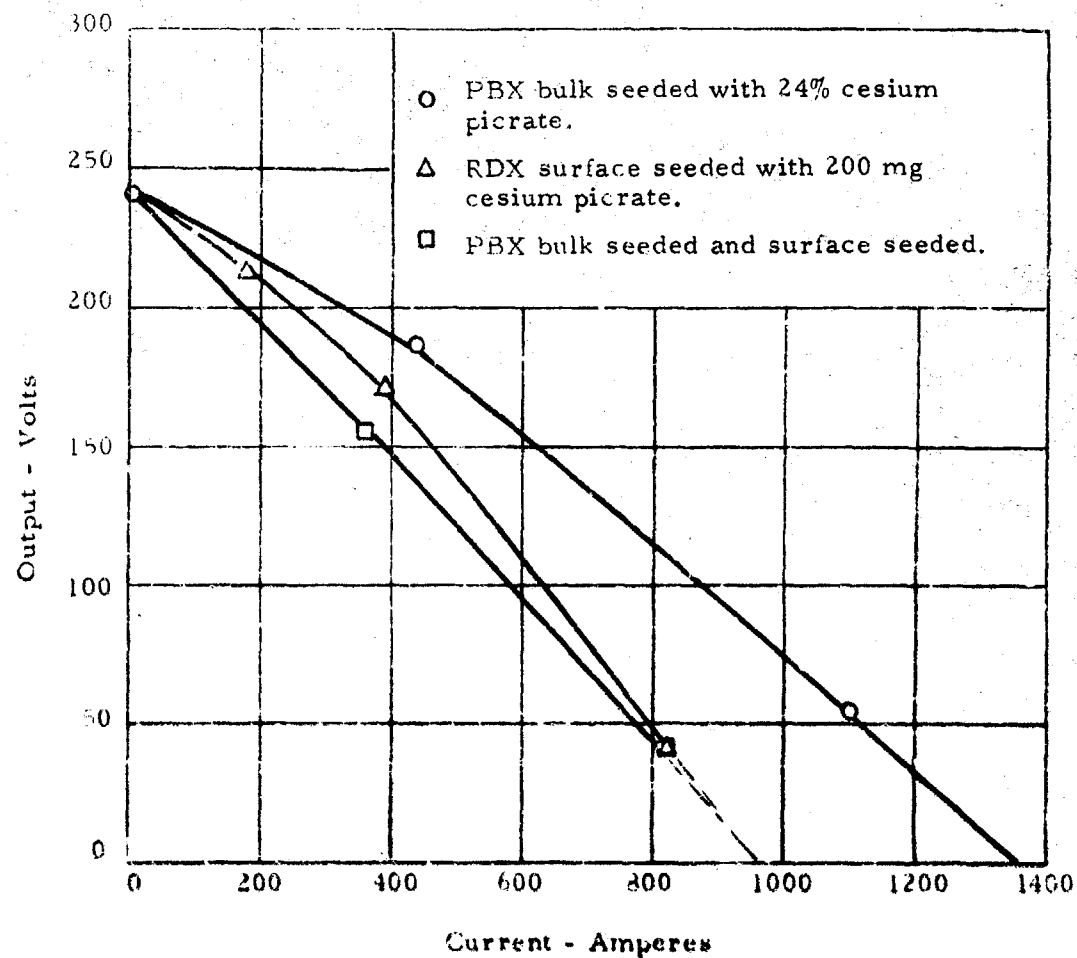


Figure 2.15

Comparison of generator characteristics for bulk and surface seeding with PBX and RDX charges.

effect is shown in Figure 2.16, which is a plot of the initial velocity as determined by the time of flight from the trigger electrode to the number 2 electrode, as a function of the weight of cesium picrate seed which is placed on the conical surface of the charge. It can be seen that the front of the conductive detonation products is slowed down approximately 20% by the addition of 1 gm of cesium picrate. Assuming a constant total energy release, it is possible to set up the relation

$$\frac{1}{2} m_0 u_1^2 = \frac{1}{2} (m_0 + \Delta m) u_2^2, \quad (2.5.5)$$

where m_0 is the mass of detonation products accelerated to a velocity u_1 in the absence of seed, Δm is the mass of seed added, and u_2 is the velocity with the seed. From the measured change in velocity as the seed is added, one can solve this relation and obtain the representative value for m_0 of 1.5 gms, or approximately 20% of the charge. The same result can be derived from the experiment in the 1 inch by 4 inch channel described in the following paragraph.

To determine the optimum seed level in the 1 inch by 4 inch channel, a series of experiments were conducted where the channel was evacuated and then filled with 10 mm Hg of argon. Different amounts of material were used for each shot. The results of these experiments are shown in Table 2.1 which lists the peak current through a 20 milliohm load resistor as a function of the mass of cesium picrate used in each of the two duPont 20B charges. Also given in Table 2.1 are the peak voltages, which may not occur simultaneously with the peak current, and the length of the pulse, as determined by the time to the sharp cut off in the voltage trace. It is seen that the peak current, and hence power output, occurs for the 200 mg seeding case. It may be noted that the pulse is lengthened as the amount

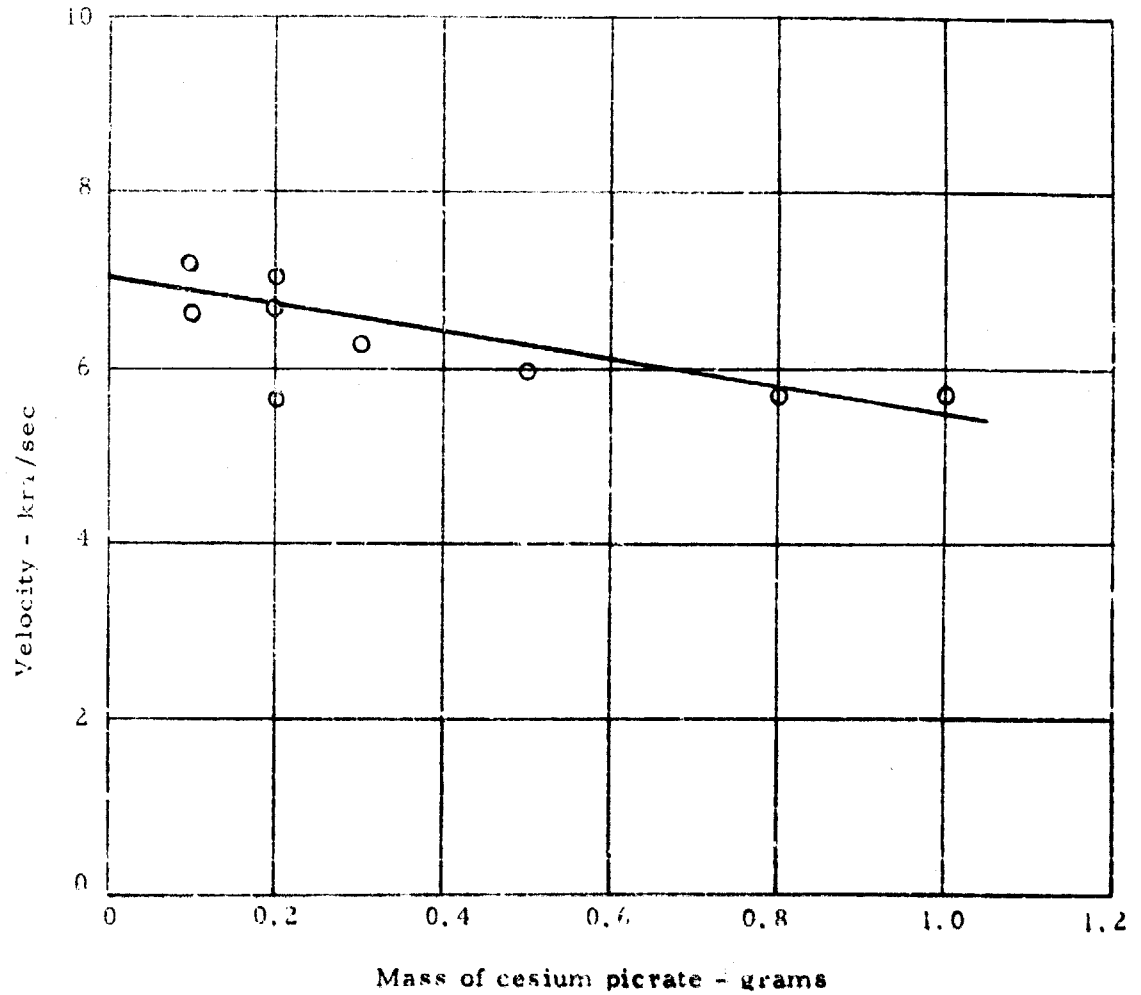


Figure 2.16

Reduction in velocity of detonation product front as cesium picrate seed is added to front surface of duPont 20B charge. Initial channel pressure is atmospheric.

TABLE 2.1
EFFECT OF SEED LEVEL ON POWER OUTPUTS
IN THE 1 INCH BY 4 INCH GENERATION

Seed, mg/charge	Peak Current, kiloamperes	Peak Voltage, volts	Pulse Length, μ sec
0	17.7	380	45
50	24.1	550	44
100	26.8	660	49
200	28.0	710	47
300	26.8	660	49
400	27.8	680	49

TABLE 2.2
EFFECT OF ARGON PRESSURE ON 1 INCH BY 4 INCH
CHANNEL OUTPUT

P _{argon} , mm Hg	P _{air} , mm Hg	Peak Current, kiloamperes	Peak Voltage, volts	Load, milliohms	Pulse Length μ sec
10		11.75	170	9.0	48
10		18.0 (est)	138 (est)	6.0	48 (est.)
10		22.5	125	4.5	48
30		18.2	129	6.0	54
100		11.23	75	6.0	48
10 no seed		8.7	65	6.0	46
	10 no argon	16.6	110	6.0	44

of seed is increased, as we have seen before, and that in these experiments, considerable power can be drawn if no cesium picrate is used, i. e., the argon is shock ionized and acts as the conductor. This is similar to earlier experiments where MHD power was drawn from shock waves, i. e., the work of Nagamatsu⁽⁸⁾ in air, and Pain and Smy⁽³⁾ in argon. In the present experiments, it should be noted that the maximum power is generated when both argon and cesium picrate are used.

To investigate the optimum level of initial argon pressure a series of experiments was conducted wherein the initial argon pressure in the 1 inch by 1 inch channel was varied. The data for these experiments are shown in Table 2.2. Unfortunately, the data were not obtained for the same load in each case, so that it is necessary to interpolate between the 4.5 milliohm and the 7 milliohm data to obtain a comparison with the other data taken with a 6.0 milliohm load. Also shown in Table 2.2 are data taken in the 1 inch by 1 inch channel for the conditions where 10 mm Hg of argon was used with no cesium picrate seed, and a comparable case where 10 mm Hg of air was used in the channel with the usual 200 mg of cesium picrate.

The major effect noted is that as the initial argon pressure is increased, the pulse is lengthened, indicating that the detonation products are slowed down by the added argon. The peak current is also lower at the highest argon pressures. This data would indicate that the highest conversion efficiency, i. e., largest energy output would occur at the 30 mm Hg argon case because of the lengthening of the pulse while maintaining a high power level.

Studies were also conducted using helium in place of argon or air in the 1 inch by 4 inch channel. The data for these experiments are

contained in Table 2.3. In each case it is seen that the highest currents, and hence output powers, were achieved using helium in the channel, as was seen in Figure 2.8. The increase in power is accompanied by a decrease in pulse length which would indicate that the helium slows the detonation products less than the air or argon. Data were given for a shot where helium was used alone without cesium picrate. Again it is seen that it is possible to obtain MHD power from shock heated gases, but that much more power or energy can be derived when using seeded detonation products in combination with a rare gas additive. It should be noted that for the experiments in the 1 inch by 4 inch channel, the entire chamber, including the explosion tube was evacuated and filled with the additive gases, which was different from the procedure used in the 1 inch by 1 inch channel where an upstream diaphragm was used.

In addition to seeding studies associated with the explosive charge, and the channel gases, tests were conducted to determine the effectiveness of downstream seeding with cesium picrate. In one series of tests, at 10 mm Hg of air, the mylar diaphragm was coated with 200 mg of cesium picrate. In the other tests, the 2 inch long electrodes were coated with 50 mg of cesium picrate. In both tests the results were identical to comparable non-seeded tests without downstream seeding. The results confirm the view that the electrical conductivity is associated with seeded detonation products and not as a result of the passage of a shock wave in the air.

In summary, we can see that the choice of the optimum seed system is rather complex and will depend upon many factors. In particular it appears

TABLE 2.3

OPERATING CHARACTERISTICS OF THE 1 INCH BY 4 INCH GENERATOR
FOR HELIUM, ARGON, AND AIR IN THE CHANNEL

Initial Gas and Pressure		Peak Current, kiloamperes	Peak Voltage, volts	Pulse Length, sec	Load, milliohms	Remarks
10 mm Hg	He	31	740	42	20.1	
	Ar	28	710	44	19.5	
	Air	21	510	43	19.5	
	He	17.1	310	38	20.1	No cesium picrate
	He	49.2	360	44	6.9	
	Ar	47.1	365	50	6.9	
10 mm Hg	Air	47	340	46	6.9	

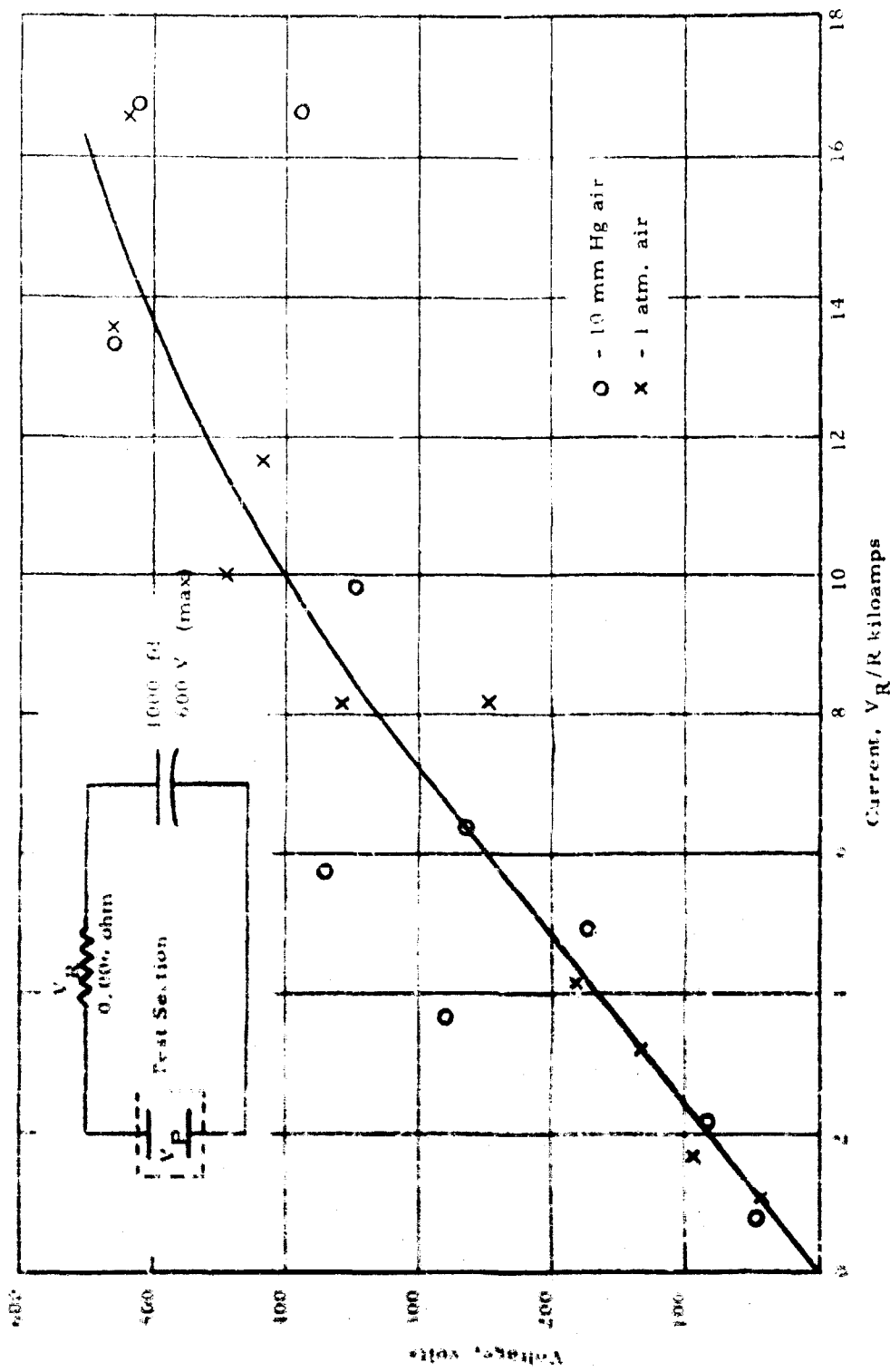
as though, once the conductivity is high enough so that the magnetic Reynolds number approaches unity, the output becomes somewhat independent of the conductivity, and other factors such as the effect of the seeding system on the detonation product velocity become important in controlling the output.

2.5.3 Conductivity Measurements

Because the electrical conductivity σ , is a sensitive function of the temperature of the electrons in the conducting gases, it appeared that information regarding the variation of conductivity with initial channel gas density would help explain the mechanisms responsible for the conductivity. Also, the conductivity data, per se, is important for the power generation experiments since, for low magnetic Reynolds numbers the power output will vary directly with the conductivity. The conductivity is also one of the most difficult parameters to measure.

The conductivity was determined by measuring the current between two electrodes on opposite sides of the channel held at a difference in potential by a 1000 μ f capacitor bank charged to an arbitrary voltage up to 600 volts. For this set of experiments the electrodes were brass, 3/8 inch in diameter. The current was determined by measuring the voltage drop across a calibrated shunt.

Figure 2.17 is a plot of the voltage-current relationship determined for the seeded detonation products for the two cases where initial test section pressure was atmospheric pressure and 10 mm Hg of air. While there is some scatter in the data, particularly at the high voltage and currents, the conductivity, as determined by this method, appears to be independent of the initial gas pressure or density. Since it has been seen that this reduction in initial pressure doubles the velocity of the front, and hence should change the Mach number of the shock,



Current, V/R kiloamps

The voltage-current relationships across the generator electrodes, $B = 0$. From this curve approximations to the conductivity can be obtained. Even though the scatter in experimental points is considerable, this figure indicates that the conductivity for initial pressures of 1 atm and 10 mm Hg is approximately the same.

FIGURE 2.17

it is expected that an increase in conductivity because of the higher temperature in the shocked gas, would be observed. However such is not the case.

The measured resistance of the seeded detonation product column is 0.038 ohms which would correspond to a conductivity somewhat greater than 10^3 mho/meter. Because of the inductance effects, which make the voltage measurement uncertain (the pick-up coil technique had not yet been worked out) and because of the uncertainty in the linear dimension of the conductive slug in these measurements, the exact value of the conductivity is uncertain by perhaps a factor of two or more.

In the power generation experiments it was possible to make a more accurate determination of the plasma current and the size of the conductive slug for purposes of determining the conductivity. These experiments were conducted in the 1 inch by 1 inch channel with an initial pressure of either 10 or 760 mm Hg of air in the channel. The magnetic field was 1.7 w/m^2 , and the standard 20B charge with 200 mg of cesium picrate was used. In the majority of the experimental shots the electrode length was 2.0 inches.

Figure 2.18 is a typical oscilloscope trace for this experiment showing the current and voltage when using a 9.45 milliohm load resistor. The sweep speed is 2 microseconds per centimeter, the voltage gain is 50 volts per cm (upper trace), while the gain for the current (lower trace) is 1070 amperes/cm. The peak current, shown in the lower trace, is 3500 amperes, which would indicate a power generation level of approximately 115 KW at the time of peak current. The power pulse lasts for about 6 microseconds, then falls off rapidly, with a dI/dt of about 10^9 amperes/sec. During the time the current is falling the voltage trace goes negative showing the inductive effect to be much larger than the ohmic voltage drop. From the measured dI/dt and

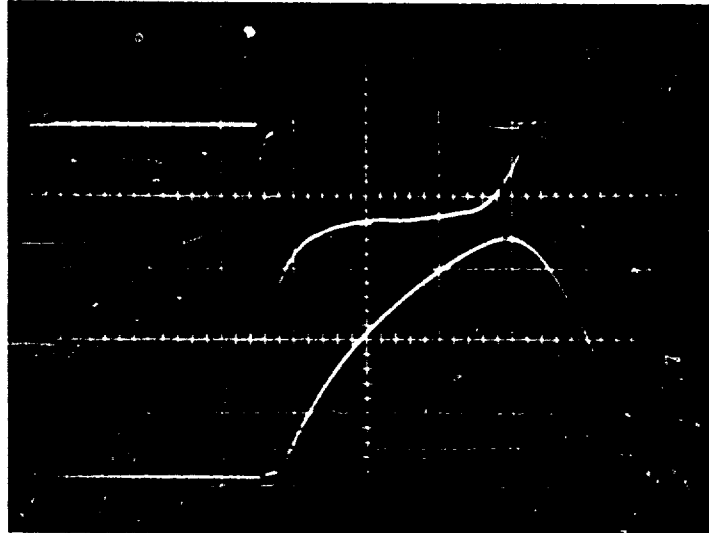


Figure 2.18

Typical oscilloscope trace from explosive driven MHD generator. Upper trace is the voltage across 0.00945 ohm resistor, at 50 volts/cm gain. Lower trace is current through load, gain is 1070 amperes/cm. Initial pressure is 10 mm Hg, magnetic field 17 KG, and sweep speed 2μ sec/cm.

the measured voltage drops, it is estimated that the inductance of the external load is $0.07 \mu\text{h}$. Thus, despite efforts to maintain the load inductance as low as possible, the current is inductance limited over part of the range of the experiment. In this case the conductance of the plasma column can be determined from the data taken at the peak current when $dI/dt = 0$.

The peak current and voltage data from a large number of shots similar to the one shown in Figure 2.18, but with different load resistors, are plotted in Figure 2.19. Also shown in Figure 2.19 are a limited number of data points for shots where the initial channel pressure was atmospheric. The solid lines shown connecting the various data points represented the generator voltage-current characteristic, or load line, for the two initial pressures. The conductivity is indicated by the slope of the voltage-current characteristic curve, which gives the internal resistance of the generator. If the dimensions of the current carrying channel are known, and a uniform electric field can be assumed, the conductivity can be calculated from the generator internal resistance.

The similarity in slope between the two characteristics, i. e., 0.109 ohms for the atmospheric pressure curve, and 0.0717 ohms for the 10 mm Hg curve, supports the previous evidence shown in Figure 2.17, that the conductivity is practically independent of the initial channel pressure and hence is independent of the Mach number.

Figure 2.20 is a plot of data taken using a $1/2$ inch diameter copper electrode, and a test section pressure of 10 mm Hg , similar to the data shown in Figure 2.19. The centers of the round electrodes were located at the same point on the channel as the centers of the 1 inch by 2 inch electrodes.

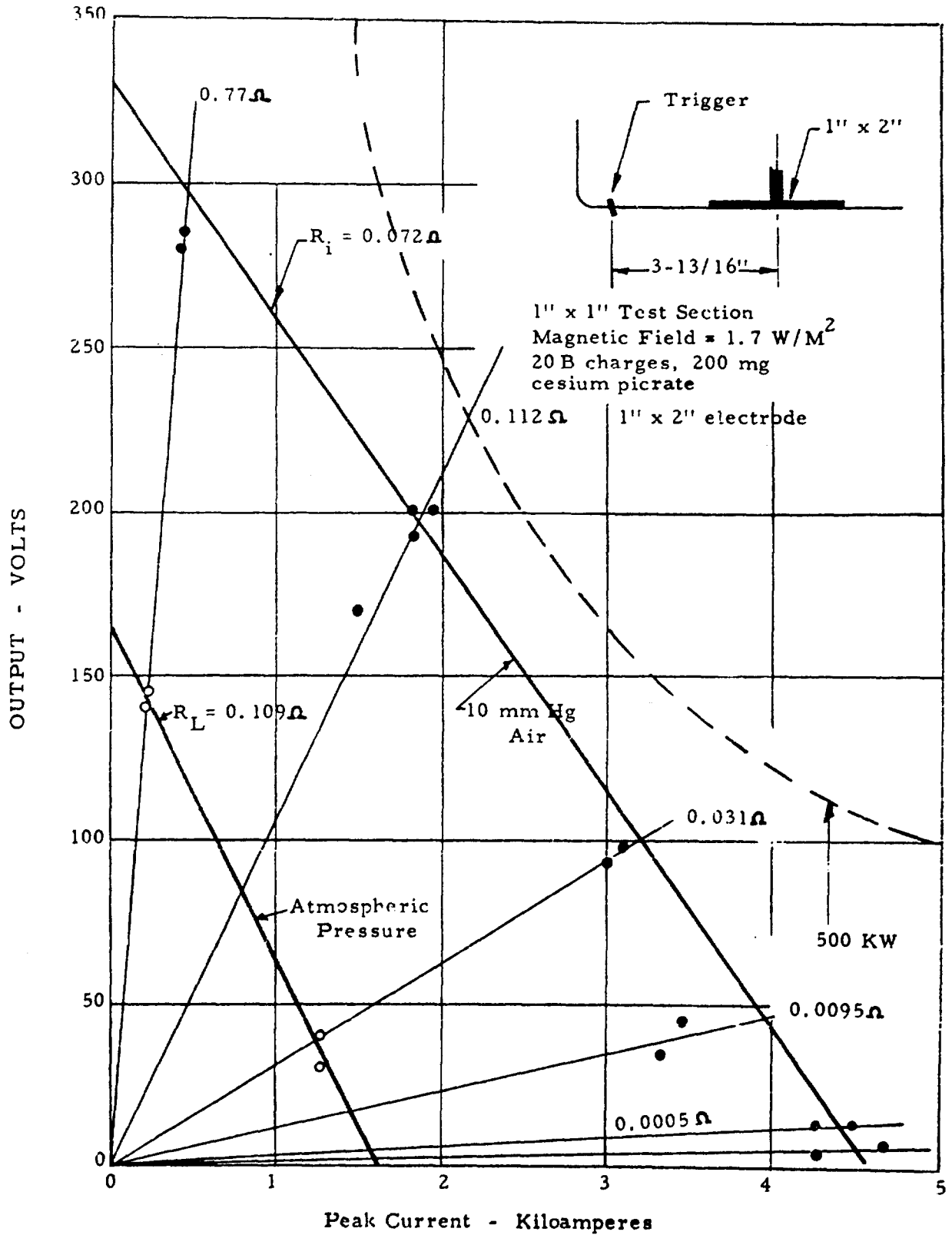


Figure 2.19
Voltage-Current characteristic of explosive driven MHD generator for conductivity determination.

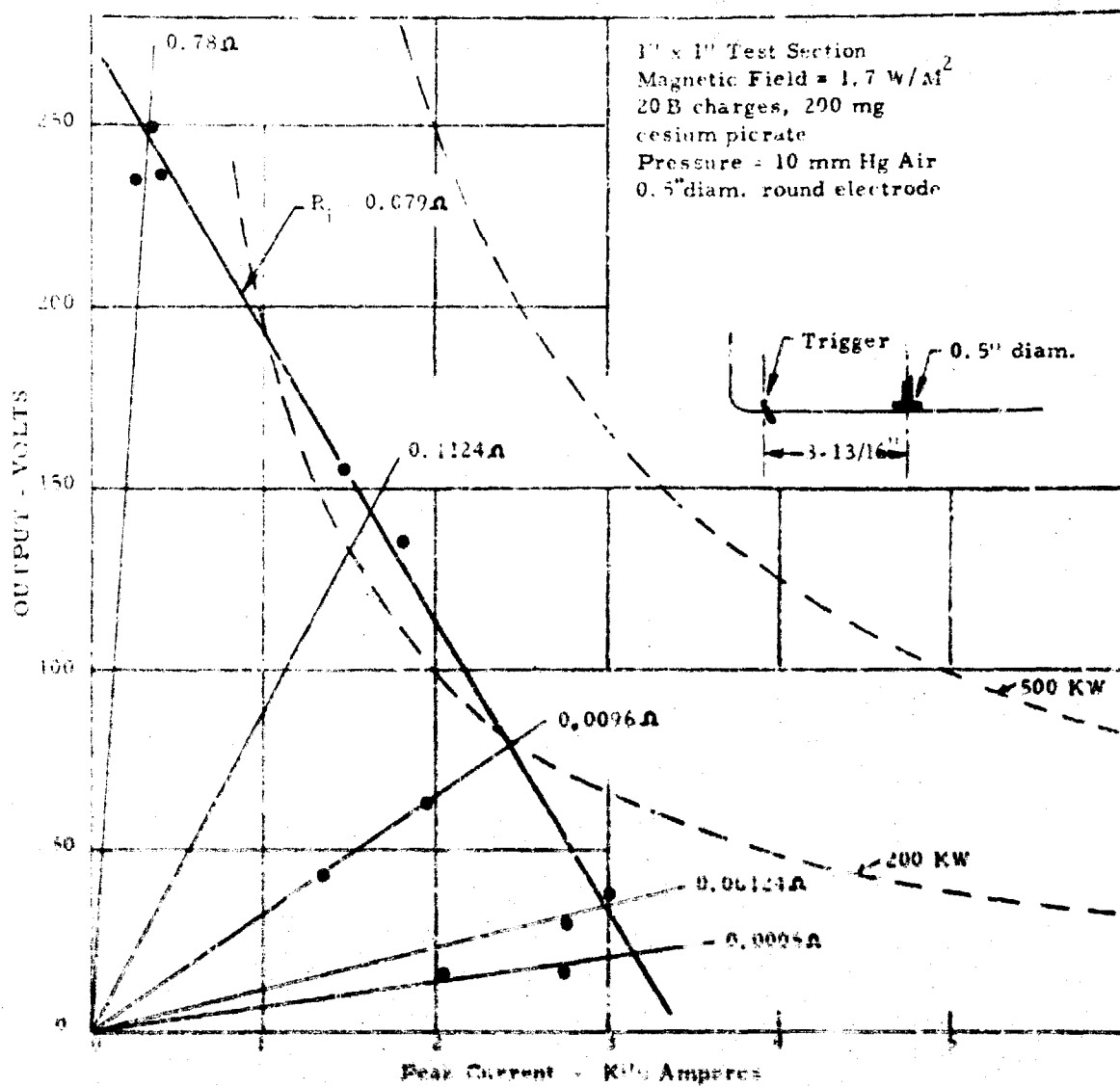


Figure 2.20
 Voltage current characteristic of
 explosive driven MHD generator
 with 0.5 inch diameter electrodes.

From Figure 2.19 it may be determined that the internal resistance of the generator with the smaller electrodes, is 0.0795 ohms, or only a factor of 1.1 higher than when the 1 inch by 2 inch electrodes were used. Since the electrode area differs by a factor of 10, it is assumed that the small difference in resistance results because the area occupied by the highly conducting detonation products is small compared to the size of the large electrodes. This view is supported by an examination of pulse length versus electrode length. The velocity of the gas is roughly 10 km/sec or 1 cm/microsecond. Therefore, the transit time for a 2 inch electrode would be 5 μ sec. It can be seen in Figure 2.18 that the current maximum occurs at about 6 microseconds, which would indicate that the conductive slug is of the order of 1 cm long.

Data on pulse length was taken using electrodes of the following lengths: 2.0 inches, 1.0 inch and 0.5 inch. Extrapolating this data to zero electrode length gave a pulse length of 1.5 microseconds which would correspond to a thickness of 1.5 cm for the conductive slug. Under the assumption that the conductive material uniformly fills a 1.5 cm length of the flow channel, and that the electrode length is long compared to the thickness of the slug so that electrode fringing factors need not be considered, the conductivity of the channel is 1000 mhos/meter. If an allowance is made for the 40 volt electrode drops which are indicated by the probe measurement, the conductivity of the seeded detonation products is 1100 mho/meter. This conductivity, in a direction perpendicular to a strong magnetic field would correspond to a plasma temperature of 9000^oK, using the Spitzer relation⁽⁹⁾

$$\sigma = \frac{7.75 \times 10^{-3} T^{3/2}}{T_e A} \text{ (mho/m) } . \quad (12.5)$$

where it is assumed that the product of the ionic charge, Z , times the logarithm of the Debye cut-off parameter, Λ , has the numerical value of 6. The reason for the high apparent temperature is not known. Spectrographic measurements made of detonating explosives which have been soaked in butane give apparent temperatures of this order. The high apparent temperature would also imply that most of the cesium is ionized.

In the power generation experiments, which are described in Section 2.4, we see that the ionized detonation products are conductive for times up to 50 microseconds. In these experiments it is also seen that the voltage-current relation is very non-linear, whereas for the experiments with short electrodes reported in this section, the voltage-current characteristic curve is reasonably linear. Part of this discrepancy is due to the fact that the peak current occurs at a different time in the generator as the load is changed. For high load resistances, the peak current and voltage occur early in the pulse while the conductive slug is near the front of the generator. As the load resistance is decreased, allowing a larger current to flow, the peak current moves to the downstream 1/3 of the channel. The peak voltage generally occurs later in the pulse, as the conductive slug leaves the electrode structure. Thus it would appear that the generator internal resistance is decreasing with time. However, from the data taken with small probes, it appears as though the decrease in internal resistance occurs because of an increase in the axial dimension of the conductive slug, and not because of an increase in conductivity with current as would be implied by the non-linear voltage-current plots. Further investigation of this topic is indicated.

In summary, it may be stated that very high conductivities are observed in the seeded detonation products and the conductivity exists for times sufficiently long that an appreciable fraction of the kinetic energy of the detonation products can be converted to electrical energy.

2.5.4 Variation in Output with Load Resistance

Important information can be gained by examining the output of the explosive-driven MHD generator as the load is changed from open circuit conditions, to short circuit. In the normal MHD generator theory, the open circuit voltage is given by the relation

$$V_o = uBd , \tag{2.5.7}$$

where u is the gas velocity, B is the magnetic field strength and d is the separation between the electrodes. If the electrodes are then connected to an external load so that currents can be drawn through the generator, then the voltage across the load will be given as

$$V = V_o - IR_i = IR_l , \tag{2.5.8}$$

where I is the current through the generator, R_i is the internal impedance of the generator and R_l is the load impedance. In the more general case, which must be considered here because of the short pulse length, inductive effects must be included. Under these conditions we have

$$\begin{aligned} V &= IR_l + L_l \frac{dI}{dt} = V_o - IR_i - \frac{d}{dt} (L_i I) \\ &= V_o - IR_i - I \frac{dL_i}{dt} - L_i \frac{dI}{dt} , \end{aligned} \tag{2.5.9}$$

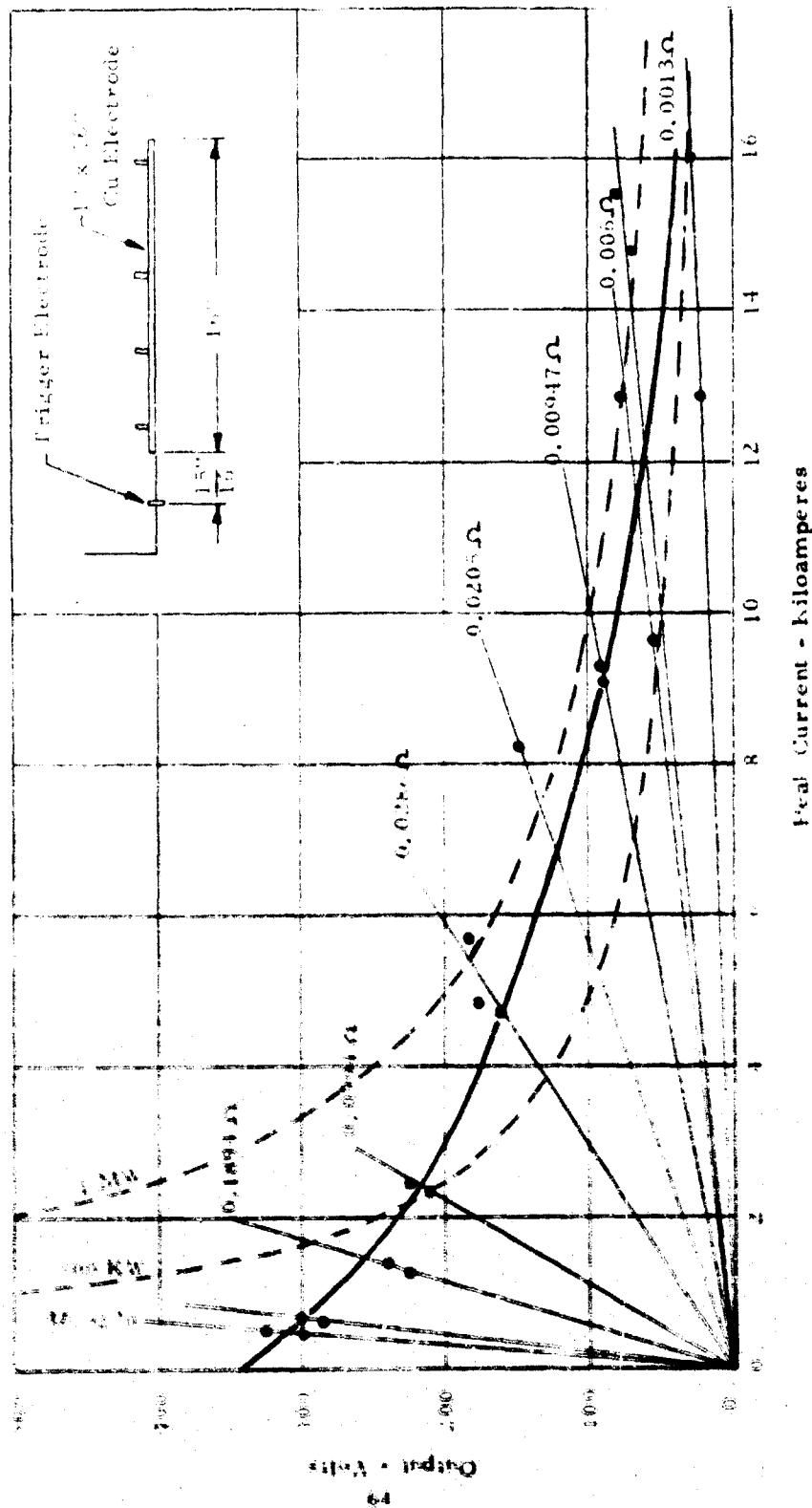
where L_l and L_i are the inductances of the load and the internal inductance of the generator, respectively.

By variation of R_e and L_e , the external parameters most readily available for change, and by measuring I and V , it is possible to estimate R_i and L_i , if it can be assumed that V_o is constant over the change in parameters. However, as will be noted later, it is possible to slow the gases down by approximately 10% by the extraction of energy with low values for the load resistance. However, as a first approximation it will be assumed that V_o is constant. If the measurements are made at the peak current, then $dI/dt = 0$, and this relation simplifies to

$$V = IR_e = V_o - I_m \frac{dL_i}{dt} - I_m R_i \quad (2.5.10)$$

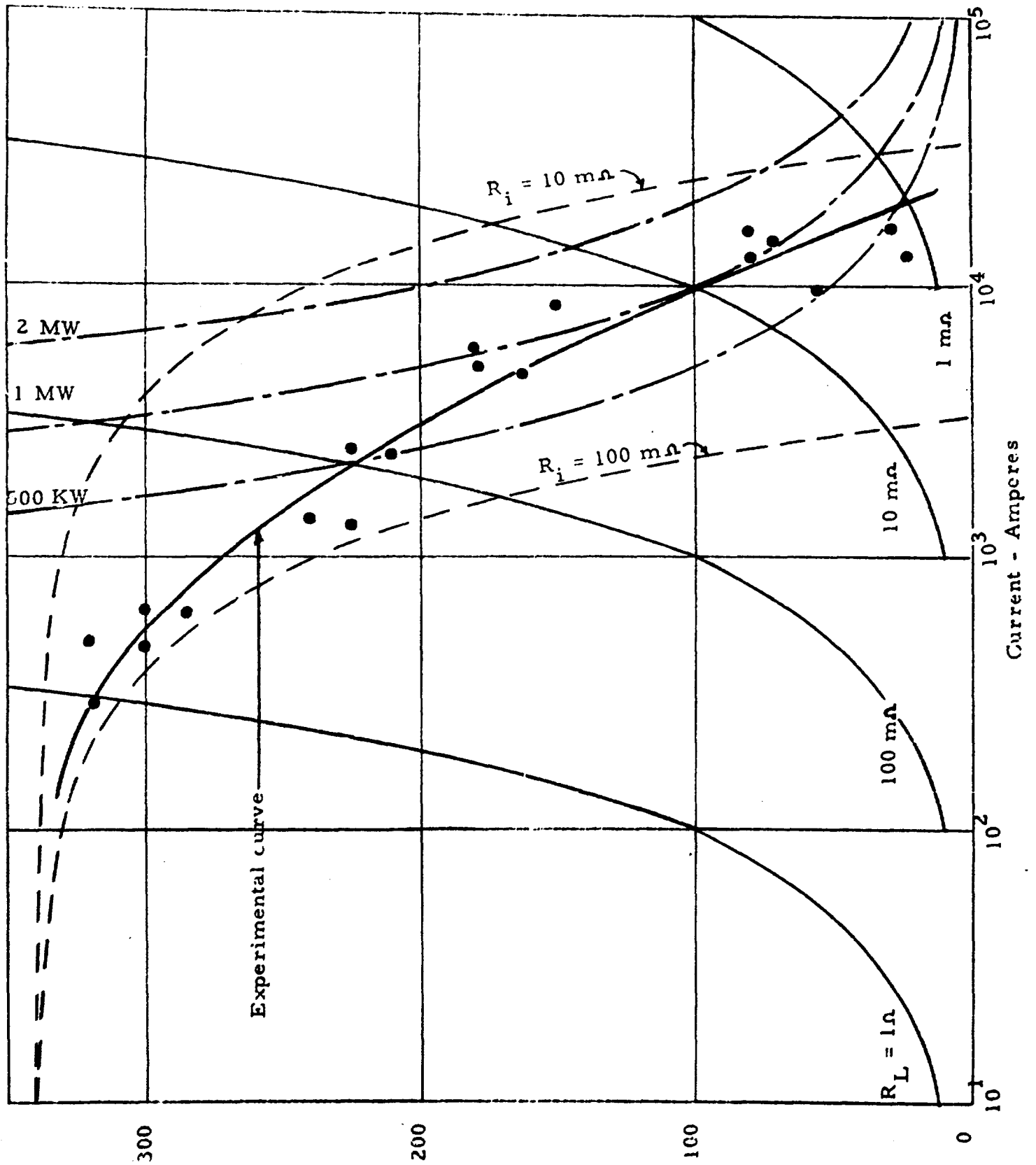
where I_m is the peak current.

By plotting V as a function of I_m , then, one can evaluate R_i and dL_i/dt , assuming the R_i does not vary with the current level. Figure 2.21 is a voltage-current plot of the V and I_m data taken in the 1 inch by 1 inch test section, using the 16-inch long continuous electrodes and with the channel initially filled with 10 mm Hg of air. The first thing which is evident is that the voltage current relation is very non-linear. The initial slope, at low currents corresponds to an internal resistance R_i of 70 milliohms, which is in agreement with the short electrode data shown in Figure 2.19. As the current level increases the curve flattens out, with internal resistance approaching 5 milliohms in the range between 10 and 20 kA. Because of the wide range of currents which are covered in these experiments, it is perhaps better to plot the data on semilog paper as is shown in Figure 2.22. In this plot, lines of constant resistance have a characteristic shape, but they are not straight as in the linear plot. One thing which becomes more readily apparent in this plot is the value of the short



Output characteristics of 1 inch by 1 inch explosive-driven MHD channel for various load resistances. Magnetic field 1.7 w/m², initial pressure 10 mm Hg, air.

Figure 6.21



Output - Volts

Figure 2. 22

Output voltage at peak current for the 1 inch x 1 inch channel at 10 mm Hg, air.

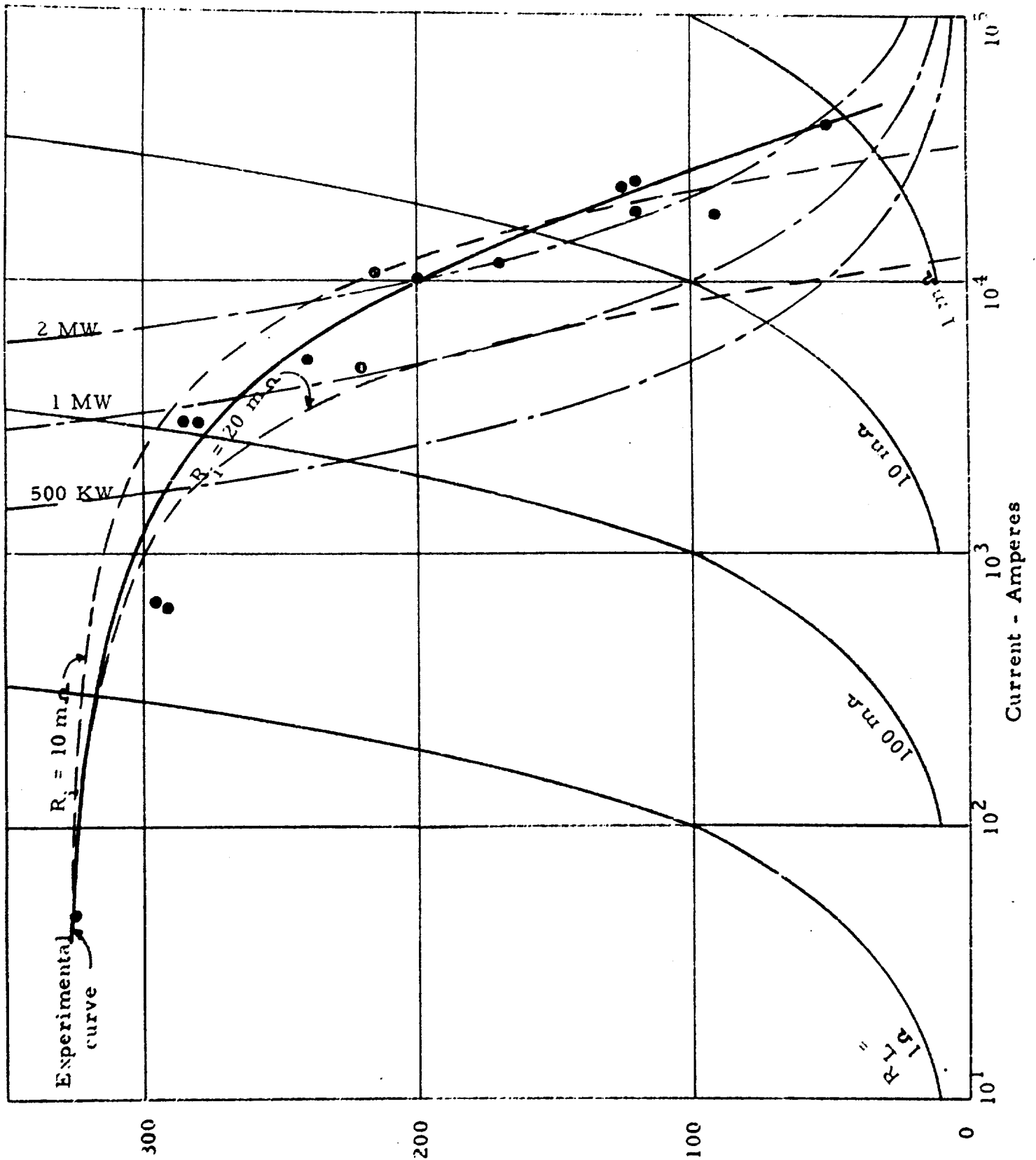
circuited current which is estimated as 25 kA. Also shown on Figure 2.22 are dotted lines which show the expected variation in V with I assuming a constant internal impedance R_i , and $dL/dt = 0$ with V_0 assumed equal to 340 volts. It can be seen that the apparent internal impedance decreases with current. Making the additional assumption that R_i is equal to 70 milliohms, as is indicated by the low current data, it is then possible to quite accurately fit the data with the relation

$$V = 340 - 0.07 I_m + 8 \times 10^{-6} I_m^2, \quad (2.5.1)$$

where I_m is in amperes and V is in volts. Presumably the last term in the above equation represents such factors as the time changing inductance term, which could include the magnetic bootstrapping effects, and non-linear conductivity which would appear similar to the transition to an arc mode.

Also drawn as dashed lines on Figure 2.22 are lines showing constant power output. It is seen that under the conditions in the explosive-driven MHD generator the maximum power output was relatively insensitive to load resistance over the range from about 6 to 60 milliohms as we have seen in Section 2.4. The peak power in these experiments in the 1 inch by 1 inch channel using air at 10 mm Hg as the filling gas was about 1.3 MW. Much higher power levels were obtained in the experiments where argon was used as the additive seeding gas.

The data for the argon experiments are shown in Figure 2.23. The details of these experiments were identical to those reported above except that the channel was evacuated and then filled to a pressure of 10 mm Hg with argon.



Output - Volts

Figure 2.23

Output voltage at peak current for the 1 inch x 1 inch channel at 10 mm Hg, argon.

The results of the two experiments are similar except that the peak current is about a factor of two higher for the argon experiment. The peak power in the argon run was about 3 MW. As before, it is possible to fit the data with a series expansion in the current variable of the following form:

$$V = V_0 - IR_i + \mathcal{G} I^2 = 325 - 0.015 I + 3 \times 10^{-7} I^2, \quad (2.5.12)$$

where \mathcal{G} is the second coefficient of the expansion. Comparison with the data for air shows that V_0 is only slightly lower than for air, whereas R_i with the argon additive is a factor of 5 lower, and \mathcal{G} is a factor of 25 lower.

The lower value for V_0 is consistent with the decrease in velocity observed as the pressure of argon is increased, and represents the difference in mass of the comparable volumes of air or argon which are swept up by the detonation product front flowing down the channel. The reasons for the change in R_i and \mathcal{G} are more subtle. Measurements were made of the characteristics of the generator for experiments where the channel was maintained at 10 mm Hg of argon, but no seed was used in the explosive charge. In one experiment where a 6 milliohm load resistor was used, a current of 9.2 kA was measured, as compared to the 20 kA current shown in Figure 2.23. This experiment implies that the argon is ionized by the explosive shock and is capable of achieving high levels of conductivity, of the order of 700 to 1000 mho/meter, which is comparable to the conductivity of the detonation products. Thus, there can be two possible paths for the generator current, i. e., through the ionized cesium in the detonation products and through the ionized argon. The factor of two increase in current when using cesium seed and argon accounts for the increase in output power as shown in Figure 2.9.

Similar experiments were conducted in the 1 inch by 4 inch channel and the limited data was presented in Section 2.4.

In summary it may be stated that the explosive-driven MHD generator demonstrates non-linear voltage current characteristics. The apparent internal resistance is a function of the current level, and is therefore a function of the external load. The experimental data for peak current can be represented by a function of the form

$$V = uBd - \alpha I_m + \beta I_m^2 \quad (2.5.13)$$

where α and β are experimentally determined constants. The constant α represents the conventional generator internal resistance and β represents a non-linear correction term. Because of this characteristic the output power level is more sensitive to the value of the load resistance.

Thus, it is seen that the non-linear characteristic makes the problem of matching the generator to the load critical because of the more rapid variation in power output with load than in the conventional case. As discussed in Section 2.4 the optimum load appears to scale linearly with the electrode separation d , however, additional experimental data is needed on this topic.

2.5.5 Variation in Output with Magnetic Field

As outlined in Section 2.5.4 the output voltage of an MHD generator in the low magnetic Reynolds number approximation is a function of the applied magnetic field. This relation is given by Equation (2.5.9) as

$$V = uBd - IR_i - \frac{d}{dt} (L_i I) \quad (2.5.15)$$

Therefore, if we make a measurement of the open circuit voltage, where $I = 0$ we can examine the effect of the magnetic field upon the output of the generator by comparing the data to the relation

$$V_{oc} = uBd \quad (2.5.16)$$

Figure 2.24 is a plot of the open circuit voltage of the 1 inch by 1 inch generator when it is operated with the channel initially at atmospheric pressure. The open circuit voltage is plotted as a function of the applied magnetic field over the range of fields from 0 to 2.2 w/m^2 .

It is seen that Equation (2.5.16) fits the data very well. The effective velocity u as derived from the slope of Figure 2.24 is 4.7 km/sec , whereas the measured velocity of the propagation of the front of the conductive region is 6.0 km/sec . One possible explanation for this discrepancy is that the velocity of the particles, or gas, behind a shock is equal to the shock velocity minus the velocity of sound in the shocked gases or detonation products, i.e.,

$$u = Ma_0 - c_x \quad (2.5.17)$$

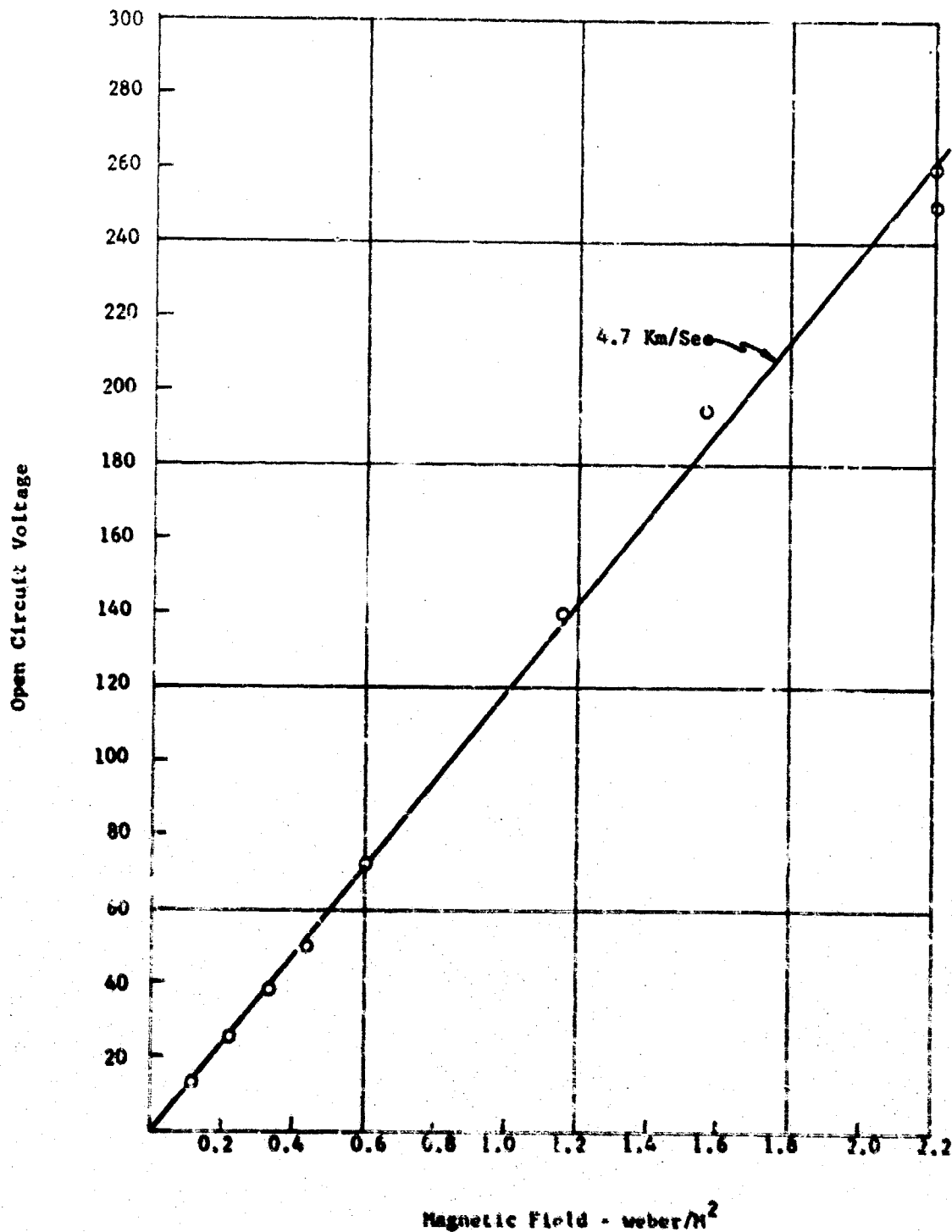


Figure 2. 24 Open circuit voltage versus applied field. From this plot the effective gas velocity of 4.7 Km/sec can be determined.

where M is the Mach number, a_0 the speed of sound in air, or the gas in which the shock is propagating, and c_x is the velocity of sound in the detonation products (see Section 2.5.1). This theory would indicate that c_x is 1.3 km/sec, or somewhat higher than the previous estimate.

The data from the power generation and conductivity experiments which were conducted at lower pressures do not agree as well with Equations (2.5.16) and (2.5.17). For example, the data expressed by Equation (2.5.11) gives the measured effective product uBd of 340 volts. For an electrode separation of 2.54 cm, and a magnetic field of 1.7 w/m^2 , the effective velocity u is 7.9 km/sec, whereas the measured velocity is 10.3 km/sec. The limited data taken with the 1 inch by 4 inch generator indicate the same sort of discrepancy. The data suggest that the output voltage is a constant fraction of about 0.8 of the uBd product. On this basis it is indicated that the problem is not due to electrode drops, or sheaths, etc., which would tend to be a smaller fraction of the open circuit output in the larger generator, but is due to some other factor.

One possible explanation is that the effect is due to circulating currents which arise because of the axial velocity distribution of the detonation products. The back and the front of the conductive slug, which move at different velocities, are connected by the electrodes.

2.5.6 Scaling and Aspect Ratio Studies

To investigate the effect of scaling factors, the outputs of the 1 inch by 1 inch and the 1 inch by 4 inch generators were compared under supposedly

identical conditions. As outlined in Section 2.3, the 1 inch by 1 inch channel had electrodes 16 inches long and was driven by 1 duPont 20B charge, whereas the 1 inch by 4 inch channel had 18 inch long electrodes, and was driven by two charges, which were placed approximately 2 inches apart, one above the other. Because soft iron was used in the 1 inch by 4 inch channel sidewalls, a magnetic field of 2.2 w/m^2 could be obtained in that channel whereas in the 1 inch by 1 inch channel with stainless steel walls the maximum magnetic field was 1.7 w/m^2 . Aside from these differences, all experiments were conducted with 10 mm Hg pressure of either air, argon, or helium in the channel and with comparable electrical loads.

In order to compare the scaling relation, the data from the two generators has been normalized by dividing the voltages by the electrode separation d , times the magnetic field B . As indicated by the simple theory for the open circuited generator this is equivalent to determining the effective gas velocity u . The data normalized in this manner are plotted in Figure 2.25 as a function of generator current. It is seen, for the 10 mm Hg air data, when the currents are less than 10 kA, that the data scale as predicted. However, at higher current levels the scaled output voltage for air in the 1 inch by 4 inch channel is much higher than for the smaller channel. This anomaly can also be seen in Figures 2.8 and 2.9.

When comparing the data taken with 10 mm Hg of argon initially in the channel, it is seen that there is a closer agreement between the two sets of scaled data, at least as to form, in the high output region. However, it should be noted that the larger generator still has a somewhat higher output than would be expected on the basis of scaling in terms of magnetic field times electrode separation. For this reason we have replotted the argon data from

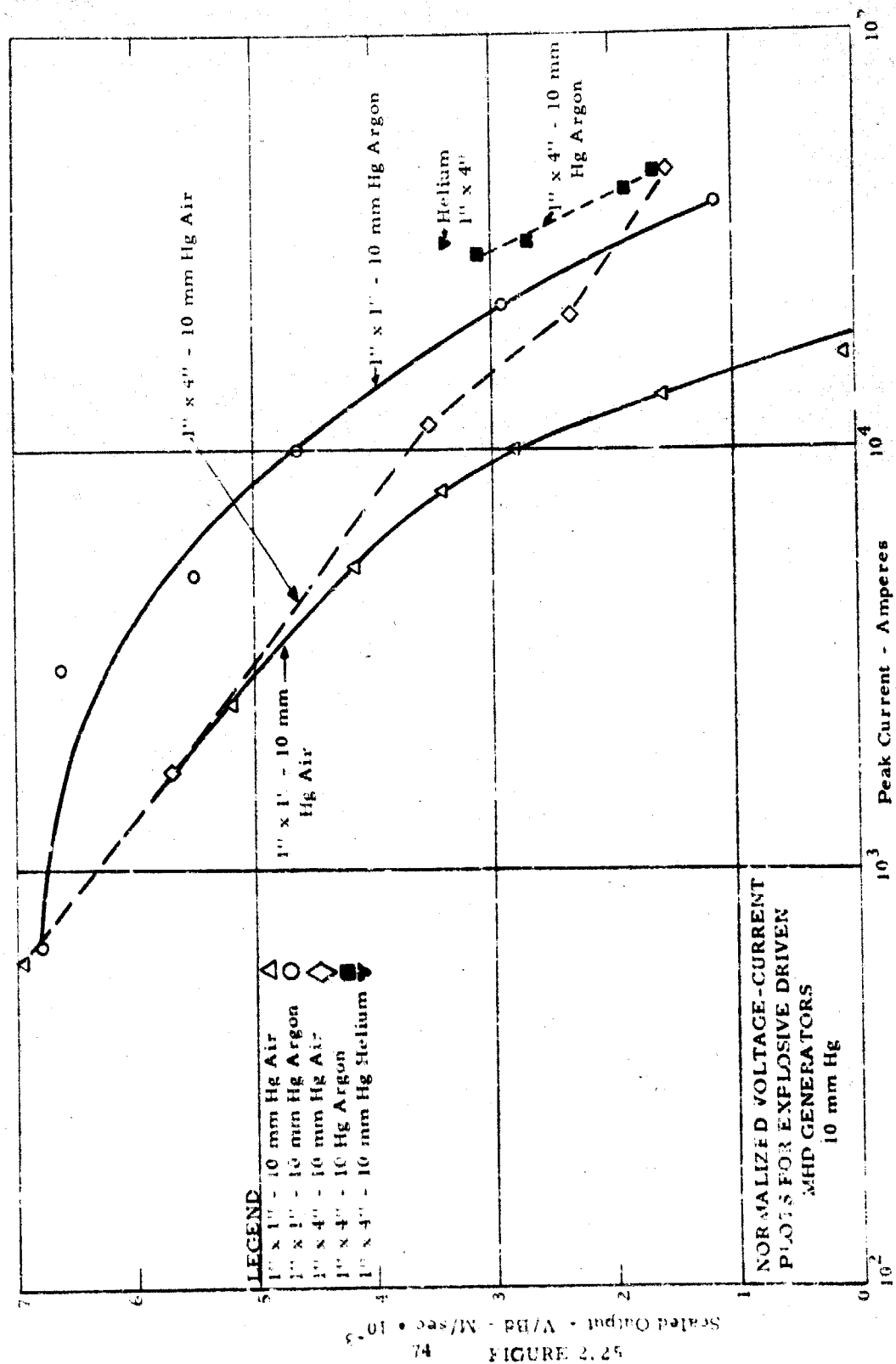
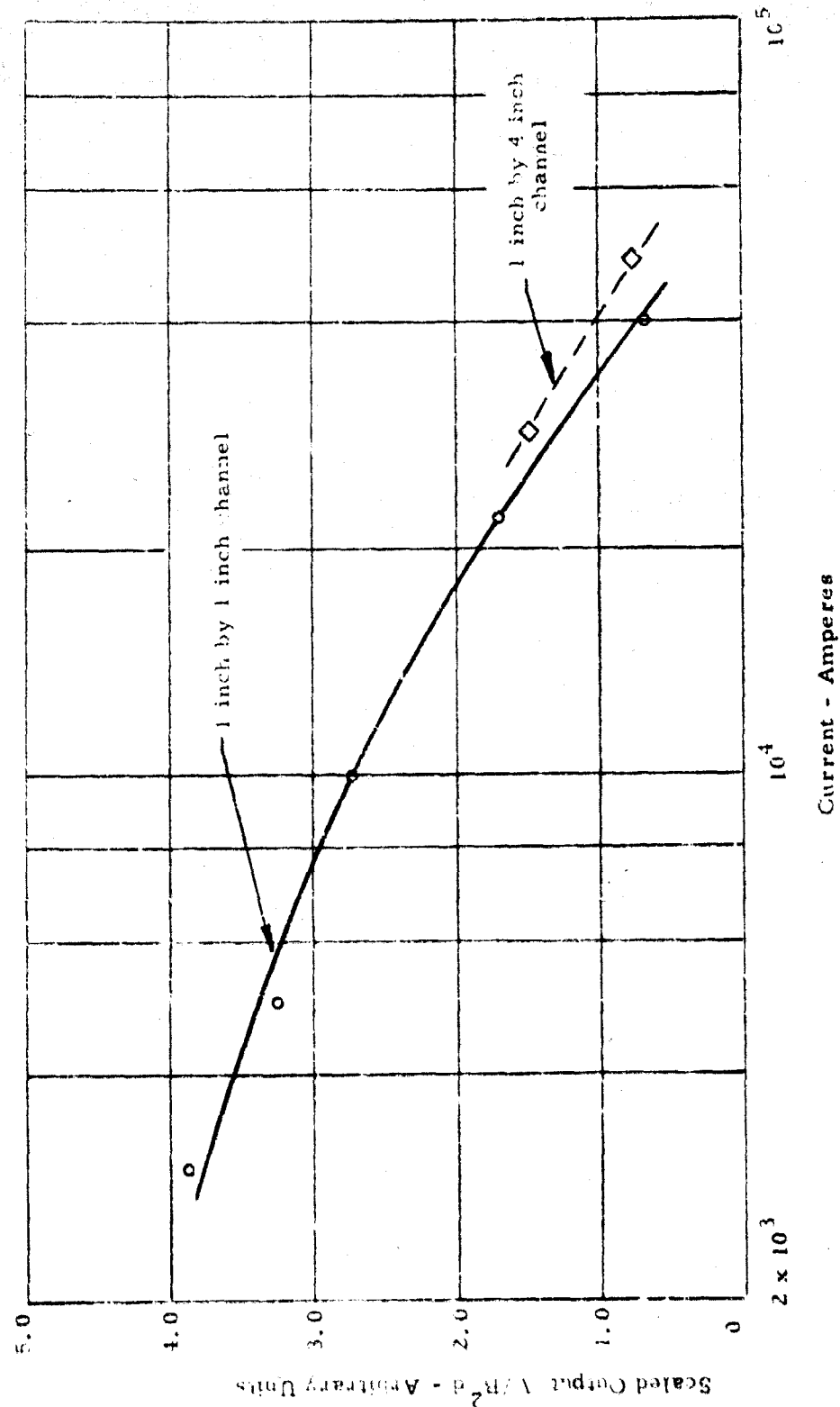


Figure 2.25 in terms of a scaling parameter which is the output voltage divided by the electrode separation times the square of the magnetic field. As outlined in Section 2.2 this would be the scaling condition for a high magnetic Reynolds number. This data are shown in Figure 2.26. Using this scaling relation it is seen that there is good agreement between the data taken in the 1 inch by 1 inch channel and the 1 inch by 4 inch channel when using argon at 10 mm Hg pressure. The fact that this scaling law can be used, is further evidence in support of the claim that a high magnetic Reynolds number does exist in the explosive-driven generator. Further experimental data is needed on the scaling parameters.

2.5.7 Variation in Blast Pressure with Initial Channel Pressure

To check the applicability of the shock wave model which was originally used to explain the characteristics of the explosive-driven MHD generator, a series of measurements was made of the pressure associated with the detonation product flow. The pressure rise was measured as a function of the initial pressure in the flow channel, using a Kistler 605-B quartz transducer which has a rise time of approximately 3 microseconds. Because of shock reflections in the crystal and noise transmission through the channel wall to the crystal, it was possible to determine only the initial pressure rise. None of the subsequent pressure profiles could be determined using the Kistler gauge.

Figure 2.27 is a plot of the peak pressure measured at a station 15 inches downstream from the entrance of the channel as a function of initial pressure of air in the channel. The peak pressure at this station is of the order



High Reynolds number scaling of explosive-driven MHD channels with initial pressure 10 mm Hg of argon.

Figure 2.26

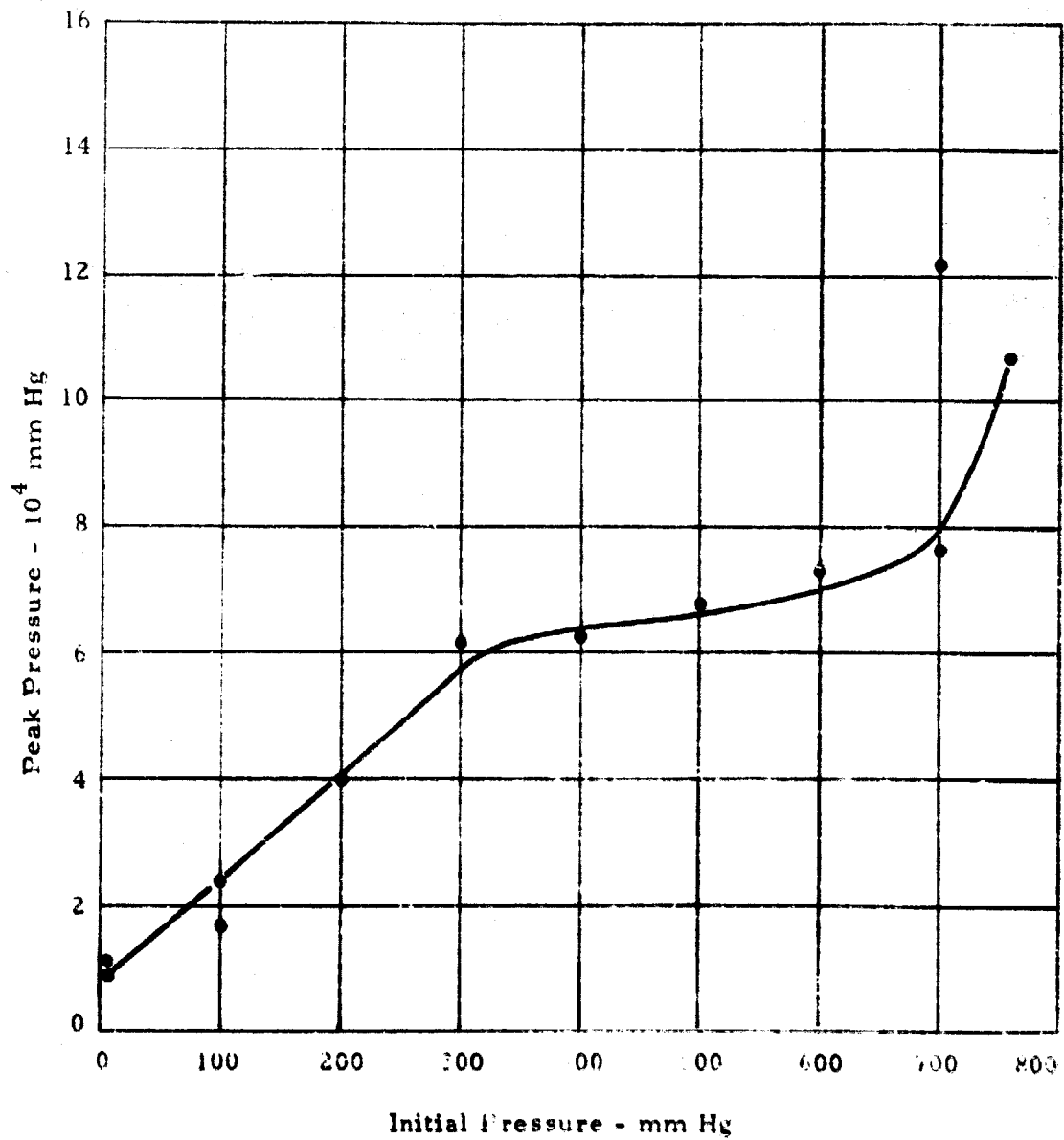


Figure 2.27

Pressure rise as a function of initial air pressure in explosive-driven channel.

of 140 atmospheres for initial pressures near atmospheric. The pressure was also measured at a station 3 inches down the channel. The highest pressure at this station was 350 atmospheres, which is in agreement with the calculation in Section 2.5.1 for the air shock associated with the isentropic expansion of the detonation products.

From the normal shock relations it can be shown that the over-pressure ΔP is related to the initial pressure and Mach number by the relation

$$\Delta P = P_0 \frac{2}{\gamma + 1} (M^2 - 1). \quad (2.5.18)$$

For the present experiments the Mach number is very large, of the order of 10 to 40, so that the following approximate relation should obtain

$$\frac{\Delta P}{P_0 M^2} = \text{constant} = \frac{2}{\gamma + 1} = 1.167 \text{ to } 1.00 \text{ for air.} \quad (2.5.19)$$

Since the velocity is measured simultaneously with the pressure measurement, it should be possible to determine if this relation is fulfilled. Examination of the experimental data which is contained in Table 2.4 shows that there is much scatter in the data. In general, the measured values are less than the theoretical prediction, the disparity being the greatest at the lowest initial pressure. One reason for this discrepancy may be the fact that the pressure transducer has a finite rise time of 3 microseconds. For the high Mach numbers and low initial densities the shock-heated high pressure region will be very thin, so that considerable error may arise in the measurements.

TABLE 2.4

CORRELATION OF PRESSURE RISE DATA
WITH MACH NUMBER IN EXPLOSIVE-DRIVEN MHD CHANNEL

P_0 mm Hg	$\Delta P \times 10^{-4}$ mm Hg	$\Delta P/P_0$	M	$\frac{\Delta P}{P_0 M^2}$
10.5	0.113	1080	33.0	1.00
10.5	0.075	716	33.0	0.66
100	1.5	150	20.0	0.38
100	2.4	240	20.0	0.60
200	4.2	210	17.7	0.67
300	6.3	210	15.1	0.92
400	6.3	157	14.1	0.79
500	6.6	132	12.8	0.80
600	7.2	120	11.3	0.94
700	12.3	176	10.2	1.69
758	10.8	140	10.6	1.24
700	7.8	111	11.3	0.86

While the pressure measurements show general agreement with shock wave theory, this is to be expected since the air, or other gas in the channel, is driven as shock supported by the expansion of the detonation products.

2. 5. 8 Explosive Parameters

The output of the explosive-driven MHD generator is a function of the detonation product velocity. In the low Reynolds number regime the output varies as the square of the velocity, whereas for the high magnetic Reynolds number case, the output varies directly with the velocity. In any case, it is desirable to produce as high a flow velocity as possible in the MHD channel. In the studies concerned with the variation in velocity with initial channel pressure, the variation in velocity of the detonation products could be described by a relation of the form

$$u = D + F(p) , \quad (2. 5. 20)$$

where D is the detonation velocity in the explosive, and $F(p)$ is an additive factor which is a function of the initial pressure in the channel. For the one dimensional expansion of a plane faced, constrained charge, $F(p)$ varies in an inverse manner with the initial pressure, approaching a constant value of the order of D as the initial pressure goes to zero.

On this basis the highest velocities would occur with an explosive having the highest detonation velocity. Aside from the requirement of high D , it is possible to achieve high velocities for ejected materials by proper geometrical arrangement of the explosive such as by using explosive cavities

utilizing the Munroe effect⁽¹⁰⁾. This knowledge was the reason for the initial selection of the 60° cone-shaped charge configuration which was commercially available in the duPont perforators.

The initial experiments were conducted using the shaped charges complete with copper liners. Low conductivities were observed. The liners were then removed for subsequent shots and the charges were seeded with either cesium carbonate or cesium picrate. The average velocity, as determined from the time of flight to the end electrode, was higher with the copper liner than without. However, because of the large increase in conductivity obtained by using the low ionization potential seed material, all subsequent shots were conducted without the liner even though the average detonation product velocity was lower. This reduction in velocity was presumably due to "unloading" of the free surface of the explosive, i. e., an edge effect in which the detonation is not complete near the surface due to the reduction in pressure. These experiments were not repeated at the lower pressure used in subsequent experiments.

In order to investigate the many factors involved in the choice of an optimum explosive composition and configuration a number of other explosive experiments were conducted. Because of the large increase in output when using low initial pressure, these experiments were conducted at 10 mm Hg, usually in air, as standard condition. Several different types of explosives were evaluated as well as several different explosive geometries. The results of these tests are summarized at the end of this section in terms of a figure of merit which roughly evaluates each explosive system in terms of the energy conversion efficiency. The figure of merit is proportional to the square of the peak current times the pulse length divided by the weight of the charge for a fixed load resistance and magnetic field.

In order to investigate effects of explosive geometry, composition C4 was used to form charges which contained the same quantity of explosive as the duPont 20B charge, but with explosive formed into a flat front instead of the 60° cone. These charges were fabricated using the bakelite charge holders of the 20B charge, the C66 booster, and 7.6 grams of composition C4. In these experiments it was possible to evaluate two quantities: the generator current, and the time for the conductive slug to travel to various electrodes which is inversely proportional to the front velocity. Table 2.5 gives the data for a number of these experiments. These data were taken in the 1 inch by 1 inch generator using a 1.28 milliohm load, which is essentially a short circuit condition. The electrodes were 0.5 inches long by 1.0 inch wide, the magnetic field was 1.7 w/m^2 , and the initial pressure was 10 mm Hg of air unless otherwise specified. These experiments included tests of the flat front charges in various confining shells to investigate the effect of the charge holder density. Charge holders of low density polyurethane and Cerrobend, a low melting point bismuth eutectic which has a very high density, were cast to the same contour as the bakelite holder normally used with the 20B charge. Also shown are the data for a bulk seeded charge using 7.5 grams of composition C4 and 500 mg of cesium picrate formed to the face contour of the 20B charge (60° cone) in a bakelite holder. The data for a comparable shot using the duPont 20B charge are listed for reference. For comparison of the velocity data, the distance from the trigger electrode to the leading edge of each electrode is listed.

The data show that when comparing the flat front charge in the bakelite holder and the 20B charge the velocities are comparable, but the short circuit current for flat front charge experiment was somewhat

TABLE 2.5
 COMPARISON OF EXPLOSIVE CHARGE HOLDER DENSITY
 AND CHARGE GEOMETRY

		I_{ss} kA	t_1 μ sec	t_2 μ sec	t_4 μ sec	Remarks
(1)	20R	2.0	3.2		18.0	200 mg cesium picrate
(2)	Flat Front	2.7	3.2		19.0	200 mg cesium picrate Bakelite shell
(3)	Flat Front	1.0 (est)	4.3		23.0	Polyurethane shell
(4)	Flat Front	2.0		9.2		Cerrobend shell
(5)	Composition C4 - 20E geometry	0.3	3.2		17.5	500 mg cesium bulk seeded

$x_1 = 4.1$ cm

$x_2 = 3.4$ cm

$x_3 = 19.4$ cm

higher. This would indicate a higher conductivity for the flat front charge detonation products.

In the shot with the low density polyurethane holder the velocity was markedly lower than for the standard 20B charge as judged from the longer propagation time to the electrodes. The short circuit current was also lower by roughly a factor of two. For this shot the current had to be estimated from the amplitude of the voltage trace where $dI/dt = 0$. For the shot with the Cerrobend holder the measurements were made at the second electrode in conjunction with probe experiments as is shown in Table 2.5, so the distance to the second electrode should be used in comparing velocities. Within the accuracy of the experiment the Cerrobend charge holders appear to result in the same detonation product front velocity as is obtained with the bakelite holder. Because of the difficulty in fabricating the Cerrobend holders and the comparable performance of the bakelite holders, the use of the commercially available 20B charges was continued.

The data taken for the bulk seeded composition C4 formed into a 60° cone show that the time for the front to reach the electrodes was almost identical with the referenced 20B shot, however, the peak current is much lower. Examination of the record shows that the current pulse was also much shorter, lasting for 2.4 microseconds, compared to 5 or 6 microseconds for the surface seeded 20B charges. The short pulse length seems to be characteristic of all shots made with bulk seeded charges.

As part of the investigation of charge geometry a limited number of experiments were conducted using the W-shaped charge developed by Falcon Research & Development Company. The details of the W-shaped charge are

presented in Reference ⁽¹⁰⁾. The performance of the W-shaped charge which contains 12.3 gms of composition C4 was compared to the duPont 20B charge which contains 7.6 grams of RDX. The experiments were conducted in the 1 inch by 1 inch channel which was fitted with the 16 inch electrodes. The magnetic field was 1.7 w/cm^2 and the initial pressure was 10 mm Hg of air. The charges were seeded with 200 mg of cesium picrate on the front surface. Table 2.6 lists the pertinent data for these experiments. Two values of load resistor were used, approximately 30 milliohms and 1.3 milliohms. The 30 milliohm was chosen because it represented the good impedance match for power output with the 20B charges. The 1.3 milliohms load was essentially a short circuit. It is seen that the Falcon W charge had a slightly larger current in each case than the 20B charge. However, when considering the Falcon charge weighed approximately 1.7 times as much as the 20B charge, the output per gram of explosive was approximately 20% less. Two things were noted with the Falcon W charge: the pulse length was somewhat less than with the 20B, on the order of 10%, which would indicate a higher velocity; and the initial voltage which is indicated by V_i in Table 2.6 was much higher for the Falcon charge. This could imply that the Falcon W charge more nearly filled the channel during the early part of the shot.

Further comparisons of the 20B charges with other explosive systems were made using the 1 inch by 4 inch channel. These experiments were conducted using single and double charges with various filling gases in the channel and included charges formed of composition C4 and duPont Detasheet. The details of these experiments are summarized in Table 2.7 which lists the type of charge, number of charges, seed material used, initial pressure and

TABLE 2.6

COMPARISON OF DUPONT 20B AND FALCON RESEARCH W CHARGES
IN 1 INCH BY 1 INCH EXPLOSIVE-DRIVEN MHD GENERATOR

Charge	R_L $m\Omega$	I_{max} kA	$V_{i_{max}}$ volts	V_i volts	Pulse Length μsec
20B	28.6	5.8	180	50	45
Falcon W	31.6	6.0	205	120	40
20B	1.30	16.0	28	25	47
Falcon W	1.31	18.75	18	60	43

type of additive gases, and load resistance for each series. The data which are summarized, include peak current, voltage at peak current, and pulse length for each shot. Also shown in Table 2.7 is a figure of merit which relates the energy output to the weight of explosive used. The figure of merit is numerically given as

$$\text{F.M.} = \frac{I_m^2 R_L T}{W}, \quad (2.5.21)$$

where I_m is the maximum current, R_L the load resistance, T the pulse length and W is the weight of the charges in grams. The data given in Table 2.7 have been normalized to the output of the channel using two 20B charges and an initial pressure of 10 mm Hg of air.

From Table 2.7 it is seen that the maximum power was derived using two 20B charges with 10 mm Hg of helium in the channel as was reported in Section 2.4. The figure of merit for the helium experiment is 1.93. The highest figure of merit, 2.12, was obtained using a single flat front composition C4 charge firing into 10 mm Hg of argon. Although the peak currents are less than obtained in the other experiments the pulse lasts considerably longer so that more energy is extracted per gram of explosive. In the Detasheet experiments some initial difficulty was experienced in initiating the explosive with conventional blasting caps. Therefore, an experiment was conducted where 7.5 grams of Detasheet was fit into a 20B bakelite holder to form a flat faced charge. The figure of merit for this charge is comparable to that for the single 20B charge. Extended linear charges, approximately 10 cm in length, were constructed using the two different thickness of Detasheet. Each charge

Charge	Seed nug Cs Pic./Charge	P ₀ & Gas mm Hg	I _{max} kA	V _{max} volts	Pulse Length μsec	R _L m	Figure of Merit
2 - 20E	200	10 - Air	21.0	510	45	19.5	1.00
2 - 20B	200	He	30.0	750	43	19.5	1.93
2 - 20C	200	Ar	25.4	720	46	19.5	1.86
2 - 20D	0	Ar	17.7	380	45	19.5	0.703
1 - 20B	200	Ar	19.3	410	47	19.5	0.915
1 - Comp. C4 Flat Face	200	Ar	18.2	355	64	20.1	2.12
2 - Comp. C4 Flat Face	200	Ar	23.6	530	61	20.1	1.78
1 - Detasheet 7.5 grms 20B holder	200	Ar	11.8	280	78	20.1	1.08
Thin Detasheet 15.1 gm	200	Ar	10.0	225	66	20.1	0.353
Thick Detasheet 15.8 gm	200	10 - Ar	10.2	190	60	20.1	0.306

TABLE 2.7

FIGURE OF MERIT COMPARISON OF 20B CHARGES, COMP. C4 FLAT
FACE CHARGES AND DETASHEET IN 1 INCH BY 4 INCH EXPLOSIVE -
DRIVEN MHD CHANNEL

weighed approximately 15 grams so it was equivalent to two 20R charges. It is seen that the peak currents achieved with the extended charges were relatively low, as is the corresponding figure of merit.

While further work on the development of optimum explosive systems for the linear channel is indicated from the work reported herein, it would appear that the most productive area for future investigation would be in the study of methods for increasing the fraction of the explosive which participates in the energy conversion process.

2.5.9 Load Placement Studies

During the course of the experimental program it was discovered that the output of the generator depended upon the physical location of the load. Currents flowing through the electrodes changed the magnetic field in front of the conductive slug by a sort of magnetic "bootstrapping" if the load was connected at the downstream end of the long electrodes. For experiments in the 1 inch by 1 inch generator feeding a 1.3 milliohm load the current was increased by a factor of two, from 6.85 kA to 15.0 kA, when the load resistor was moved from the upstream end of the electrode to the downstream location. To explain this effect the following theory, which views the generator in terms of the lumped electrical parameters, was developed. This model suggests that there may be an optimum location for the load.

Inasmuch as the generator electrodes are extended and may therefore contribute appreciably to the impedance of the generator-load circuit, the question arises as to the most favorable position for local connection of the load. As the plasma conductor moves from one end of the electrodes to

the other, the inductance and resistance of the circuit may vary appreciably in time. Clearly the functional character of the variations depends on whether the load is connected to the upstream end of the electrodes, to the downstream end, or perhaps to some intermediate point.

Some insight into this question of load position is readily derived from the following simplified lumped-parameter description of the circuit. Let L and R be the total inductance of the circuit consisting of the moving plasma conductor, electrodes, leads, and load. Let u be the speed of the plasma conductor and B , the magnitude of the applied field through which it moves. Neglecting displacement currents the Kirchhoff equation for the circuital current I is

$$\frac{d}{dt}(LI) + RI = uBd s(t) \quad , \quad (2.5.22)$$

where d is the interelectrode spacing and $s(t)$ is a unit step function in time, taking $t = 0$ as the time the plasma conductor first bridges the electrodes.

In general, u , B , L and R are time dependent. The parameters L and R depend explicitly on the position of the load. For simplicity in the present analysis let the resistance be considered essentially constant, R_0 say.

If now the inductance is expanded in a power series of a suitable expansion parameter, α , the current can be similarly expanded:

$$L(t, x) = L_0 + \alpha L_1(t, x) + \dots \quad (2.5.23)$$

and

$$I(t, x) = I_0(t) + \alpha I_1(t, x) + \dots \quad (2.5.24)$$

where x is the position of the load connections from the upstream end of the electrodes. Substituting into (2.5.22) yields the following equations for I_0 and I_1

$$L_0 \frac{dI_0}{dt} + R_0 I_0 = uBd s(t) \quad (2.5.25)$$

$$L_1 \frac{dI_1}{dt} + R_0 I_1 = -I_0 \frac{dL_1}{dt} - L_1 \frac{dI_0}{dt} \quad (2.5.26)$$

It is to be noted that the right hand side of the Equation (2.5.26) for I_1 contains a source term proportional to I_0 and is positive when the inductance decreases with time. This term accounts for the voltage induced in the plasma conductor as it moves through the magnetic field arising from the current I_0 .

If it is assumed that u and B are substantially constant, the solution of (2.5.25) is simply

$$I_0(t) = \frac{uBd}{R_0} (1 - e^{-t/\tau}), \quad 0 \leq t \leq \mathcal{L}/u \quad (2.5.27)$$

where the current rise time is $\tau \equiv L_0/R_0$ and \mathcal{L} is the length of the electrodes.

The solution of (2.5.26) is, after partial integration,

$$I_1(t, x) = \frac{L_1(t, x)}{L_0} I_0(t)$$

$$+ \int_0^t \frac{L_1(t, x)}{L_0} \frac{dI_0}{dt} dt \quad (2.5.28)$$

Given the functional dependence of L_1 on time and the position of the load connections the current can be determined.

The average power delivered to a load resistance R_L is evidently

$$\bar{P} = \frac{u}{\ell} \int_0^{\ell/u} I^2(t, x) R_L dt. \quad (2.5.29)$$

An extreme in the average power occurs when the load is positioned at x as given by $\partial \bar{P} / \partial x = 0$ or

$$\int_0^{\ell/u} I(t, x) \frac{\partial I(t, x)}{\partial x} dt = 0. \quad (2.5.30)$$

As a particularly simple example of the effect of varying the position of the load consider the limiting case for which the current rise time is long compared with the transit time of the plasma conductor along the electrodes. According to (2.5.24), (2.5.27), and (2.5.28) then

$$I(t, x) \approx I_0(t) - \alpha \frac{L_1(t, x)}{L_0} I_0(t), \quad \tau \gg \ell/u. \quad (2.5.31)$$

Substitution of the current given by (2.5.31) into condition (2.5.30) yields

$$\int_0^{\ell/u} I_0^2 \frac{\partial L_1(x - ut)}{\partial t} dt = 0, \quad (2.5.32)$$

when terms to first order in α are retained in \bar{P} . It is assumed that L_1 is a function of the distance between the plasma conductor and the load connections. For definiteness consider a primitive bilinear function, namely,

$$L_1(x - ut) = L_0 \left| \frac{x - ut}{l} \right|. \quad (2.5.33)$$

According to (2.5.32) then the condition for a maximum in load power occurs when the load connections are at a distance x from the upstream end of the electrodes as given by

$$\int_0^{x/u} I_0^2(t) dt = \int_{x/u}^{l/u} I_0^2(t) dt. \quad (2.5.34)$$

Thus, it is found that in the case for which $\tau \ll L_0/R_0 \gg l/u$ the load connections should be made at point along the electrodes on either side of which the areas under $I_0^2(t)$ are equal.

In addition to consideration of load position there is the question of the load impedance for maximum power transfer. The usual statement of the power-transfer theorem is that the load impedance should be the complex conjugate of the generator impedance; that is, a negative inductance should be inserted in series with the load. Crudely applied to the present model, the theorem would require that a capacitor on the order of

$$C \sim \frac{4L_0}{R_0^2} \quad (2.5.35)$$

should parallel a load resistance equal to the internal resistance of the generator.

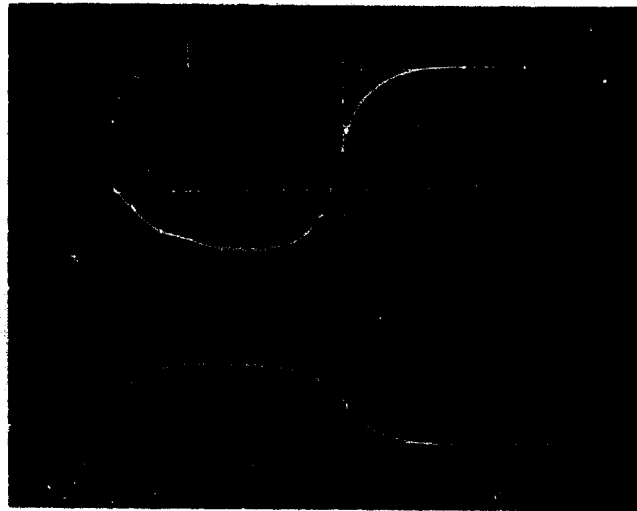
In conclusion, it is perhaps noteworthy that Equation (2.5.22) admits an integrating factor $\exp \int \frac{R}{L} dt$ which leads readily to the general solution

$$I(t) = \frac{d}{L} e^{-\int_0^t \frac{R}{L} dt} \int_0^t u B e^{\int_0^t \frac{R}{L} dt} dt, \quad 0 \leq t \leq \ell u. \quad (2.5.36)$$

The above solution for the current by successive approximations is practically useful only if the time-variant contribution by the electrodes to the total inductance is relatively small. Solution (2.5.36) is of course not restricted by this condition and may be useful for more detailed analytical investigations. It should be appreciated that in reality R , B , and u as well as L will be time varying. If these parameters can be experimentally determined, numerical methods can be used to determine the optimum position of the load.

2.5.10 Probe Studies

When using the long continuous electrode in the explosive-driven MHD channel, it is sometimes difficult to determine the position and the velocity of the front of the conductive detonation product slug. To assist in determining this information and to estimate the length of the conductive region, a series of four probes was installed in the upper electrode of the generator. This electrode would normally be negative with respect to ground and would be considered the anode inasmuch as it is required to collect electrons in order to carry the generator current. The four probes were copper wires 1.5 mm in diameter which were installed in holes drilled through the four electrode mounting bolts. The probes were insulated from the electrode structure and were flush with the surface of the electrode, in contact with the gas stream. The probes were mounted at distances of 4.5 cm, 14.6 cm, 24.7 cm, and 40.0 cm respectively from the trigger electrode. For these experiments which we conducted in the 1 inch by 1 inch channel, the magnetic field was 1.7 k/m^2 and the initial pressure was 10 mm Hg of either air or argon. Figure 2.28 is a typical oscilloscope trace for a shot in 10 mm Hg of



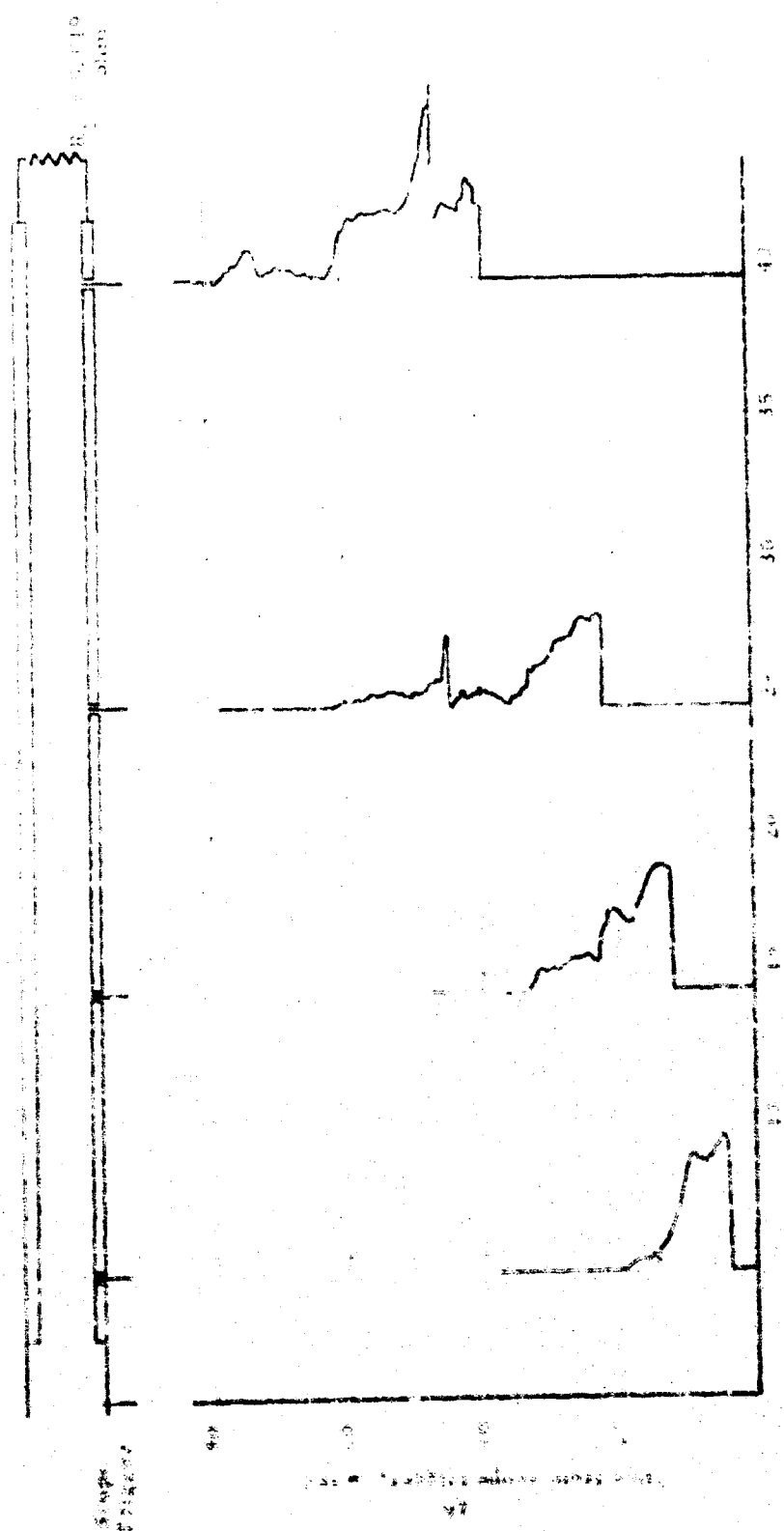
Typical oscilloscope trace showing current (lower trace) and voltage (upper trace) in 1 inch by 1 inch explosive-driven MHD generator during probe experiments. Peak current is 7.0 kA, peak voltage 140 volts, sweep speed 10 microseconds/cm. Magnetic field is 1.7 w/m^2 , initial channel pressure 10 mm Hg of air.

Figure 2.28

air. The generator load is 19 milliohms. The sweep speed is 10 microseconds per cm. The upper trace is the voltage at 50 volts/cm, and the lower trace is the current at 5.35 kA/cm. The peak current is approximately 7 kA. The peak power is approximately 1 MW and 43 joules of energy are delivered to the load. Figure 2.29 is a composite drawing which shows the four probe traces plotted with their origins at the appropriate distance along the channel in the form of an X-t diagram. It can be seen that detonation products propagate in air with a sharply defined front. It is also apparent that the slug of detonation products expands as it flows down the channel which would cause a distribution in velocities along the conducting slug. This velocity distribution, as discussed in Section 4.5.5, may account for the reduction in the open circuit voltage. It is also noted that there is a sharp spike in the traces for the third and fourth probes at about 46 microseconds, apparently when the rear of the conductive slug leaves the electrode.

It can be seen that the velocity is attenuated slightly as the detonation products move down the channel. The initial velocity is approximately 12.1 km/sec, which slows down to 8.9 km/sec between the third and fourth probes. The average velocity is 10.5 km/sec over the length of the channel with this load. An average of data taken with an 0.5 ohm load resistor, which is almost equivalent to an open circuit condition, indicates an average velocity of 10.5 km/sec. These results would imply that the removal of 40 joules of energy has slowed the detonation products by 0.2 km/sec.

A number of similar shots were made with argon as the initial gas in the channel. In the argon shots there is a precursor which causes the



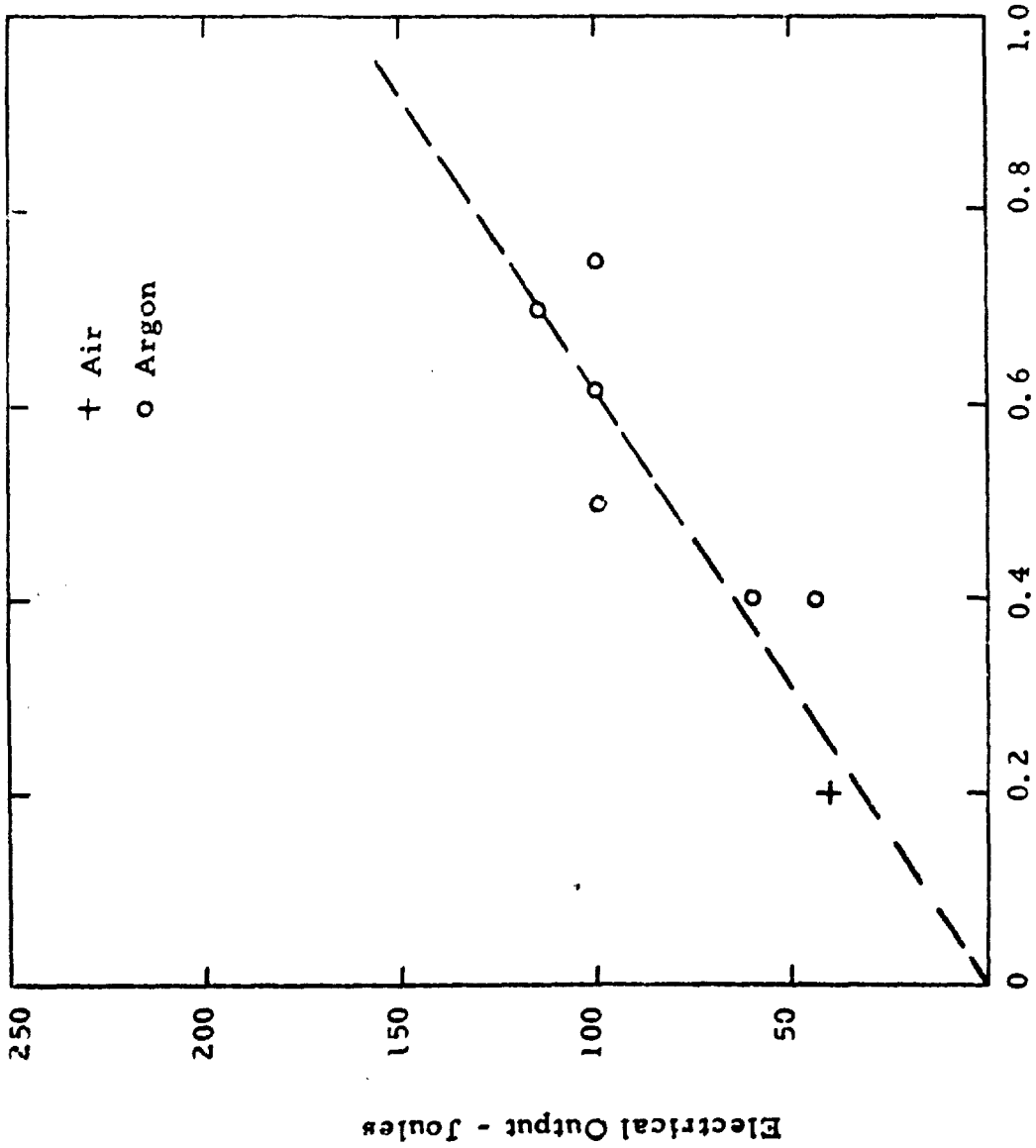
Distance from trigger point, cm

Top of graph shows traces from four 1.0 cm dia. probes installed through the top of the tube to the 1.0 cm diameter driver Mill generator. The probes are connected to the 2 tubes with 50 ohm terminated coaxial cables. Initial pressure in the test chamber is 10 mm Hg, 25.33 K. It is apparent how the conducting pulse widens with distance down the channel.

FIGURE 4.29

voltage on the probe to rise before the conductive slug arrives. It is generally possible to determine the arrival of the conductive slug by a steep increase in voltage on the probe. The data from the argon shot are contained in Table 2.8 which lists the load resistance, the peak current, and the time for the detonation products to reach the fourth probe. While there is some scatter in the data, several shots have been taken with each load resistance so that there is some degree of confidence in the results. It can be seen that as the load resistance is decreased and energy is removed from the detonation product stream, the time for the detonation products to reach the fourth probe increases, indicating a decrease in velocity.

Figure 2.30 is a plot showing the change in velocity as a function of the number of joules delivered to the external load. It can be seen from Figure 2.30 that removing 16.5 joules of electrical energy slows the detonation product front by 0.1 km/sec. This data supports the previous assumption that the velocity was not markedly changed in the present experiments by the MHD interaction.



Velocity Change - KM/sec
 Change in velocity of conductive detonation products as a function of extracted energy in explosive-driven MHD generator. Generator channel is 1 inch by 1 inch, by 16 inches long. Magnetic field is 1.7 w/m^2 . Average velocity without energy extraction is 10.4 km/sec . Figure 2.30

TABLE 2.8

DATA TAKEN DURING PROBE EXPERIMENTS IN 1 INCH BY 1 INCH
CHANNEL SHOWING SLOWING DOWN OF DETONATION PRODUCTS AS
ELECTRICAL ENERGY IS GENERATED

Load Resistance ohms	Current kA	Power MW	Energy joules	Time to Travel 40 cm
9.5	0.048	0.025	1.2	38.5
0.5	0.685	0.24	11	38.5
0.5	0.642			39.0
0.096	3.1	0.92	441	40.0
0.096	3.1			40.0
0.051	4.71	1.25	60	40.0
0.051	5.14			40.0
0.0195	10.7	2.0	100	40.0
0.0195	10.2			41.0
0.0145	11.75	2.0	98	41.0
0.0045	23.6	2.4	115	41.0
0.0045	22.5			41.5
0.0013	na	2.08	100	41.0
0.0013	39.1			42.0

3.0 LONG DURATION PULSED POWER

3.1 Introduction

The conversion of chemical energy stored in condensed explosives into useful electrical energy through MHD methods described in Section 2.0 of this report has produced encouraging results for times up to approximately 100 microseconds. Many applications for pulsed electrical power will require pulses for longer durations than can be achieved with detonating systems. Therefore, this phase of the program was oriented toward conversion systems using slower burning, deflagrating compounds with the objective of achieving pulses ranging from 1 millisecond to 1 second or more.

In these experiments, deflagrating compounds are used to generate hot gases in a combustion chamber. These gases contain low ionization potential materials, which are partially ionized at the flame temperature. The ionized gases are then expanded into the MHD power generation channel which has a transverse magnetic field. Electrical power is generated by the relative motion of the conducting gases through the magnetic field. Calculations and experiments indicate a conductivity level of 1000 mho/meter.

The following sections briefly describe the experimental apparatus and the summarize experimental data obtained. Background information on the design of the apparatus, the choice of propellant systems and the detailed results of previous experiments are contained in References (1) and (2).

3.2 Experimental Apparatus

3.2.1 Design Objectives

The major design objective was to achieve versatility of the test apparatus, permitting relatively easy modifications to be made of as many

gas dynamic parameters as practical. The configuration chosen was such as to produce high velocity gases with high conductivity. The important parameter to be maximized in these experiments is the product of conductivity times the velocity squared, σu^2 . To a first approximation, this will result in the maximum power production per unit volume for a given value of magnetic field. The high conductivity was achieved by the high temperature combustion of light metals (B and Al) with alkaline metal nitrate oxidizers (KNO_3 and $CoNO_3$).

The basic facility used in the long duration pulse power experiments is shown in Figure 3.1. A photograph of this disassembled hardware is shown in Figure 3.2. Figure 3.3 shows how the test section was modified for the power generation experiments which are reported herein.

3.2.3 Combustion Chamber

The hot ionized gases are generated in the combustion chamber, then expanded through a nozzle into the test section. The combustion chamber was sized for a deflagrating charge of 100 gms. Details of the combustion chamber are shown in Figure 3.4. Provision was made in the face plate for appropriate tungsten or carbon nozzles which were varied as to size and material.

The nozzle plate was subject to many changes. Early experiments with a 1/8-inch diameter hole in a stainless steel plate resulted in clogging with attendant reduction in orifice size. This clogging was assumed to result from condensation of combustion products, especially the solidification of liquid alumina impinging on a cold nozzle plate when using Al/ $CoNO_3$ charges. Subsequent plates were fabricated from brass, with a carbon face toward the

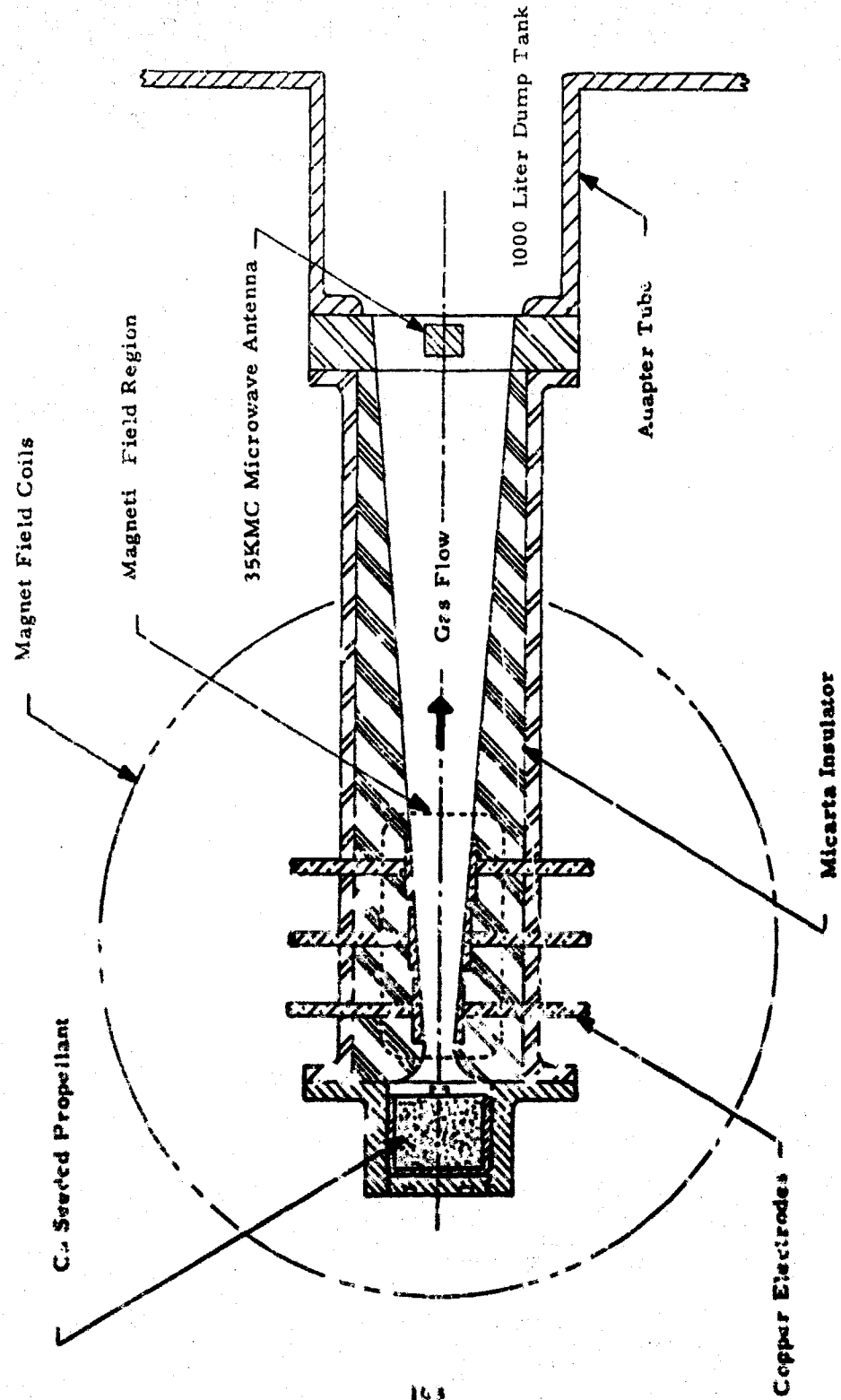
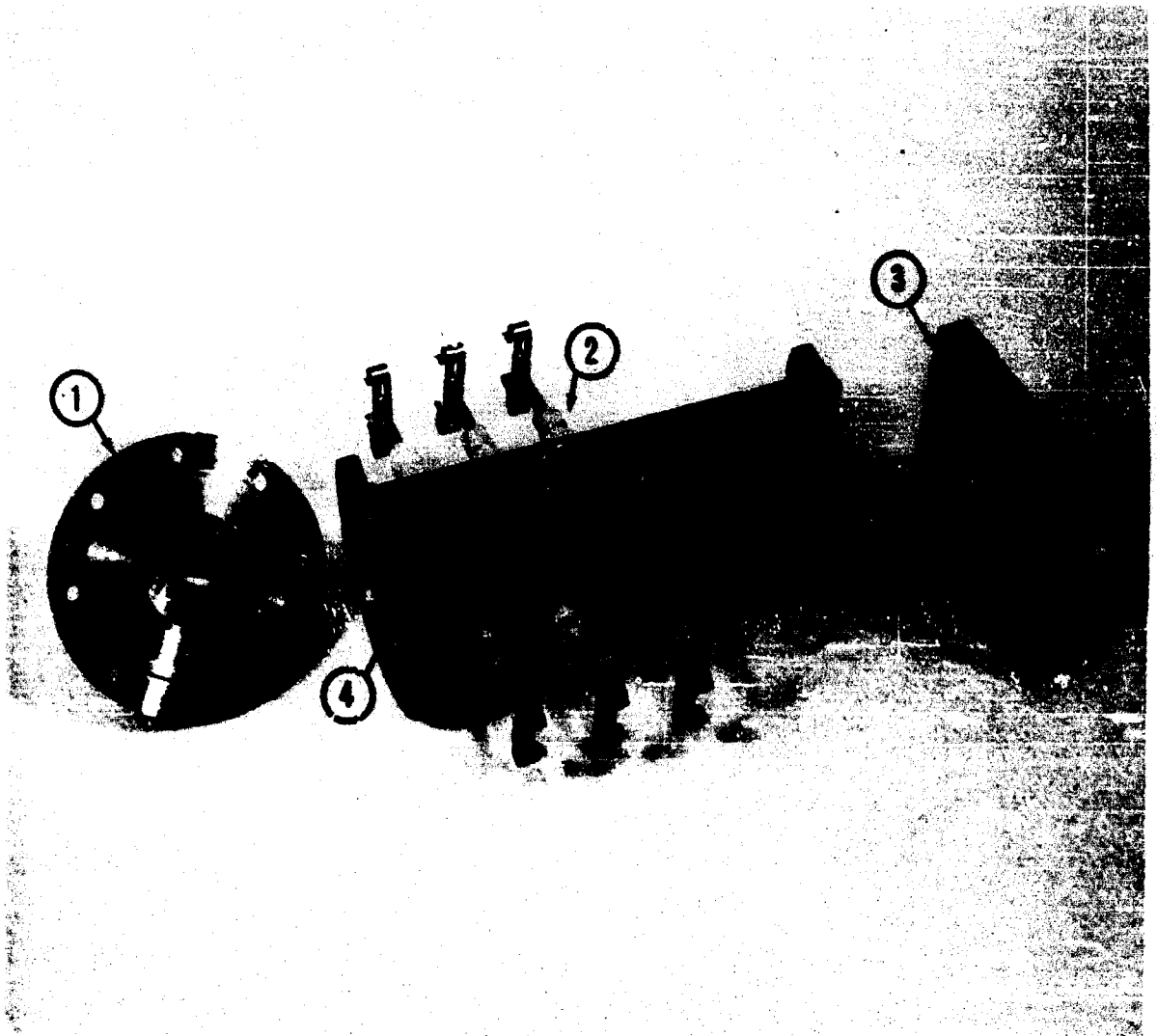
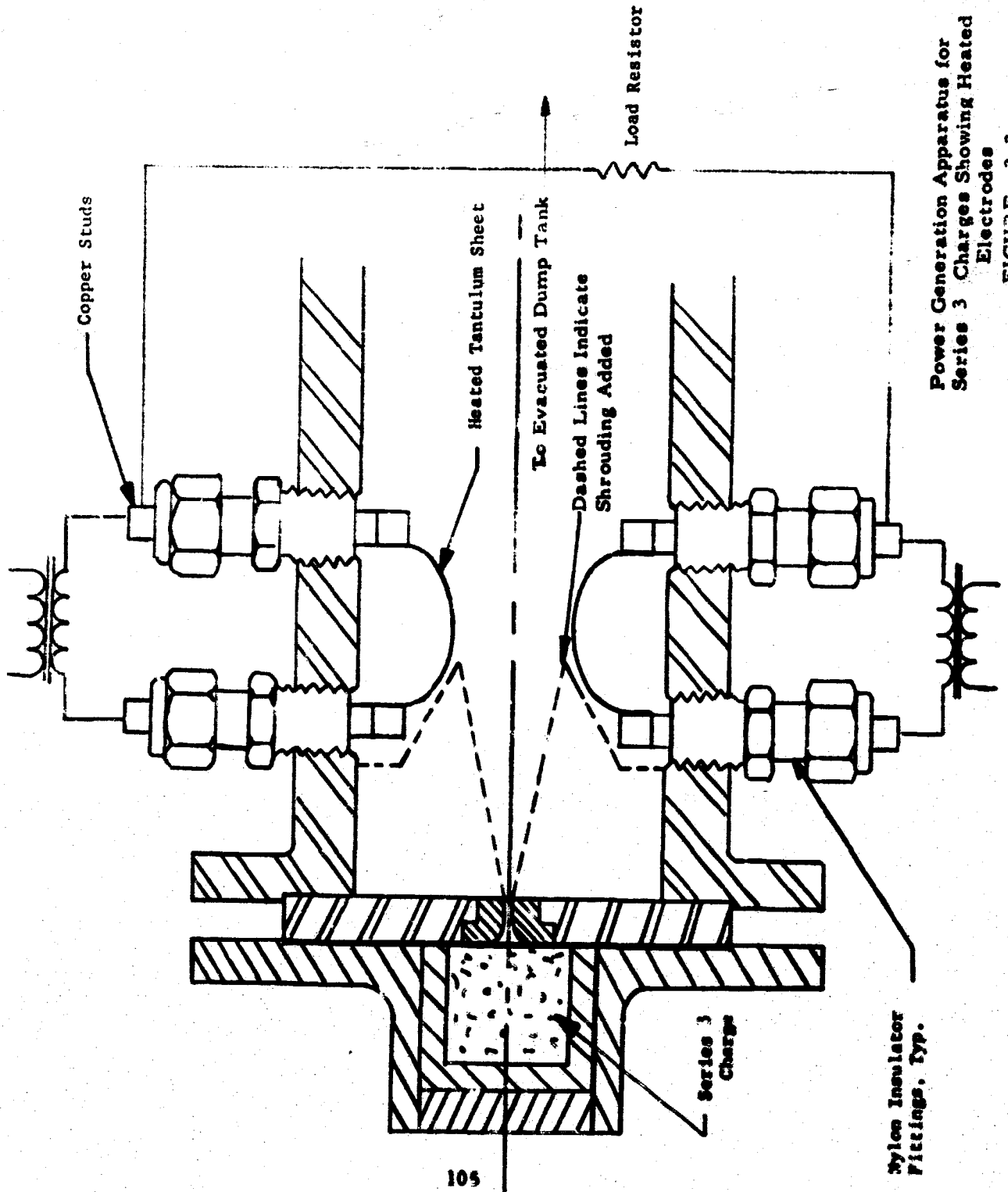


FIGURE 3.1 Long Duration Pulse Power Facility, used for Series I Charges



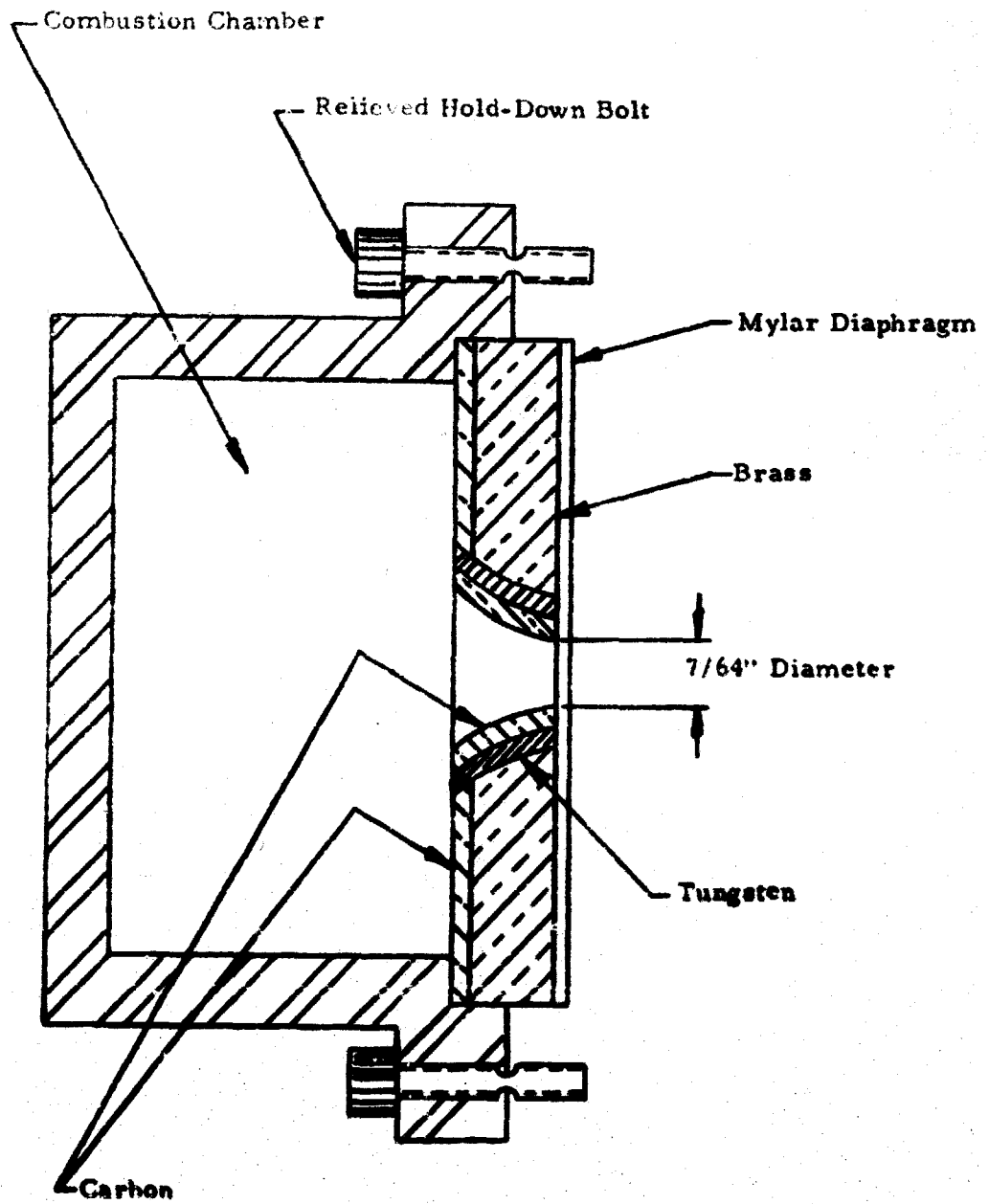
1. Combustion chamber section
2. Zytel insulator
3. Microwave instrumentation flange
4. Electrode face
5. Micarta sidewalls

Figure 3.2
Disassembled view of supersonic MHD channel



Power Generation Apparatus for Series 3 Charges Showing Heated Electrodes

FIGURE 3.3



Cross Section of Combustion Chamber and Nozzle Plate.

Figure 3.4

combustion chamber to reduce heat loss and with tungsten nozzle inserts faced with carbon. The size of the nozzle orifice played an important role in all runs. Conductivity is a sensitive function of combustion chamber pressure which is controlled by the nozzle orifice area for a given mass flow rate. Ignition of the explosive was vitally effected by pressure, i. e., the burning rate is pressure sensitive. If the pressure does not build up rapidly the charge will not ignite. The velocity of the hot gases in the MHD generator section is also controlled by the nozzle orifice size. The best operation was obtained in this system using the Al/CsNO₃ charges with a 7/64-inch diameter orifice designed and fabricated as shown in Figure 3.4.

The chamber casing is fabricated of stainless steel tubing with 1/2-inch thick walls. Provision was made for a threaded breach plug to facilitate loading. Ports were provided for pressure measurements and for ignition wires.

The hold down bolts on the combustion chamber were relieved in cross section as shown so that they would fail and vent the chamber at a pressure of approximately 1000 psi. This occurred during one run at 900 psi when the nozzle plugged.

3.2.3 Test Section

Test sections used in experiments are shown in Figures 3.1 and 3.3. The basic configuration shown in Figure 3.1 had a small throat which gradually increased to a maximum chamber size at the dump tank end of the chamber. As can be seen from the photograph, Figure 3.2, this channel has straight interior sidewalls so that the channel was of constant width with gradually increasing height, permitting much easier calculations as a one-dimensional expansion.

The channel, as shown in Figure 3.3, has been modified to include heated tantalum electrodes as well as to include modified channel walls used to provide a two-dimensional supersonic expansion of the flow channel.

The test section is preceded by a rupturable mylar diaphragm (sometimes augmented with aluminum foil sheets) to maintain pressure into combustion chamber for ignition. The outer casing of the test section, together with all down-stream fittings and components, are sealed to provide for evacuation or pressure when required.

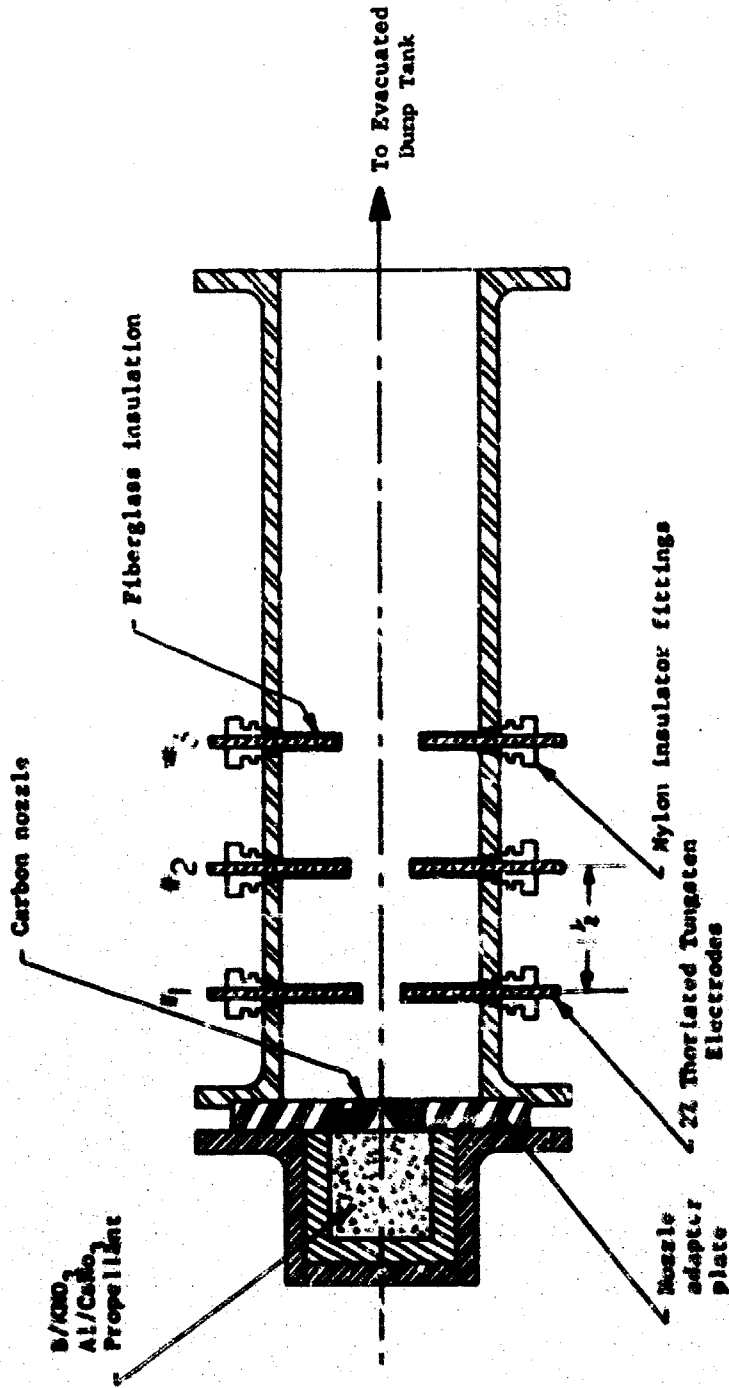
3.2.4 Electrodes

Electrodes of the basic configuration were fabricated of solid copper as shown in Figure 3.1 and were sheathed with 1/8-inch zytel fittings for insulation. Other configurations used straight 1/8-inch O.D. 2% thoriated tungsten rods (see Figure 3.5) or the heated electrodes fabricated of tantalum sheet as shown in Figure 3.3 which were heated either by 60-cycle current or an exterior 6 volt battery.

3.2.5 Magnet

A small electromagnet with pole faces approximately 2 inch by 4 inches and capable of producing up to 1.0 w/m^2 has been used with this apparatus. This is a level similar to that which can be produced by a permanent magnet. The use of permanent magnets in a pulsed power generator may be desirable for certain applications. The position of the magnet pole faces relative to the electrodes used in the basic configuration is shown in Figure 3.1.

Electrode Pair	Separation
1	1/2"
2	3/4"
3	1"



Schematic for the 60 cycle conductivity measurement.
FIGURE 3.5

Exhaust System

The gases discharge from the test section into a dump tank of 1000 liter capacity. The gaseous products of the discharge can be highly corrosive and toxic, hence they are exhausted from the dump tank through the roof of the laboratory building. The dump tank is connected to a vacuum pump such that it may be evacuated before each shot. The pressure in the tank serves to regulate the pressure in the downstream end of the test section. The 1000 liter volume has been calculated to be adequate such that the change in pressure during the burning time of the propellant charge will be of the order of a few percent.

Conductivity and Power Measurement Instrumentation

The electron densities and mobilities predicted for the various chemical systems considered for use in these experiments indicated that the conductivity, σ , is variable over a wide range and is difficult to calculate with any accuracy. However, it is the most important parameter in the power generation process. A major objective of experiments and instrumentation then, has been to determine conductivity as accurately as possible.

The primary approach to this measurement is to determine the shape of the characteristic voltage versus current (V-I) curves. It is recognized that true conductivity is masked by generator end effects, sheath voltage drops, probe effects and fringing effects, however, auxiliary experiments can be employed to evaluate these correction factors. The largest of these factors is the electrode sheath voltage drop which was evaluated during a series of conductivity measurements reported in Section 3.4.

In order to determine the generator internal resistance, from which the conductivity can be determined, the voltage and current through the generator are recorded for various external loads. The generated electric fields are of the order of 10 volts/cm with a 10 kilogauss magnetic field, so that with a 3 cm electrode separation, the open circuit voltages are of the order of 40 volts. With the indicated conductivities, the peak currents are of the order of 10 amperes or less. Provision was made to record the current and output voltage continuously as various load resistors are automatically switched into the circuit. The cycle between open circuit and short circuit is repeated several times a second. From a plot of the voltage-current characteristic, the internal resistance or conductance of the generator can be determined.

In addition to the instrumentation for directly obtaining the V-I curves, 10 Gc microwaves have been employed in a microwave interferometer system. The measurement of microwave attenuation and phase shift is made at the downstream end of the test chamber where the gas density at supersonic flows is at a minimum. These measurements indicated that the electron density was greater than 10^{13} cm⁻³. Other systems for measuring the conductivity are discussed in a later section.

3.2.8 Pressure Measurement Instrumentation

The pressure in the combustion chamber was measured by a 1 to 1000 psi fast response strain gauge transducer. This measurement is mainly used for determining the combustion rate and the mass flow rate. A similar transducer is also mounted at the exit of the test section to determine the pressure drop so that the velocity can be calculated.

3.2.9 Recording System

The data from the assorted sensors, the voltages across the load resistances and the voltages across the current shunts were recorded on a Consolidated Electrodynamics Corporation Model 5-114 multichannel recorder. Up to 18 channels can be recorded simultaneously. Fluid damped galvanometers capable of 100 cycles per second response were used.

3.3 Power Generation Experiments

The objective of this program is the generation of long pulses of power by MHD principles, using solid propellants as the energy source. During the contract period many runs have been made during which MHD power was generated. The seeded solid propellants which were used had a very high electrical conductivity. It was expected that the power outputs should have been much higher than those actually observed. However, one main disadvantage of these runs has been the small scale of the experiment, dictated by safety considerations. It is believed that electrode drops observed in the conductivity measurements to be reported in Section 3.4 were a major factor limiting the power output. These experiments suggest a favorable scale-up potential. In these experiments four different types of charges were used. For the first series (Series 1) the charge was a standard ammonium perchlorate resin propellant which had been seeded with $CsNO_3$. The remaining three sets of experiments were conducted with aluminum-cesium nitrate charges which incorporated various amount of boron-potassium nitrate in the initial layers for ignition assistance. Table 3.1 gives the details for the various charges.

TABLE 3.1

Charges Used in Long Pulse Power Generation

Series 1.

Six charges of this series were prepared and used to test the facilities.

NH₄ClO₄ 76 parts by weight
 Genpol A-20 Resin 14 parts by weight
 Styrene, *n*-Butyl Catechol 10 parts by weight
 100 parts by weight

(Three of the above had 1 part by weight CsNO₃ powder added in bulk before casting, the other three had 2 parts CsNO₃ added).

Series 2.

Prepared in layers with Layer 1 nearest ignitor.

Layer	wt(gm)	B/KNO ₃	Al/C NO ₃
1	1	100%	0
2	4	40%	60%
3	8	8%	92%
4	5	0	100%

Series 3.

Prepared in layers with Layer 1 nearest ignitor.

Layer	wt	B/KNO ₃	Al/C NO ₃
1	1 gm	100%	0
2	4	40%	60%
3	8	8%	92%
4	25	0	100%

Series 4.

Prepared in layers with Layer 1 nearest ignitor.

Layer	wt	B/KNO ₃	Al/C NO ₃
1	1	100%	0
2	4	40%	60%
3	8	8%	92%
4	25	0	100%

The initial power generation runs, using the Series 1 and Series 2 charges, were conducted in the channel arranged as shown in Figure 3.1, or in an alternate arrangement where 2% thoriated tungsten rod electrodes were used, similar to the geometry used in the conductivity experiments. These experiments indicated open circuit potentials of about 30 volts, which would yield supersonic velocities in the smooth contoured flow channel. Measurements with the stub electrodes yielded subsonic velocities indicating that shocks were occurring. No current could be measured within the sensitivity of the apparatus, which had been calibrated for a very highly conductive plasma flow.

For work with the Series 3 charges the externally heated tantalum sheet electrodes shown in Figure 3.3 were employed. It was hoped that the high temperature of the electrodes would not only deter condensation of flow products; but in addition, the tantalum should emit thermionically providing a cathode with a lower potential drop. The electrodes were heated by 60 cps alternating current. The spacing for the gap between electrodes was determined from optical observations of the edge of the jet made during previous runs.

For the first run with this apparatus, a single 0.122 ohm load was connected across the electrodes. The open circuit voltage across a set of downstream electrodes was used to monitor the gas velocity. The electrodes were heated to a brightness temperature of 1900°K (2020°K true) two seconds prior to firing.

Figure 3.6 shows the recorded current through the load. The power generated is disappointingly low, never exceeding 2 watts. The current was at least a factor of 10 greater than the calculated thermionic emission of tantalum at 2000°K (16 ma/cm^2 vs 1 amp. cm^2). The voltage probes indicated that the

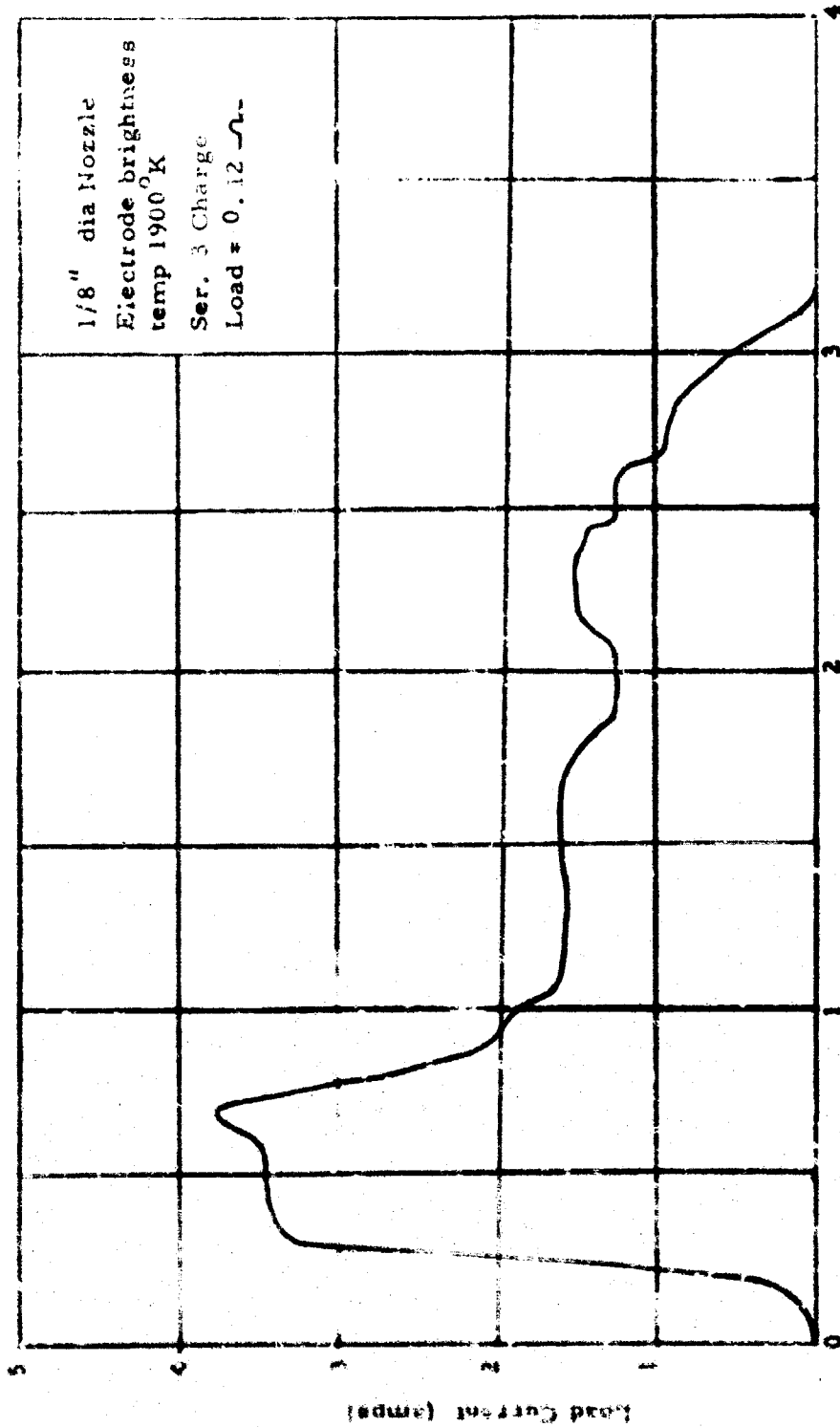


Figure 3.6. Load current vs. time

gas velocity was about 1.450 km/sec at the downstream station, which is definitely supersonic. One possible explanation for the low power level is that the electrodes did not contact the plasma and should have been moved inward for better contact. Another possible explanation considers the existence of a large sheath drop despite electrode heating.

To determine if electrode temperature was a factor, a run was made with the electrodes at $T_b = 2050^\circ\text{K}$. The motivation was that if the currents extracted are limited by an emission process at the dirty cathode, then perhaps a higher cathode temperature would help. The load was changed to 1 ohm with the magnetic field remaining the same (1.07 w/m^2). The shot was normal. The resulting voltage drop across the load for this shot is shown in Figure 3.7. The maximum power level is 29 watts. The current trace had a shape similar to that of the previous shot. The maximum currents for both shots were of the same magnitude. The open circuit voltage on the downstream probe was abnormal. At run commencement the voltage went to ~ 3 volts where it remained until burnout. This could indicate subsonic flow at this location or shorting across the sidewalls.

From this run it can be concluded that either the poor electrode contact or subsonic flow, or both, were factors limiting the power output in these experiments. Subsonic flow can be caused by the presence of the electrodes which produce local shock waves. The maximum power generation, about 30 watts, occurred during the burning of layer 3 of the propellant at a pressure between 300 and 400 psi. Layer 3 consists of 8 gms of 92% CaNO_3/Al and 8% KNO_3 . The higher power level at the high pressure could be the result of four factors which are all a part of the propellant formulation:

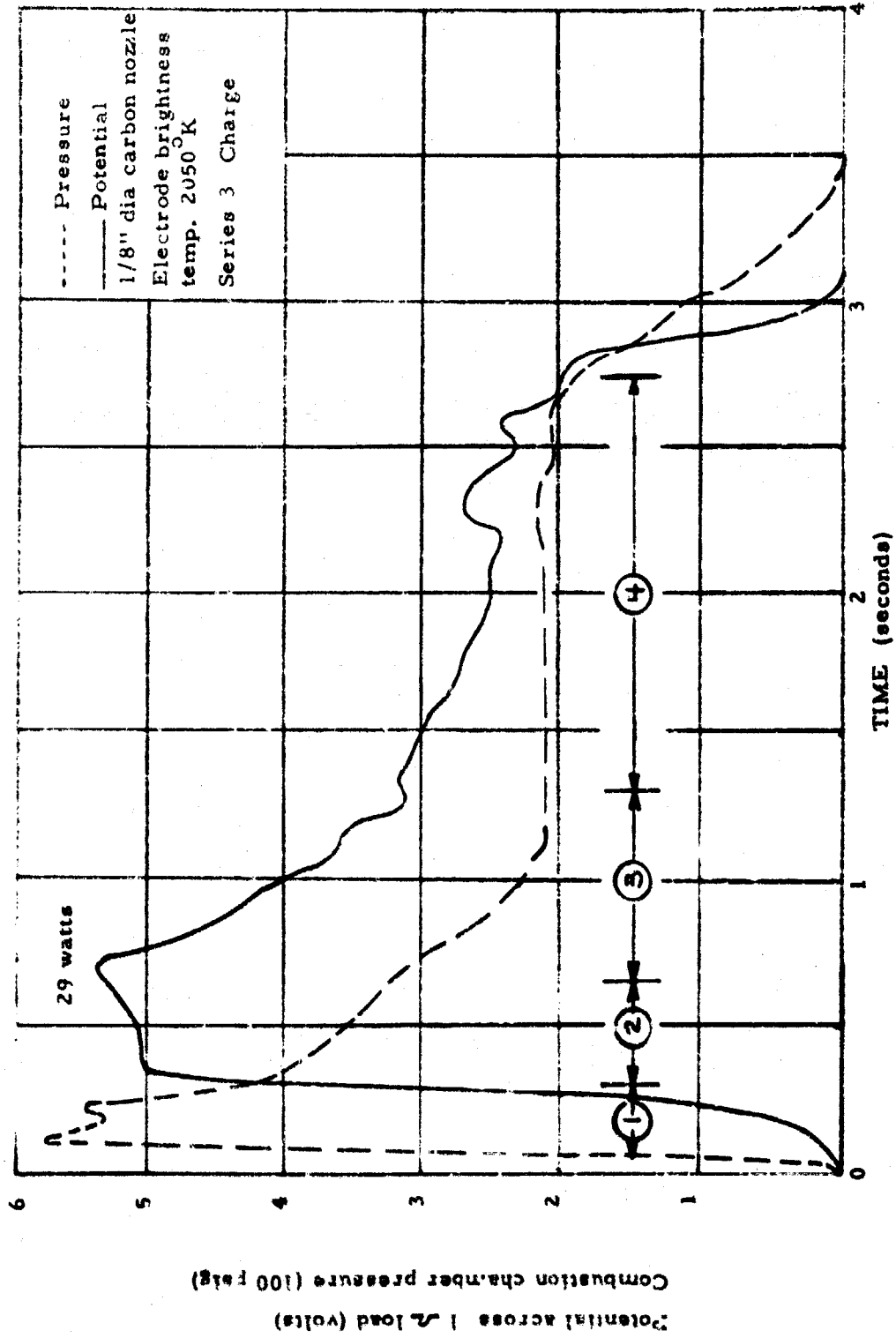


Figure 3.7 Voltage output and burning pressure (circled numbers approximate layer of charge burning at that time). See Appendix B, Figure B.2)

MHD research, inc.

The B/KNO₃ increases the burning rate. This raises the chamber pressure for a constant nozzle area; hence the combustion temperature is higher. Since the initial electron density is highly temperature dependent, the resultant jet is hotter and has more free electrons; hence, higher conductivity. The power varies directly with the conductivity.

(a) When the combustion pressure is high the resultant mass flow and gas velocity are increased producing a higher induced voltage. Power is proportional to velocity squared.

(b) When some B/KNO₃ is present, the average molecular weight of the products is lower, producing a higher velocity jet for a given initial temperature.

(c) At any given temperature a mixture of K and Cs bearing products may yield a higher electron density than that of a compound containing only Cs because of the large mass difference between K and Cs. There are about three times more potassium atoms/gram of burned material than cesium. Even though there is a large difference in ionization potential it is possible to obtain a higher electron density from a mixture in these experiments since the temperatures are high enough (~4000°K) so that large percentages of both Cs and K are ionized.

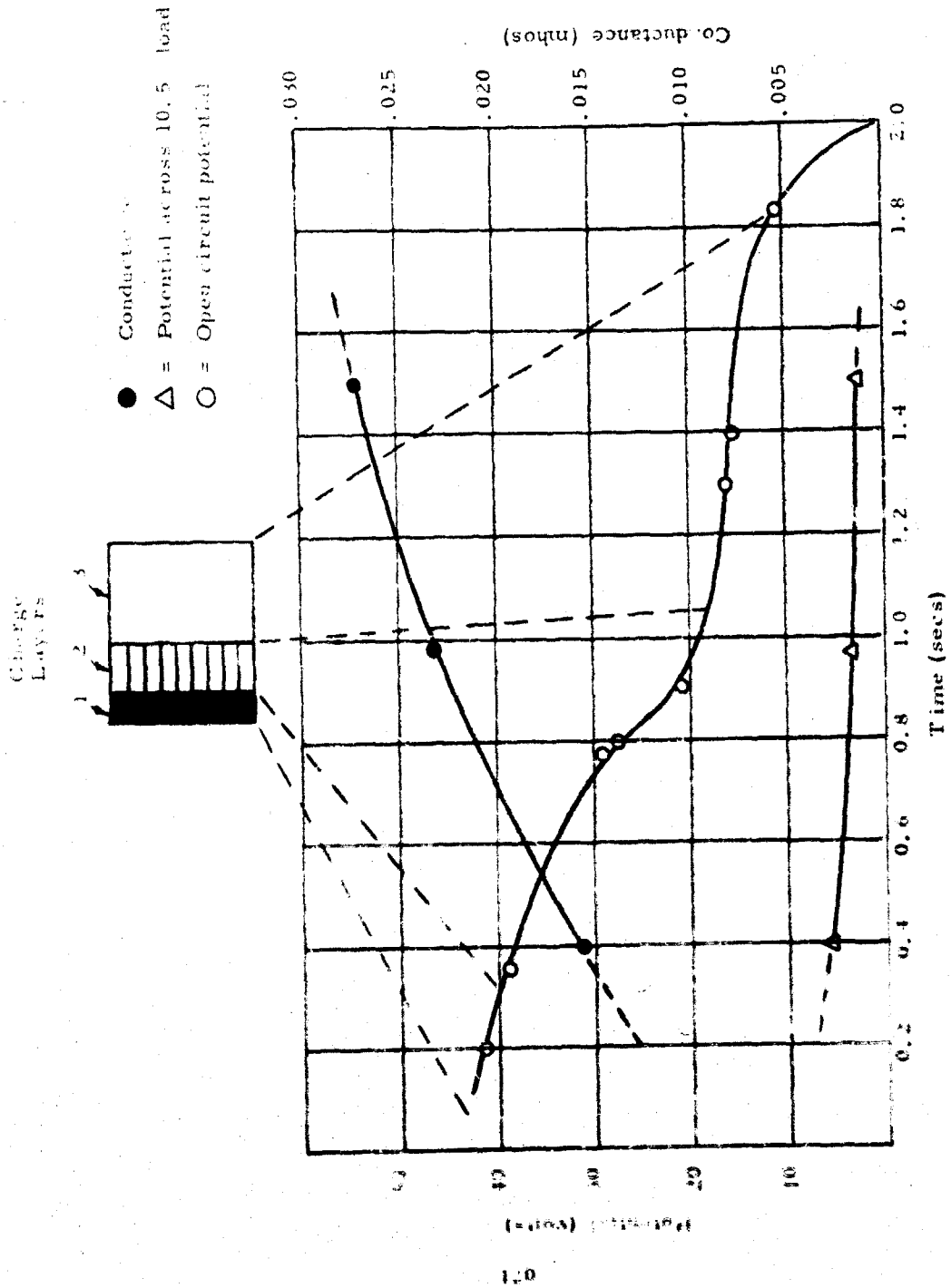
(d) The manufacturer of the charges had indicated that electron yields for the Al/CsNO₃ charges are satisfactory only when the combustion pressure is higher than 300 psi; this tends to support statement (a) above.

Due to the wide difference in indicated gas velocity during the different runs, it was decided to abandon the free jet approach and shroud the electrodes with a supersonic nozzle. This is indicated by the dashed lines in

Figure 3.3. The electrodes were widened to 3/4 inch to form a rectangular flow channel (3/4 inch by 1 inch at the center of the electrode station) giving an area ratio of 80. This would indicate a flow Mach number of 4.7 for a gas with $\gamma = 1.2$. A motor-driven rotary switch apparatus was arranged to cyclically apply four different loads (10, 1.0, 0.1, and 0.01 ohms) to the electrodes.

The channel was tested with the Series 3 charges in a run where the electrodes were heated immediately prior to firing. The run was normal and occurred without incident. On development of the recording chart, it was seen that the characteristic pressure trace was recorded. However, the current trace went off-scale steeply on initiation of the first layer of the charge. It was found that the gain had been set too high through plugging in the wrong galvanometer. The current during the run was always in excess of 3 amps. Inspection of the channel after the run showed that supersonic flow had existed in the diverging section. Proof is given by shock reflection patterns on the sidewalls at the end of the diverging section. There was extreme erosion of the mica forming the supersonic portion nearest the throat and some slag deposition downstream near the electrodes.

The configuration shown in Figure 3.3 was then used in a run with the Series 4 charges. The Series 4 charge differs mainly in that the 100% B/KNO₃ layer is not used. Figure 3.8 shows the open circuit voltage, and the voltage across a 10.5 ohm load resistor as a function of time during this run. From the two data points, open circuit and 10.5 ohm load, voltage current curves can be plotted to yield the generator internal resistance, or conductance, which is also shown in Figure 3.8. The pressure trace is similar to those shown in Figures 3.6 and 3.7 and is not reproduced here.



Voltage and conductance data for Series 4 charge run.

Figure 3.8

It is seen that the velocity, as indicated by the open circuit voltage, decreases with time, as the combustion chamber pressure drops. The flow is initially supersonic, as indicated by the high open circuit voltage, then becomes subsonic at about 1.0 seconds. However it is seen that the highest conductance, which is proportional to conductivity, occurs during the burning of the Al/CsNO₃ portion of the charge. The peak power generated during this run was approximately 3 watts which occurs early during the run when σu^2 is a maximum. It would thus appear that a B/KNO₃ - AlCsNO₃ mixture would be preferred for pulsed power generators. Further work in the evaluation of optimum propellant formulations is indicated.

In general it may be concluded that there are several limitations in using the present sized apparatus for these studies. For the small sized channel the generated voltage, approximately 30 or 40 volts, is less than the electrode sheath drops. Therefore the sheath effects are a dominant factor and overshadow the power generation mechanism. Future experiments should be conducted in a channel with a wider electrode separation and/or with a stronger magnetic field.

3.4 Conductivity Measurements

One of the major efforts in this series of experiments was in the measurement of the conductivity of the seeded propellant flow stream. In addition to the determinations of conductance made during the power generation runs, experiments were conducted to measure the conductivity by means of the following techniques:

1. 60-cycle current-voltage relations,
2. 14 mc radio frequency coupling measurements, and
3. 35 Gc microwave interferometer.

The complete details of these experiments are reported in Reference (2).

The radio frequency coupling measurements and the microwave interferometer data provided limited information because of the high conductivity. However, they did confirm the measurements made at 60 cycles in that the measurements made 25 cm downstream indicated a conductivity of 100 mho/meter, at the time of peak combustion chamber pressure.

The 60-cycle conductivity measurements were conducted in the flow channel shown in Figure 3.5 with 122 volt rms 60 cycle alternating current applied to the electrode pairs. It was expected that free jet expansion would occur; hence, the electrode spacing was varied to approximate the expected envelope of hot gas liquid products.

Two runs were conducted to measure the conductivity. In the first, a 3/16 inch diameter carbon nozzle was used and the pressure did not build up sufficiently to maintain combustion; the charge burned for 1/8 inch and went out. The total burning time was 0.4 seconds. During the run the current was so high through electrode pair #1 that the shunt solder melted causing the shunt to fall out of the circuit. The final layer (layer 2) burned in this run consisted of 40% B/KNO₃ and 60% Al/CsNO₃.

The 361 galvanometers have a flat response to 8 KC; hence, faithful reproduction of the current is assured when operating at 60 cps. A maximum of 370 amps was drawn at the first electrode pair about 30 milliseconds after ignition. The voltage drop across the electrodes, as indicated by the instantaneous voltage at the start of current conduction, was measured to be initially 73 volts total for both anode and cathode. This value decreased to 29 volts 160 milliseconds after ignition. The measured conductance at 160 milliseconds (after overcoming the voltage drop across the electrodes) was 3 mhos/m.

The measured conductance can be reduced to an equivalent conductivity in a number of ways. Assuming the column of conduction to be confined to a cylindrical channel between the electrodes, the conductivity would be 4600 mho/meter. However, the confinement of the current to this channel is not realistic and an appropriate fringing factor should be used. An electrolytic mockup of this experiment was constructed and the fringing factor measured in this mockup was 2.6. The indicated conductivity for the measured conductance would, therefore, be 1.8×10^3 mho/meter. A further adjustment should be made because the edge of the insulation quickly burns off the electrodes. It is estimated that the electrode area changes such that the effective fringing factor should be 4 or 5, based on the original area. This would change the conductivity estimate to a maximum of 1000 mho/meter.

In this experiment the #2 pair started to draw current about 80 milliseecs after ignition and the #3 pair started about 230 milliseconds after ignition. A check of the conductance of the #2 pair at 300 milliseconds yields a conductivity 6700 mho/meter with no correction for fringing. Since the separation distance is greater than for electrode #1, a fringing factor greater than 5 would apply, making the conductivity at this station also close to 1000 mho/meter.

Check of conductivity at #3 electrode could not be made since it did not start conducting until 230 milliseconds after ignition and then conductivity was limited to one direction (rectifier action) with very large electrode drops.

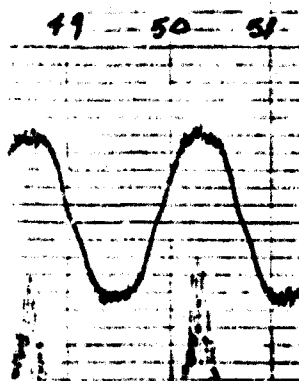
It may appear that the conductivity measurements are on the high side since the current (measured as 370 amps) heats the gas, increasing the level of ionization. However, the average electrical power input for the above mentioned run was 20 kw per electrode or less. The thermal power was

approximately 10 times this value. Hence, very little heating should be expected.

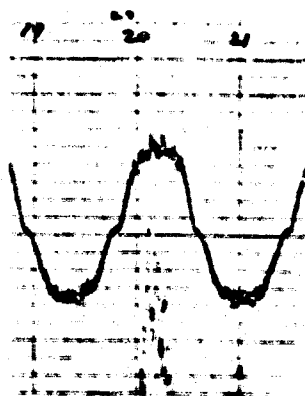
To prevent a flameout, the next run used a smaller nozzle (1/8 inch dia) and ran successfully for 0.62 seconds. In anticipation of high currents at #1 electrode a ballast resistor of 2.2 ohms was added in series with the electrode gap. The other electrodes remained the same as the previous run. All electrodes began conduction (in both directions) 10 milliseconds after ignition and ceased simultaneously when the charge was expended.

Figure 3.9 shows characteristic traces for electrode #1 at three different times. A value of conductivity derived from the last current (at 620 millisecc) yields 600 mho/meter, 1/3 the value of the previous run (1800). As the ballast resistor limits the current (55 amps peak) this would support the view that heavy currents are joule heating the plasma resulting in false conductivity values. Electrodes #2 and #3 which did not use a ballast resistor gave conductivity measurements higher than the #1 electrode. Comparison of the #2 electrode with the previous shot yielded a decrease of conductivity by a factor of two from the previous shot.

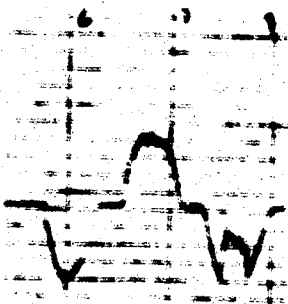
Figure 3.9 illustrates the change in electrode voltage drop as a function of time; notice the deadband decreasing. Without forced heating of the electrode by the impressed current and heat transfer from the flow stream, one would not expect a current to begin flowing with less than 50 volts. In the present experiments where $B = 1.0 \text{ w/m}^2$, $u = 2 \text{ km/sec}$, and d the electrode separation is 2.5 cm, the maximum generated voltage, $u \times B \times d$ would be only 50 volts. Experience of other investigators has shown the existence of electrode drops of this order. This result is one possible explanation for the poor output from the power generation runs not employing the heated electrodes.



A. .50 sec after ignition, less than 10 volt drop



B. .20 sec after ignition, approximately 30 volt drop



C. .06 sec after ignition, approximately 65 volt drop

FIGURE 3.9

Run #2 - 30 March 1963 Current traces on #1 electrode 1 3/8 inches
downstream, 1/2 inch separation, 1/8 inch diameter. Gain 110 amp/in

MHD research, inc.

The power output was approximately 5 watts. A number of generator load curves were taken which showed an increase in conductivity when the cesium nitrate-aluminum powder portion of the charge was burning. While this approach appears to have promise, it is indicated that further experiments should be conducted on a somewhat larger scale.

4.0 CONCLUSIONS

It has been demonstrated that short pulses of electrical power can be generated by MHD principles using either condensed explosive or solid propellant materials as the energy source. The work with the condensed explosives has been particularly successful in that large pulses of power have been obtained with relatively high conversion efficiencies. The scaling of these results to larger sizes to produce systems with greater outputs appears relatively straightforward. Additional work is needed to determine the optimum values for the various parameters, however, the basic principles are well understood and the direction for future work to increase output and efficiency can be clearly outlined.

The work with the solid propellant driven supersonic channel has been encouraging, however the results were not as spectacular as with the explosive charges. It was possible to generate power from the highly conductive flow stream, but scale effects appeared to be important. Much additional work is indicated in the areas of propellant composition and channel configuration for the two-phase (gas and liquid) flow. With the measured conductivity and the known high temperatures, very high specific power outputs should be attainable using this technique.

APPENDIX A - SCALING AND GEOMETRY CONSIDERATIONS
OF EXPLOSIVE-DRIVEN MHD GENERATORS

P. R. Smy and C. N. McKinnon

Measurements on the shaped charge-driven pulsed MHD generator indicate that high power, high energy outputs will be obtained when this type of device is scaled to a larger size. Already 23 MW (lasting about 30 μ secs) has been delivered to a resistive load. Important considerations that arise therefore, are:

1. What scaling relations apply to this device?
2. Can the device compete favorably with capacitor storage or some other form of conversion?
3. How can the power be delivered for times longer than tens of μ secs, so more total energy is delivered to a load?
4. What other forms might such a high-powered device take?

Before considering the scale-up of an explosive-driven generator, the proper perspective can be gained by looking at existing (competing) methods for the generation of electrical pulses of high power.

The most obvious competitor is the capacitor bank. A typical capacitor bank occupying a total volume of 1 cubic meter might possess a stored energy of 2×10^4 joules and provide a peak power of 10^{10} watts. Power supplies and switching equipment would of course take up more space. One drawback of this system is that, although a capacitor bank discharge can be initiated with little delay, the capacitors must be charged prior to discharge. The

MHD research, inc.

capacitors can be maintained in the charged condition indefinitely, however, this puts a severe stress on the dielectric and reduces their lifetime and even in this event the inevitable leakage current would require a supply of electrical power to the bank. In this respect, capacitors are storage devices and not independent energy sources.

The properties of compactness and zero power consumption in the "primed" state make an explosive-driven generator an attractive proposition compared to capacitors. A very large amount of chemical energy is stored in a very small volume of explosive and no power is required to maintain the explosive in its "primed" state apart from the power consumed by the triggering device. Neglected here is the power requirement for the magnetic field as this could be supplied by permanent magnets in certain instances. The problem is to convert this explosive energy into electrical energy.

Another competitor in the generation of pulse power are the new piezoelectric materials, which transform a direct mechanical stress into high voltage electrical power. The piezoelectric energy output that can be expected from a cubic meter is about 3×10^4 joules, which could be delivered in about 10^{-3} secs for a power output of the order of 10^7 watts. The problem is in providing the mechanical pressure of 15,000 psi over the desired surfaces. Again, explosive energy may be capable of providing the quick mechanical stress necessary for high power pulse generation.

Scaling

To design an efficient pulsed power generator it is necessary to know those properties of the generator which must be optimized. For

most applications it seems that the desirable properties are high power, high energy, compactness, and in certain instances, small or zero power consumption in the "primed" condition. These properties are of course desirable in a continuous generator, but it should be noted that efficiency, a property essential in a continuous generator, has been omitted. It is this omission that lends a certain flexibility to the design of a pulsed MHD generator.

In the present experiments, the explosion products were channeled through a linear MHD generator to provide a peak power of approximately 23 MW for a period of about thirty microseconds. The volume of the generator for this power level is about 1100 cm^3 . Properties of the gas in the region of interaction with the magnetic field, as calculated from experimentally determined quantities are:

$$\text{Velocity } u \sim 10 \times 10^3 \text{ m/sec,}$$

$$\text{Electrical conductivity } \sigma \sim 2 \times 10^3 \text{ mho/m.}$$

The Rankine-Hugoniot equations imply a minimum gas density of about 5 kg/m^3 .

With these experimental results, it is possible to estimate the power output from a generator with the much larger dimensions of 1 meter x 1 meter x 1 meter, and so compare the generator performance directly with the capacitor bank or piezoelectric system described above.

In an MHD generator in which the magnetic field strength is B , the power output per unit volume is:

$$\frac{P}{\text{vol}} = \frac{\sigma u^2 B^2}{4}$$

Thus with the experimental values for σ , u , and with B equal to 1 weber/m² (feasible for permanent magnets), the resulting power density is about 5×10^{10} watts/m³. Unfortunately, although this power output density is obtained with the present generator, it is unlikely that P_{vol} could have such a high value with the much larger generator. There are two reasons for this:

1. At present the region of conducting gas is located within 4 cms of the shock front and thus (for strict scaling) only a small fraction (4%) of the total generator volume (1 meter x 1 meter x 1 meter) will be effective in power production at any given time. Of course it can be expected that this rather limited region of high conductivity might be extended by further experimentation with seeded materials and by use of large explosive charges.
2. As the dimensions of the generator are increased, the appropriate magnetic Reynolds number (R_m) becomes much greater than unity,

$$R_m = \mu_0 \sigma L u .$$

In this equation μ_0 is the permeability of the conducting medium (usually taken as the free space value) and L is a length characteristic of the interaction region. When R_m is greater than unity, the induced

(generated) current perturbs the applied field⁽³⁾
and places an upper limit on the power output of the
generator of

$$P_{\max} = \frac{B^2 Au}{2\mu_0}$$

where A is the flow cross-section.

The upper limit imposed here is a result of the generator design, and does not take into account the possibility of recovering inductively energy extracted from the gas system and stored magnetically. The usual "low" R_m relationship

$$P \approx \sigma u^2 B^2$$

no longer applies.

The conditions for the present generator are:

$$L \approx 2 \times 10^{-2} \text{ meters}$$

$$R_m \approx 0.12.$$

Therefore, the expected output power density should be 2×10^{10} watts/m³. For the generator with L equal to one meter, R_m has a value of six, and so the appropriate generator power density is more accurately given by the high relationship. Therefore,

$$P_{\max} (L = 1 \text{ meter}) = 8 \times 10^9 \text{ watts.}$$

This is somewhat less, but on the same order, as that given by the low R_m relationship. Another very similar effect which also becomes

MHD research, inc.

important if R_{in} is much greater than unity, is the internal inductance of the generator. It can be shown that the power output from the generator will be substantially inhibited for the time it takes the gas shock front to transverse the generator due to this inductive effect.

It can be seen that on the basis of either of the above mechanisms, the power output density will decrease with increasing generator volume. However, a one cubic meter generator would still produce respectable quantities of power:

$$P \approx 10^9 \text{ watts .}$$

Extrapolating from present experiments, a duration of 10^{-4} secs seems reasonable, giving an energy output of:

$$E = 1 \times 10^5 \text{ joules.}$$

This is more than competitive with other pulse power sources.

If low electrical power consumption prior to triggering is not a prime consideration, then electromagnets could be used (rather than permanent magnets); this would boost the applied field strength up to say 5 webers/m² and so boost the power and energy output by a factor of 25. In any event, the source of magnetic field would occupy a substantial volume and would probably increase the total size of the power source by a large factor with the results that an MHD generator and condenser bank both capable of delivering between 10^5 and 10^6 joules would occupy much the same volume.

3. The problem of scaling such a generator is not simple because of the unusually high velocities and conductivities generated by seeded explosives, with the result that generators of modest size pro-

duce a high R_m interaction in which the usual low R_m generator relations do not apply.

2. Proposed Radial MHD Generators

From the above discussion it seems that the explosive driven rectangular MHD generator is a relatively inefficient device when readily attainable magnetic field strengths are used, the reason being that the dynamic pressure, ρu^2 , of the incident flow is much greater than the available magnetic pressure,

$$\frac{B_0^2}{2\mu_0}$$

Also it appears that much of the explosive energy is wasted in inelastic expansion of the explosion chamber due to the small solid angle that the generator subtends at explosive. Even optimum charge shaping results in no more than 5% of the chemical energy converted into directed motion in the MHD channel.

A notable improvement in both respects should be achieved by using a cylindrical configuration in which a stick of explosive explodes radially. In this case the density of the exploding gas must perforce decrease with increasing radius to provide a more efficient match between the dynamic and magnetic pressures and also ensure a much greater interaction cross-section. The two types of radial MHD interactions which have been considered are adaptations of the well-known \odot and \otimes pinch discharges.

MHD research, inc.

"⊖-Pinch" MHD Device

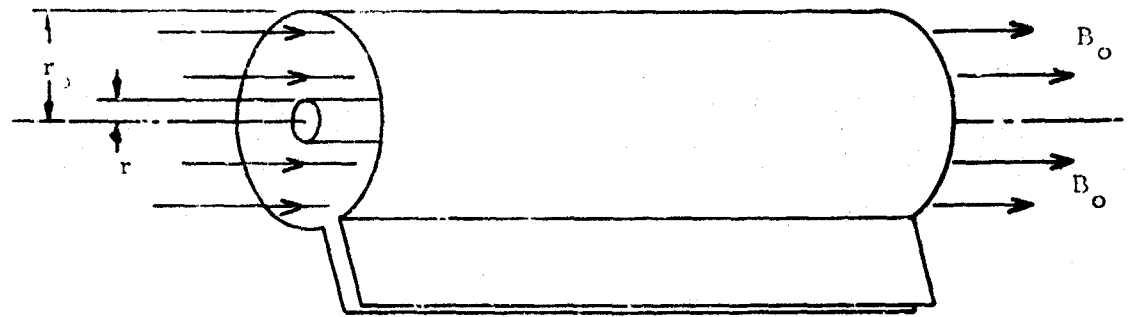
This device would consist of a radial explosion in a region of axial field surrounded by a solenoid, (see Figure A.1). For simplicity we will consider the solenoid to be short circuited initially. With the solenoid short circuited, the total flux through the solenoid remains constant. To some extent the expanding radial explosion is diamagnetic and so the magnetic field will be compressed by the explosion into an annulus at the periphery of the coil. This compression of magnetic field lines corresponds to an increase in the magnetic energy of the system

$$\int_{\text{vol}} \frac{B^2}{2\mu_0} dv .$$

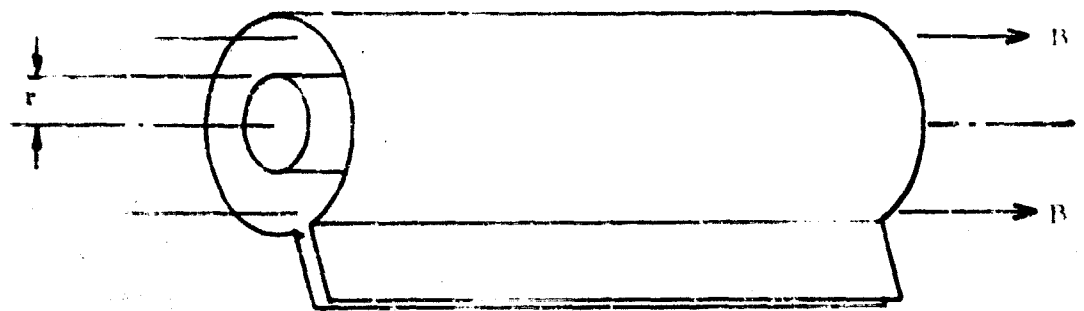
Much of this magnetic energy is readily convertible into electrical energy by switching a suitable external impedance into the solenoid circuit as the compression of field lines nears a maximum. The smallest volume of the annulus (if we assume negligible attenuation of radial explosion velocity) is determined by the velocity and conductivity distribution within the exploding column, and this limit is a consequence of the imperfect diamagnetism of the exploding column. This cross-section will be

$$= \frac{2\pi r_0}{\mu_0 \frac{dr}{dt}}$$

It should be emphasized that this is a very approximate relation. It should be fairly simple to obtain a much more accurate relation for a simple model, but this has not been attempted since the actual physical properties of the system



Before Ignition



After Ignition

Figure A.1 - Orlowski MHD generator

MHD research, inc.

are not well known. Assuming the above relation is correct, we can work out the enhanced magnetic energy of the system. If the initial field is B_0 and the solenoid radius is r_0 , then applying flux conservation we have

$$B = \frac{\mu_0 \sigma \frac{dr}{dt} B_0 r_0}{2}$$

and so the final magnetic energy is,

$$\frac{\mu_0 \sigma \frac{dr}{dt} l}{2} \frac{B^2}{2\mu_0} \sim \frac{R_m}{2} \times \text{original magnetic energy.}$$

Taking $A = 1 \text{ meter}^2$, $l = 1 \text{ meter}$, $B_0 = 1 \text{ weber/meter}^2$, and $R_m \sim 6$, we have a final magnetic energy, E_m , of 1 megajoule.

Most of this magnetic energy could be converted into electrical energy in a time: $\tau = \frac{l}{u \sigma \mu_0} = 30 \mu \text{ secs.}$

This would correspond to a power of approximately 3×10^{10} watts.

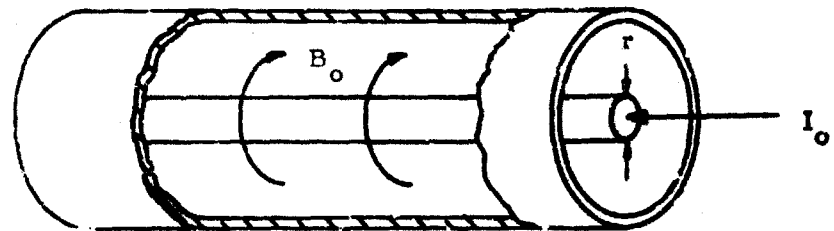
While these figures are undoubtedly optimistic, it seems probable that both power and energy would be greater than one-tenth of the above values. This inductive removal of energy has several advantages. For example, it eliminates electrode sheath effects together with their associated power losses and by varying the number of turns of the solenoid, one can vary the output impedance to match a particular load.

"Z-Pinch" MHD Device

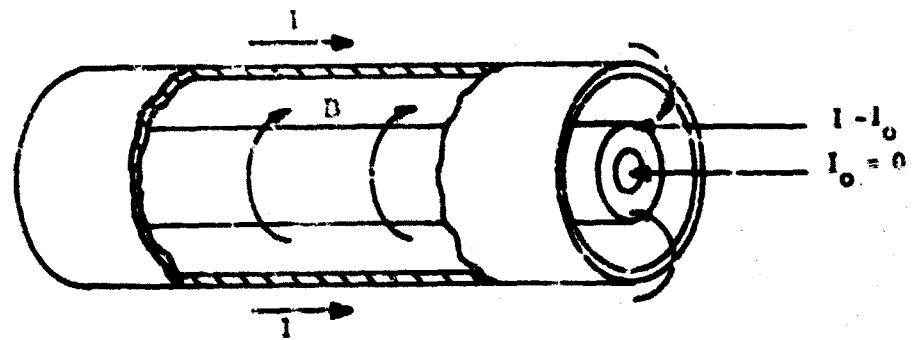
In the "θ-pinch" device, only field strengths which could be obtained using permanent magnets were considered. In the "Z-pinch" device, see Figure A.2, the initial interacting magnetic field is generated by a current along the axis of the system, i. e., along the center of the cylinder of explosive. This might be achieved by pulsing current through a thin wire coated with explosive, vaporizing the wire and so detonating the explosive. The wire would be held between the center of two parallel metal electrodes with the return lead consisting of rods situated around the periphery of the device to form a coaxial assembly. The system effectively acts as a current amplifier; the azimuthal magnetic field and the radial velocity of the explosion produce an axial E field which augments the existing axial current and so strengthens the magnetic interaction. We will consider a radial explosion in which the exploding column increases in radius at a constant rate from an initial radius r_0 , the conductivity of the exploding gas is constant, and the initial current is I_0 . As before, we neglect magnetic retardation of the gas on the grounds that this can be eliminated by using sufficient explosive. If appreciable retardation does occur, then the conversion of a large fraction of the kinetic energy of the explosion into electrical energy has been achieved. For simplicity, we consider the electrodes to be short circuited and calculate the enhanced magnetic energy of the system. If $\frac{B}{\mu_0}$ is the field at some point, r , from the axis and I is the total current passing within this distance from the wire then

$$B = \frac{2 I \mu_0}{r} .$$

MHD research, inc.



Before Ignition



After Ignition

Figure A.2 "Z-Pinch" MHD Generator

If v is the radial velocity at any point (the assumption of constant uniform velocity is made for theoretical simplicity; it is virtually certain this would not apply in practice), then the induced electric field at a point, r , from the axis is

$$E = \frac{v \times 2 I \mu_0}{r} ,$$

and so the total current

$$\begin{aligned} I &= I_0 e^{\sigma \mu_0 v (r - r_0)} \\ &= I_0 e^{R_m} . \end{aligned}$$

With a system whose dimension L equals $1/2$ m, and R_m equals 3, it is seen that considerable current and hence electrical energy amplification might be obtained. Here again the power output might be inhibited to some extent by the self-inductance of the generator for the useful case of R_m much greater than one. This system is very sensitive to R_m . For example, if σ equals 5×10^3 mhos/meter, then

$$\frac{I}{I_0} = e^{15} \text{ rather than } e^3 .$$

Significance of R_m in These Configurations

There are basically two types of power conversion systems described in the foregoing devices. In the cartesian MHD generators which have been described, energy is extracted from the system at the same rate that it is converted from kinetic to electric energy. It is this feature that allows an

MHD research, inc.

expression of maximum power output to be derived. In the radial configurations, the kinetic energy of the stream is first stored magnetically and then recovered by inductive methods. Thus, the peak power output of such a system is regulated by the recovery method, and not by the energy flux of the stream or the initial energy content of the magnetic field. The value of R_m determines to a large degree, the effectiveness of the magnetic storage type of device, because as $R_m \longrightarrow \infty$, this type of device becomes efficient. Increasing R_m beyond a certain limit would be of little value in the cartesian generator with direct extraction. However, if inductive removal of energy is utilized with this geometry, it can be generally stated that optimum operation of MHD generators will occur at the highest possible R_m .

We have frequently taken the applied field strength to be 1 weber/m², i.e., a field strength readily obtainable with permanent magnets. If we consider the use of the higher fields obtainable with electromagnets then the ratio:

$$\frac{\text{energy output}}{\text{initial magnetic energy}}$$

becomes a very significant parameter since in this case the initial magnetic energy can in any case be readily converted to electrical energy by switching off the magnetizing current.

If field strengths greater than 1 weber/m² are required in the above radial generators, it follows that R_m must be appreciable greater than unity for the generators to be practical.

Both radial generators become efficient sources of power when their dimensions are increased to about 1 meter; however, it is necessary that all the exploding gas be highly conducting rather than a region of a few cms thickness as at present.

APPENDIX B - ANALYSIS OF ENERGY STORAGE CAPACITY
OF RADIAL FLOW-PULSED MHD GENERATORS

A preliminary analysis has been conducted to determine the anticipated energy storage in radial flow-pulsed MHD generators based upon conductivity values determined in the linear generator. The analysis was conducted for an overall system weight of about 2000 pounds (this being a weight of interest for satellite operations) and it has been assumed that twenty power pulses would be required during the lifetime of the system. The useful lifetime for the system is anticipated as 3 months due to the type of cooling used for the magnet coils. In addition, the particular system considered has been designed solely for use in a space environment (i. e., the low pressure surrounding a satellite would be used to maintain solid hydrogen at about 4°K).

It is very clear that a major portion of the weight of such a pulsed power system utilizing MHD techniques is in the magnet. Substantial improvements in overall performance and power output (hence conversion efficiency) should be obtained by using the highest magnetic field strengths obtainable. For instance, if $Re_M \gg 1$ then the power output in a pulsed generator, as shown in Appendix A, should be:

$$P_{\max} = \frac{2 B^2 A v}{\mu_0}$$

where A is the cross sectional area of the flow moving with a velocity v and μ_0 is the permeability of free space. Thus, rather than put great emphasis on increasing the gas conductivity σ , it is necessary to maximize B^2 . The most feasible way to do this is to use superconducting coils.

MHD research, inc.

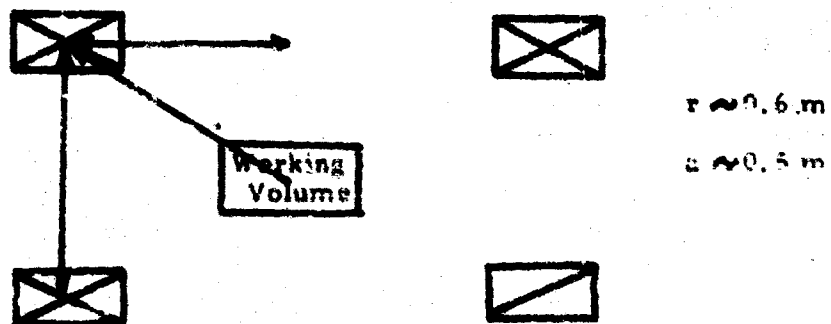
In the analysis, it is assumed that 50,000 gauss will be attainable with superconducting coils at 5°K. The average specific gravity of the superconducting wire is taken as 8 and the current density, i/A , attainable, as 10^5 amps/cm².

The energy density in the magnetic field at this strength is

$$\frac{E_B}{V} = \frac{B^2}{2\mu_0} = \frac{25}{2 \times 4\pi \times 10^{-7}} = 10^7 \text{ joules/m}^3.$$

If the working volume is 10^{-1} m^3 then $E_B = 10^6$ joules.

A Helmholtz coil would be used to generate the 5.0 w/m² over a volume of 10^{-1} m^3 . Taking the coil radius as 0.5 m and separation as 0.5 m



then the magnetic field is given by

$$B = \frac{4\pi I a^2}{10^7 r^3}$$

or the current,

$$I \text{ (total in 2 coils)} = \frac{10^7 B r^3}{4\pi a^2}$$

$$= 3.3 \times 10^6 \text{ amperes.}$$

For design purposes a conservative value of, $I_{\text{total}} = 5 \times 10^6$ amperes is used.

Now the current density,

$$\frac{I}{A} = 10^5 \text{ amps/cm}^2$$

so that the total conducting area (cross section of the coils) would be

$$A = \frac{I}{J} \times I = 50 \text{ cm}^2 \text{ or } 25 \text{ cm}^2/\text{coil}.$$

To allow for copper insulation and connections the area of each coil will be doubled so that

$$A_{\text{(each coil)}} = 50 \text{ cm}^2.$$

Thus, total volume of superconducting material plus associated insulation at an average specific density of 8 is:

$$\begin{aligned} \text{Volume} &= lA \\ &= 2(2\pi(0.5) \times 5 \times 10^{-3}) \\ &= 3.1 \times 10^{-2} \text{ m}^3 \end{aligned}$$

$$\begin{aligned} \text{and the mass} &= \rho V \\ &= 8 \times 10^3 \frac{\text{kg}}{\text{m}^3} \times 3.1 \times 10^{-2} \text{ m}^3 \\ &= 250 \text{ kg} = 550 \text{ lb.} \end{aligned}$$

In order to restrain the coils, titanium bands would be used 5 cm thick with a total mass of 340 kg or 750 pounds.

The use of superconductors adds to the system the increased complexity of cryogenics. Since one of the more attractive uses for a pulse power system would be in space, some thought has been given to the best manner of cooling a

MHD research, inc.

superconducting coil in terms of overall mass of the cooling system and its complexity. The temperature required for superconducting coils to operate efficiently is about 5°K or less. Liquid helium, of course, with a boiling point of 4.2°K is the first thought for use in the system. However, from the point of view of system mass, helium is unattractive due to its low heat of vaporization. In addition, the use of a cryostat to liquefy the helium would add mass, increase complexity and require electric power. On the other hand, solid hydrogen has a much higher thermal capacity as a thermal heat sink.

When liquid hydrogen is exposed to an ambient pressure of 50 mm Hg or less, a small percentage will "flash" to vapor and the remaining major portion will freeze to a solid form at a temperature of 14°K or less. At an ambient pressure of approximately 1 mm Hg, the sublimation temperature of the hydrogen "ice" will be reduced to 10°K , and at 10^{-5} mm Hg further reduced to 5°K . This relationship between temperature and pressure is shown in Figures B-1 and B-2.

As the vacuum environment surrounding a cryogenic cooling system in space will be less than 10^{-6} mm Hg, the temperature of the solid hydrogen heat sink can be maintained at temperatures as low as 5°K by proper control of venting.

A preliminary analysis was conducted to estimate the useful volume to weight ratio for a cryogenic container suitable for cooling superconducting magnet coils. It was estimated that 1 m^3 of volume was required and that a steady power dissipation of 0.2 watts occurred due to the coils. With proper

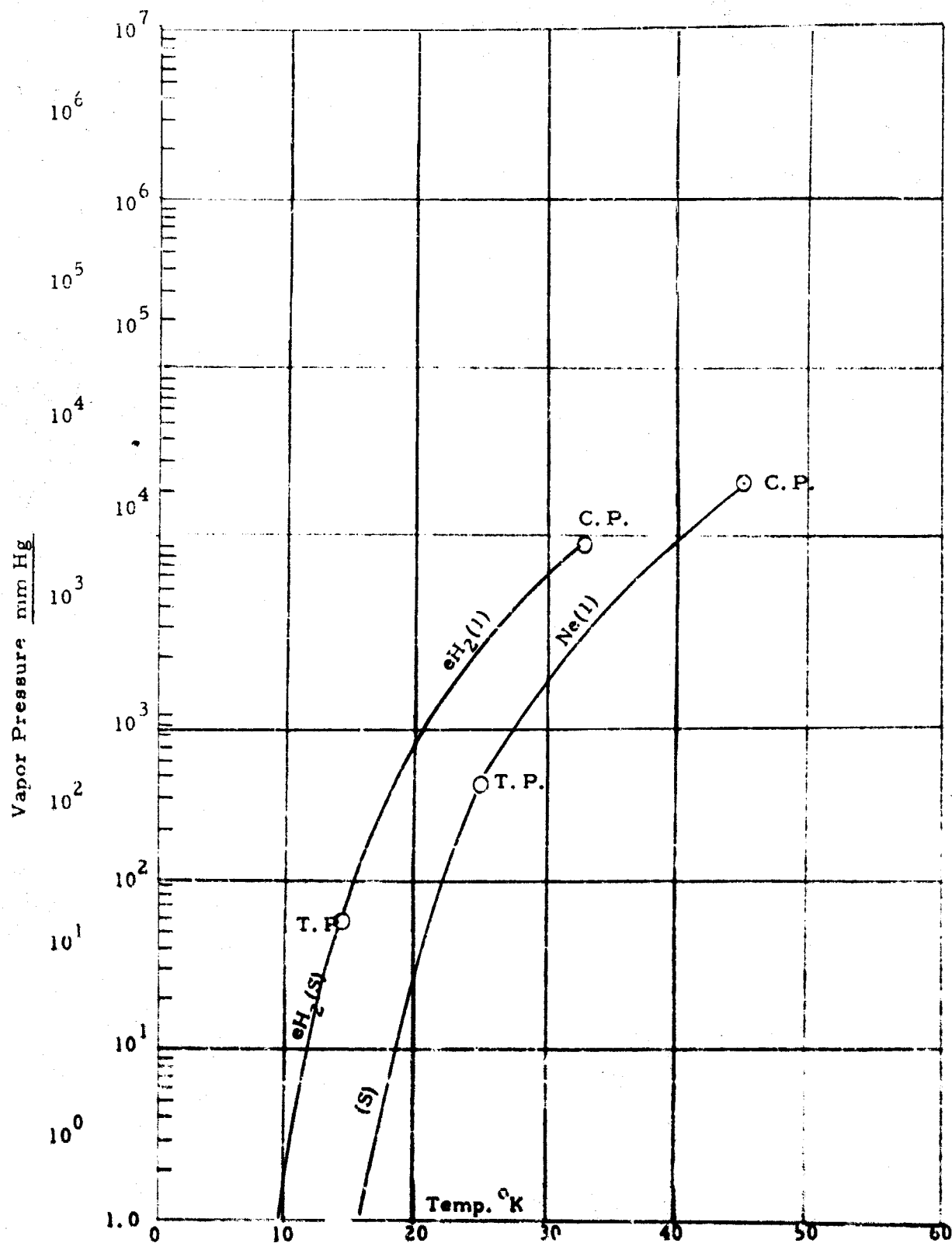
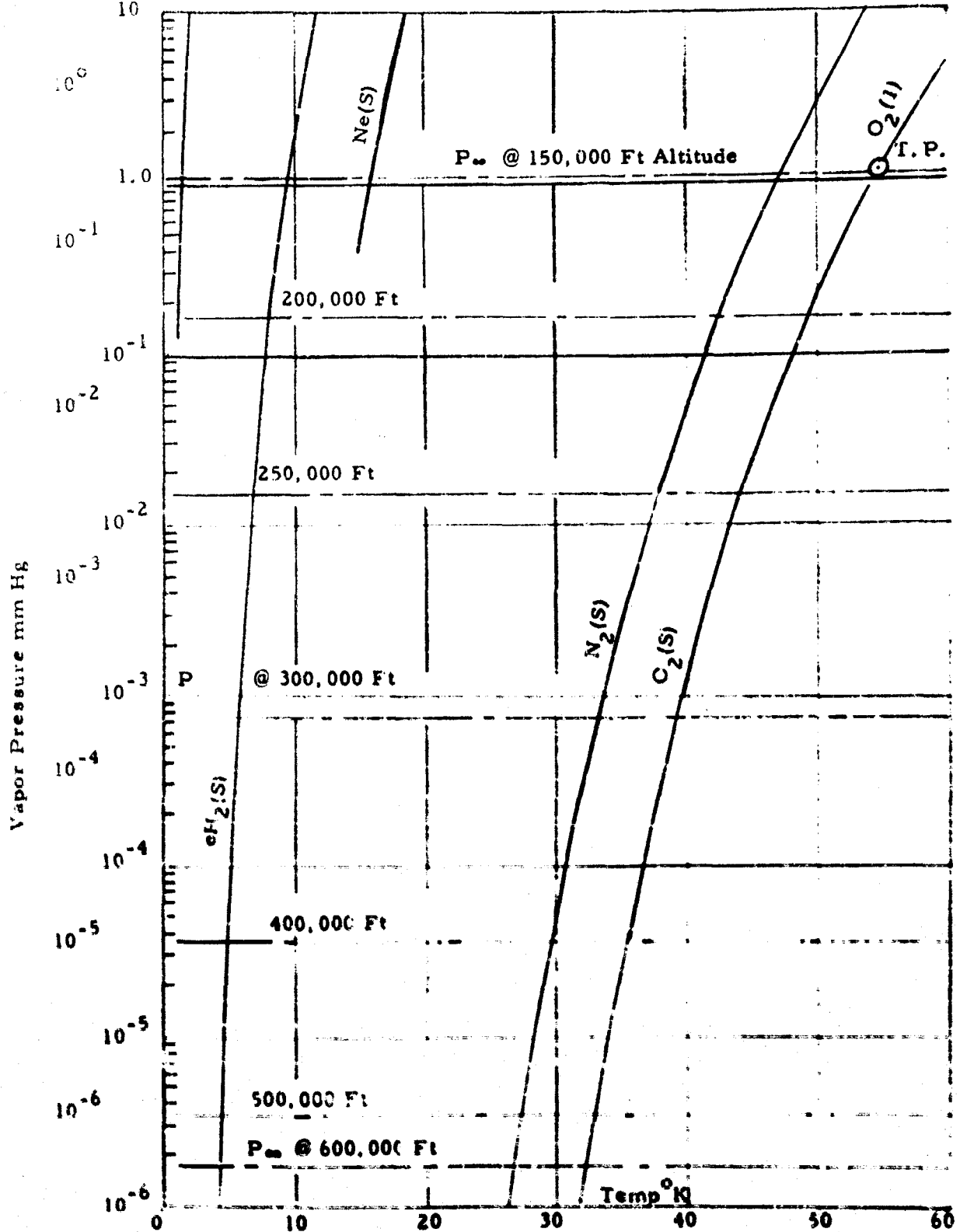


FIGURE B.1
 Vapor Pressure vs. Temperature
 (Equilibrium) Hydrogen and Neon



Vapor Pressure vs Temperature
 (Equilibrium) Hydrogen, Neon, Nitrogen and Oxygen
 FIGURE B.2

insulation and vacuum venting, power absorbed from the outside could be kept to the same level, 0.2 watts. The total weight of hydrogen required for cooling is only about 30 kg with an insulation weight of about 35 kg. Allowing structural compactness, the total weight of the system would be about 125 kg, 275 pounds, for a useful volume of 1 m^3 .

The 1 m^3 system with the above mentioned power drain could maintain a coil temperature of less than 5°K for over one year at altitudes greater than 100 miles. If mission requirements were reduced to 3 months, the amount of hydrogen required would be decreased to less than 15 kg for a total system mass of 110 kg, 240 pounds. It would be exceedingly difficult, if not impossible, to attain this volume to mass ratio with a helium system.

The coils would be energized by a battery and some form of power conditioning system. In order to bring the coil to full field strength in a reasonable time, a fairly high discharge rate battery will be required.

For a one hour discharge rate, several battery characteristics are listed below:

Nickel-cadmium	-	50 kj/pound,
Silver-cadmium	-	100 kj/pound,
Silver-zinc	-	250 kj/pound.

If the discharge time is decreased to 4 minutes, the energy per pound decreases by about 40%. For the purposes of calculation it will be assumed that 150 kj/pound can be obtained and that the coils fully energized store 2×10^7 joules. Then, 130 pounds of batteries would be required to create the field in the superconducting coils. Power conditioning equipment should approximately double this figure.

MHD research, inc.

The power per unit volume that can be produced is based upon presently obtained values of σ and v . Conservative values for these quantities are:

$$\text{velocity } v \sim 5 \times 10^3 \text{ m/sec ,}$$

$$\text{conductivity } \sigma \sim 3 \times 10^3 \text{ mho/m ,}$$

$$P/\text{vol} = \frac{\sigma v^2 B^2}{4} .$$

Now if:

$$B = 5 \text{ w/m}^2$$

$$P/\text{vol} = \frac{3 \times 25 \times 25 \times 10^9}{4} = 470 \times 10^9 \text{ watts/m}^3$$

$$= 4.7 \times 10^{11} \text{ watts/m}^3 .$$

If the active volume is limited to the 0.1 m^3 over which $B \sim 5 \text{ w/m}^2$ then the maximum power level would be 4.7×10^{10} watts. However, experiment has shown that a "slug" of gas only about 5 cm in length is active in generating power. In the present case this would reduce the power level to 4.7×10^9 watts.

The time duration of this power would be approximately:

$$t = \frac{d}{v} = \frac{.25}{5 \times 10^3} = 50 \mu\text{sec} .$$

Thus, the expected energy into a load would be

$$E = P \times t .$$

$$= 4.7 \times 10^9 \times 50 \times 10^{-6} .$$

$$= 240 \times 10^3 \text{ joules} .$$

$$= 240 \text{ kilojoules} .$$

Now 1 pound of explosive contains 2.2×10^6 joules which would require a conversion efficiency of over 10% to obtain 0.24×10^6 joules, electrical. For conservative purposes it is felt that 2 pounds of explosive would be more reasonable, requiring a conversion efficiency of under 6%.

Twenty explosive cartridges would have a mass of 40 pounds.

The cartridge replacement mechanism might be expected to weigh 60 pounds.

The explosion restraining tube would be a high strength titanium alloy at specific gravity of 5 and should have a mass of no more than 250 pounds.

Summary Table of the System

Coils	550 lbs.
Supports	750 lbs.
Cryogenics	240 lbs.
Power Supply	260 lbs.
Explosives	40 lbs.
Cartridge System	60 lbs.
Explosion Tube	<u>250 lbs.</u>
Total Weight	2,130 lbs.

Total energy out is 240 kilojoules with a pulse duration 50 sec.

There is the potential of going to 10^6 joules if the efficiency could be increased from 5 to 20 percent. This, however, would have to wait experimental and engineering development.

REFERENCES

- (1) Jones, M. S., et al, "Research on the Physics of Continuous and Pulsed MHD Generators", Semi-annual Technical Summary Report, MHD Research, Inc. Report 632, February 1963.
- (2) Jones, M. S., et al, "Research on the Physics of Continuous and Pulsed MHD Generators", Second Semiannual Technical Report, MHD Research, Inc. Report 640, August 1963.
- (3) Pain, H. J., and Smy, P. R., Experiments on Power Generation from a Moving Plasma, Journal of Fluid Mechanics 11, 51, February 1961.
- (4) Jones, D. L., The Energy Parameter B for Strong Blast Waves, National Bureau of Standards Technical Note 155, July 1962.
- (5) Koski, W. S., Lucy, F. A., Shreffler, R. G., and Willig, F. J., Fast Jets from Collapsing Cylinders, Phys. Fluids 23, 1300, December 1952.
- (6) Rosciszewski, Jan, Solid Propellant Driver Shock Tube, ARS Journal, p 1426, September 1962.
- (7) Zeldovich, Ia. B., and Kompaneets, A. S., Theory of Detonation, Academic Press, New York and London, 1960.
- (8) Nagamatsu, H. T., Sheer, R. E., and Weil, J. A., Non-Linear Electrical Conductivity of Plasma for Magnetohydrodynamic Power Generation, ARS Paper 2632-62, Space Power Systems Conference, Santa Monica, California, September 1962.
- (9) Spitzer, L. J., Physics of Fully Ionized Gases, Interscience Publishers, New York, 1956.
- (10) Burnham, M. W., "Explosive Parameters for Magnetohydrodynamic Energy Conversion", ASD PDR-63-37, September 1963.

DISTRIBUTION LIST

	<u>No. copies</u>
Director, Advanced Research Projects Agency The Pentagon Washington, D. C. 20301 Attn: Dr. John Huth	2
Office of Naval Research Power Branch (Code 429) Washington, D. C. 20360 Attn: John A. Satkowski	6
Commanding Officer Office of Naval Research Branch Office Box 39 Navy #100 Fleet Post Office New York, New York	1
Cognizant ONR Area Branch Office	1
U. S. Naval Research Laboratory Washington 25, D. C. Attn: Technical Information Division	6
Wright-Patterson Air Force Base Aeronautical Systems Division Ohio Attn: Don Warnock (ASRMFP-2)	1
Air Force Office of Scientific Research Washington 25, D. C. Attn: Dr. Milton M. Slawsky	1
U. S. Naval Ordnance Test Section Propulsion Applied Research Group China Lake, California Attn: Leroy J. Krzycki (Code 4506)	1
Rome Air Development Center Rome, New York Attn: Mr. Frank J. Mellura	1

MHD research, inc.

	<u>No. copies</u>
U. S. Naval Ordnance Laboratory NA Division White Oak, Maryland Attn: Wallace Knutsen Library	1 2
Defense Documentation Center Cameron Street Alexandria, Virginia 22314	20
U. S. Army Research & Development Laboratory Fort Belvoir, Virginia Attn: Frank Shields (ERD-EP)	1
NASA, Lewis Research Center 21,000 Brookpark Road Cleveland 35, Ohio Attn: Wolfgang Moeckel Dr. B. Lubarsky	1 1
U. S. Atomic Energy Commission Division of Reactor Development Direct Energy Conversion Section, RD: AED Germantown, Maryland	1
Dr. T. Brogan AVCO - Everett Research Laboratory 2385 Revere Beach Parkway Everett, Massachusetts	1
Dr. J. Cole Department of Aeronautics California Institute of Technology Pasadena, California	1
Mr. Arthur Sherman General Electric - Valley Forge Valley Forge Space Technical Center Philadelphia 1, Pennsylvania	1
Dr. M Talaat Martin-Marietta Corporation Nuclear Division Baltimore 3, Maryland	1

	<u>No. copies</u>
Dr. W. D. Jackson Electrical Engineering Department Massachusetts Institute of Technology Cambridge 39, Massachusetts	1
Dr. B. C. Lindley Nuclear Research Centre C. A. Parsons & Co., Ltd. Fossway, Newcastle Upon Tyne 6 England	1
Dr. Robert Eustis Thermosciences Division Stanford University Stanford, California	1
Mr. John Wright Central Electricity Research Laboratories Cleeve Road, Leatherhead, Surrey England	1
Dr. Richard Schamberg Rand Corporation 1700 S. Main St. Santa Monica, California	1
Dr. Sam Naiditch Unified Science Associates 826 Arroyo Parkway Pasadena, California	1
Dr. W. S. Emmerich Westinghouse Research Laboratories Beulah Road, Churchill Borough Pittsburgh 35, Pennsylvania	1
Dr. R. T. Schneider Allison Division General Motors Corporation Indianapolis, Indiana	1
Dr. D. G. Elliott Jet Propulsion Laboratory Pasadena, California	1

MHD research, inc.

Mr. Robert Cross
Research and Technology Division
Air Force Systems Command
Bolling AFB
Washington 25, D. C.

No. copies

1

Detachment 4. ASD
ASQW
Eglin AFB, Florida

1

Dr. Vernon H. Blackman
MHD Research, Inc.
1535 Monrovia Ave.
Newport Beach, California

1

Advanced Research Projects Agency (ONR), Washington, D. C.
RESEARCH ON THE PHYSICS OF PULSED MHD GENERATORS.
 Final report, Dec 63, 16 pp incl illus, tables, appendices.
 Unclassified Report

Two systems are discussed for producing short pulses of electrical power by MHD principles. The first system is driven by condensed explosives and produces pulses lasting from 1 microsec to 100 microseconds. The peak power generated is about 25 MW, with an energy output of 350 joules. The conversion efficiency, chemical to electrical, is 1%. Higher conversion efficiencies can be readily achieved.

The second system uses the combustion of aluminum with cerium nitrate as the energy source for a supersonic MHD channel. The measured conductivity of the combustion products was 1000 mho/in. The highest measured peak power output was 25 watts. The experimental data indicate a large electrode drop which must be overcome before currents can flow in the generator. A favorable scaling potential is indicated.

1. Electric Power Sources
2. Electric Power Production
3. Energy Conversion
4. Generators
5. Plasma Physics
6. Magnetohydrodynamics
7. Project Code 4800, Order No. 2042
8. Contract Nonr-3659(00)
9. MHD Research, Dec.
10. Newport Beach, California
11. Jones, M. S., Evans, E. W., McKimson, C. N.
12. MHD Report 646
13. in ASTIA collection

Advanced Research Projects Agency (ONR), Washington, D. C.
RESEARCH ON THE PHYSICS OF PULSED MHD GENERATORS.
 Final report, Dec 63, 16 pp incl illus, tables, appendices.
 Unclassified Report

Two systems are discussed for producing short pulses of electrical power by MHD principles. The first system is driven by condensed explosives and produces pulses lasting from 1 microsec to 100 microseconds. The peak power generated is about 25 MW, with an energy output of 350 joules. The conversion efficiency, chemical to electrical, is 1%. Higher conversion efficiencies can be readily achieved.

The second system uses the combustion of aluminum with cerium nitrate as the energy source for a supersonic MHD channel. The measured conductivity of the combustion products was 1000 mho/in. The highest measured peak power output was 25 watts. The experimental data indicate a large electrode drop which must be overcome before currents can flow in the generator. A favorable scaling potential is indicated.

1. Electric Power Sources
2. Electric Power Production
3. Energy Conversion
4. Generators
5. Plasma Physics
6. Magnetohydrodynamics
7. Project Code 4800, Order No. 2042
8. Contract Nonr-3659(00)
9. MHD Research, Dec.
10. Newport Beach, California
11. Jones, M. S., Evans, E. W., McKimson, C. N.
12. MHD Report 646
13. in ASTIA collection

Advanced Research Projects Agency (ONR), Washington, D. C.
RESEARCH ON THE PHYSICS OF PULSED MHD GENERATORS.
 Final report, Dec 63, 16 pp incl illus, tables, appendices.
 Unclassified Report

Two systems are discussed for producing short pulses of electrical power by MHD principles. The first system is driven by condensed explosives and produces pulses lasting from 1 microsec to 100 microseconds. The peak power generated is about 25 MW, with an energy output of 350 joules. The conversion efficiency, chemical to electrical, is 1%. Higher conversion efficiencies can be readily achieved.

The second system uses the combustion of aluminum with cerium nitrate as the energy source for a supersonic MHD channel. The measured conductivity of the combustion products was 1000 mho/in. The highest measured peak power output was 25 watts. The experimental data indicate a large electrode drop which must be overcome before currents can flow in the generator. A favorable scaling potential is indicated.

1. Electric Power Sources
2. Electric Power Production
3. Energy Conversion
4. Generators
5. Plasma Physics
6. Magnetohydrodynamics
7. Project Code 4800, Order No. 2042
8. Contract Nonr-3659(00)
9. MHD Research, Dec.
10. Newport Beach, California
11. Jones, M. S., Evans, E. W., McKimson, C. N.
12. MHD Report 646
13. in ASTIA collection

Advanced Research Projects Agency (ONR), Washington, D. C.
RESEARCH ON THE PHYSICS OF PULSED MHD GENERATORS.
 Final report, Dec 63, 16 pp incl illus, tables, appendices.
 Unclassified Report

Two systems are discussed for producing short pulses of electrical power by MHD principles. The first system is driven by condensed explosives and produces pulses lasting from 1 microsec to 100 microseconds. The peak power generated is about 25 MW, with an energy output of 350 joules. The conversion efficiency, chemical to electrical, is 1%. Higher conversion efficiencies can be readily achieved.

The second system uses the combustion of aluminum with cerium nitrate as the energy source for a supersonic MHD channel. The measured conductivity of the combustion products was 1000 mho/in. The highest measured peak power output was 25 watts. The experimental data indicate a large electrode drop which must be overcome before currents can flow in the generator. A favorable scaling potential is indicated.

1. Electric Power Sources
2. Electric Power Production
3. Energy Conversion
4. Generators
5. Plasma Physics
6. Magnetohydrodynamics
7. Project Code 4800, Order No. 2042
8. Contract Nonr-3659(00)
9. MHD Research, Dec.
10. Newport Beach, California
11. Jones, M. S., Evans, E. W., McKimson, C. N.
12. MHD Report 646
13. in ASTIA collection